PROPAC

Air conditioner with less than 150 gram propane

A project within the TERMO programme. A Swedish Energy Agencay research program for sustainable heat pump and refrigeration techology.

P48254-1

Klas Andersson

February 2022

Energimyndigheten

Foreword

The project achievements are the result of a team work between academic experts, small local Swedish companies and large international enterprises. It has been a pleasure to see all competences come together, in good spirit, to take a small step towards a more sustainable world. Thanks all for your contributions.

The project depended on the foundation laid by patient, foreseeing research work, in the field of small charges of natural refrigerants, by Professor Björn Palm and his colleagues at the division of Applied Thermodynamics and Refrigeration at the Royal Institute of Technology in Stockholm. Professor Björn Palm has given me the opportunity to follow and learn from his team.

I would like to express my gratitude for the courage shown by the Swedish Energy Agency by approving the application for this project, coming from a private company.

Finally, I would like to thank Professor Emeritus Eric Granryd for his mentorship. His patience with guiding me through endless trials and errors has been invaluable.

Lidingö

Februari 2022

Klas Andersson

Sammanfattning

Den här rapporten beskriver teknologi för en miljövänlig luftkonditionering av splittyp som kan ses hängande på väggarna i hundratals miljoner runt om i världen. Målet med Propac projektet var att demonstrera ett system som fungerar under realistiska förhållanden och använder mindre än 150 gram propan, ger 3.5 kW kyleffekt med rimlig effektivitet och ljudnivå.

Kondensorn som användes var av standard mikrokanaltyp tillverkad av platta aluminiumrör med små, rektangulära kanaler och med lödda flänsar mellan rören.

Projektet testade flera varianter av modifierad och vidareutvecklad mikrokanalteknik som förångare. Standardvärmeväxlare byggdes om och vidareutvecklades för mindre fyllnadsmängd och förbättrad värmeöverföring. En ny förångare tillverkades exklusivt för projektet, inklusive köldmediefördelare. Jämn distribution av köldmediet till de 1000 individuella, parallella köldmediekanalerna i förångaren är en nyckelfaktor för lågt tryckfall, hög värmeöverföring och låg fyllnadsmängd.

En effektiv intern värmeväxlare, som överför värme från det varma, flytande kondensatet till den kalla suggasen före kompressorn, är en nyckelkomponent för system med liten fyllnadsmängd. En enkel prototyp byggdes och testades i systemet. Projektet utvecklade också en ny typ av intern värmeväxlare baserad på ny teknologi, mer kommersiellt genomförbar och med utmärkt prestanda vad gäller hög värmeöverföringsprestanda, lågt tryckfall och minimal laddning.

En scrollkompressor med DC-motor för AC i elfordon, utvecklad för köldmediet 1234yf, användes. Den kännetecknas av små interna volymer, liten oljemängd och brett kapacitetsområde (800-8500 rpm). En smörjolja valdes för att passa den unika kombinationen av köldmedium och kompressor.
Expansionsanordningen var av standard elektronisk typ.

Systemkomponenterna och mätsystemet kommunicerade via olika typer av kommunikationsprotokoll vilket gjorde att det var nödvändigt att utveckla en unik styr- och mätmjukvara, PropacControl, för projektet.

Projektmålet, 3.5 kW kylkapacitet nåddes med 147 gram propan och med en verkningsgrad (COP_2), inklusive fläkteffekt, på 3.5. Anslutningarna mellan in- och utedelen var 6 m. Ökat luftflöde gav både högre kapacitet och effektivitet men orsakar också högre ljudnivåer.

Summary

This report describes technology for an environmentally friendly split air conditioner, seen hanging on the walls in hundreds of millions around the world. The objective was to demonstrated a system, operating under realistic conditions, using less than 150 gram propane, providing 3.5 kW cooling capacity with reasonable efficiency and noise level.

The condenser used was of standard microchannel type made by extruded flat aluminum tubes with narrow, rectangular channels inside and with soldered fins in-between the tubes.

The project tested serval variants of modified and further developed microchannel technology as evaporator. Standard heat exchangers where rebuilt and further developed for less charge and improved heat transfer. A new evaporator was manufactured exclusively for the project, including refrigerant distributor.

Even distribution of the refrigerant into the more than 1000 individual, parallel refrigerant channels in the evaporator is a key factor for low pressure drop, high heat transfer and low charge.

An efficient internal heat exchanger, transferring heat from the warm, liquid condensate to the cold suction gas before entering the compressor, is a key component for utilization of small charge system of this type. A simple prototype was built and tested in the system. The project also developed a new type of internal heat exchanger based on new technology, more commercial feasible and with excellent performance in terms of high heat transfer performance, low pressure drop and minimal charge.

A DC-motor scroll compressor for AC in electric vehicles, developed for the refrigerant 1234yf, was used. It is characterized by small internal volumes, small oil charge and wide capacity range (800-8500 rpm). A lubrication oil was selected to fit the unique combination of refrigerant and compressor. The expansion device was of standard electronic type.

The system components and measurement system communicated via different types of communication protocols why it was necessary to develop a unique control and measurement software, PropacControl, for the project.

The project target, 3.5 kW cooling capacity was reached with 147 gram of propane and with an efficiency (COP_2), including fan power, of 3.5. The connection lines in-between the in- and outdoor unit was 6 m. Increased air flow gave both higher capacity and efficiency but comes with increased noise.

Table of content

1 Introduction

The global market for air conditioners was 112.8 million units 2020. Year 2027, 150 million units are expected to be produced. A common type among these is the split units hanging on the walls around the globe as illustrated in Figure 1. This project studies and demonstrates technique for an environmentally friendly split unit providing 3.5 kW cooling capacity. It is one of the most common sizes of the split air conditioners.

Figure 1. AC-split outdoor units.

Until recently they were filled with about 1.3 kg of the refrigerant R410A, with GWP of 2088, corresponding to 2714 kg_{eq} CO_2. Since a couple of years, a transfer towards the refrigerant R32, with GWP 675, was initiated. A typical unit has about 0.8 kg R32, corresponding to 540 kg_{eq} CO_2. The transfer towards R32 is not a sustainable long-term solution. Figure 2 shows the phase out schedule for refrigerants according to the EU F-gas directive. The acceptable average GWP value for all refrigerants put on the market, assuming the same total amount of refrigerants set on the market as 2015, should be below 675 (the GWP-value of R32) already 2024. Moreover, R32 is mildly flammable (Ashrae class A2L) and a synthetic, non-natural, fluorinated hydrocarbon (HFC).

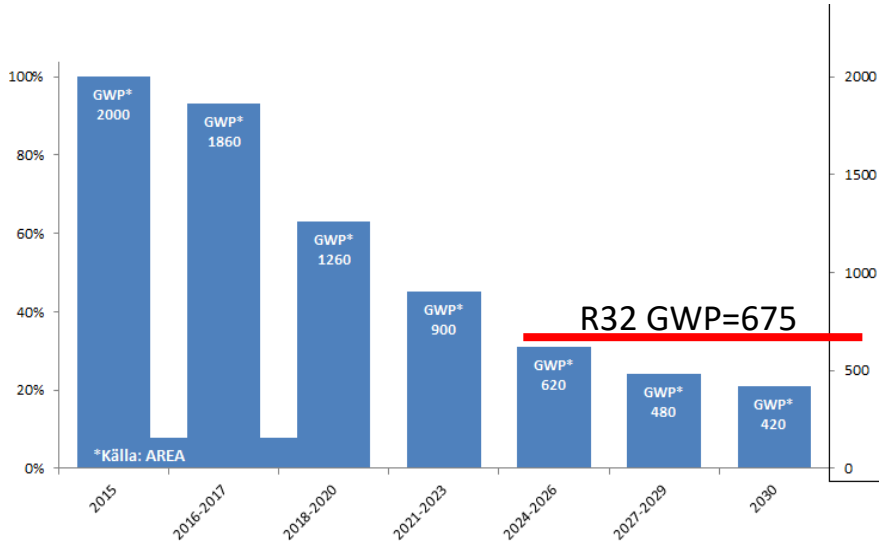

Figure 2. EU phase out schedule of high GWP refrigerants

In parallel with the transfer towards R32 there has been an increasing number of units using R290 (propane) in Asia. For example, hundreds of thousands of R290 units have been placed on the Indian market. These units typically have a charge of more than 300 gram propane. In western countries this can not be accepted due to the high flammability of propane.

According to the standard EN 378 it is recommended to have a total charge of less than 150 gram of Ashrae flammability class A3 (most flammable class) refrigerants (like propane) to avoid aggravating complications in terms of size of room, location in and/or ventilation of the space of installation. Less than 150 gram of charge thus make a huge simplification since most potential hazardous situations then can be taken care of within the system boundaries. An example how to do this is given in IEC60335-2-40. The supplier of such a system can pay less attention to how the system is installed, similar as for a household refrigerator using less than 150 gram isobutane (R600a).

Another, new group of synthetic, fluorinated hydrocarbon refrigerants with very low GWP is the HFO:s. They differs from the HFC:s by having a double bound between carbon atoms in the molecule. This makes them unstable when released into the atmosphere why they quickly decompose to substances with low GWP. The problem is that the resulting substances formed are so called “Fore ever chemicals” with very long life time and they are questioned for their environmental impact.

A way, for once and for all, to avoid synthetic refrigerants and related environmental concerns and ensure safety is to use less than 150 gram of natural but flammable refrigerant, like propane. Beside the low density, propane has shown to be a good refrigerant in many aspects. (Pavel, 2014). Reducing refrigerant charge will be important for most systems (IIR 25th info. note, 2014). Smaller charge comes with smaller internal volumes and corresponding smaller size of components. Using less material is both cost efficient and good for the environment.

The focus in this project has therefore been to study techniques for lowering the refrigerant charge whilst maintaining minimum required efficiency according to standards. A benchmark investigation at the beginning of the project set the project target to 3.5 kW cooling capacity, COP_2=3.5 at 15 m^3/min indoor air flow and 30 m^3/min outdoor air flow. The air flow limits are set by Electrolux expertise based on their experience of when acceptable noise levels can be reached. The question was if these numbers could be reached with 150 gram propane as refrigerant. This project is based on experiences from earlier studies at the Royal Institute of Technology (Fernando et al, 2008) and a study of ground source heat pump with minimum charge of propane (Andersson, 2018). This time the same approach was applied on a split air conditioner.

2 Project team

Project manager

Klas Andersson, Klas Andersson Engineering

Partners

Granryd Consulting

Senior, authority in the field of refrigeration. A facilitator of all good that comes out of the project and a preventer of too many too large mistakes. Representative: Professor Emeritus Eric Granryd

Electrolux

Sales and manufacturers AC globally. Supports the project with refrigeration expertise, test laboratory facilities, benchmark input and market knowledge. Representatives: Ph.D. Mazyar Karampour and Arturas Daugela

SANDEN Delivering Excellence

Leading, global manufacturer of compressors for electric vehicles. Supports with novel knowledge about compressor characteristics with propane, lubricant considerations (in cooperation with Shrieve) and operation advice. Representative: Ph.D. Paul Bouteiller

Lundahl

Responsible for the development of the control and measurement system “PropacControl”.
Representative: Gunilla Lundahl

SANHUA

Global supplier of refrigeration accessories. Supports the project with system components and advise how to use them. Provides standard and new developments of heat exchangers and related theoretical analysis. Representatives: Izzet Eskinazi and Yuriy Solyak

ebmpapst

Global manufacturer of fans. Provides fans, built in assemblies and fan control support. Gives expert advice for optimal fan-heat exchanger adoption. Representative: Erik Brisenheim

Manufacturer of special aluminum sheets, with integrated solder and flux, for heat exchanger manufacturing and brazing. Advises in new heat exchanger developments. Provides heat exchanger prototypes made in state of the art brazing laboratory.
Representative: Ph.D. Claudi Martin Callizo

Department of Energy Technology, Division of Applied Thermodynamics and Refrigeration. Leading academic research institute in the field of micro channel heat transfer and minimum charge of natural refrigerants. Supports the project with academic input within the field. Representative: Professor Björn Palm

Provides the project with refrigerant and soldering equipment. Supports in brazing with open flame for prototyping.
Representatives: Niclas Andersson and Helge Koponen

3 The System

3.1 Overview

A number of different versions of the system were built throughout the project. The basic system layout was the same as illustrated in Figure 3, including measurement positions. One version had no filter-dryer (orange in Figure 3). One set of fans had a nozzle with a given K-factor from which the air flow was calculated from the measured pressure drop over the nozzle (Δp-flow). An internal heat exchanger between the suction gas and liquid line was used (Heat in Figure 3).

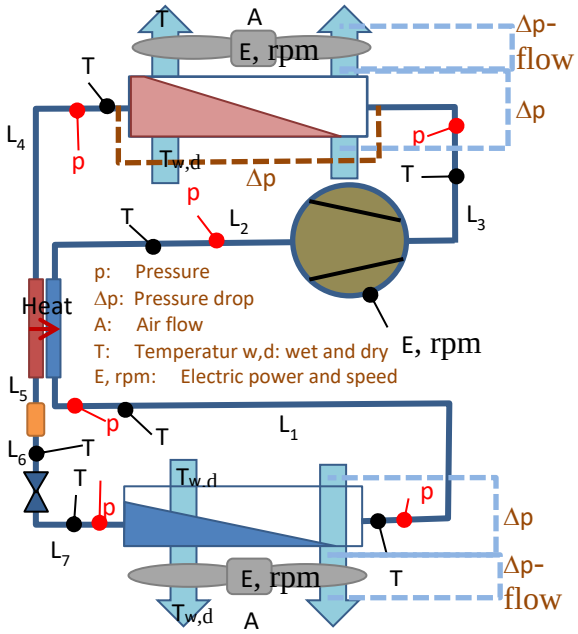

Figure 3. Propac system with measurement positions

The systems were built and initially tested and tuned at the facility of Klas Andersson Engineering (KAE). The facility did not hold laboratory quality in terms of measurement accuracy of the cooling capacity. When reasonable, approximate performance was reached the system was moved to the Electrolux test laboratory in Stockholm for more accurate measurements. The Electrolux facility also provided test chambers where accurate air inlet states could be set.

This chapter describes the different versions of components used in in the project. At the end three main versions of the system denominated Propac #1, #2 and #3, for which the most interesting results were achieved at the Electrolux laboratory are defined.

3.2 Expansion device

The expansion valves and related sensors and control unit was from Sanhua according to Table 2 and Figure 4.

Table 2.

Expansion valve	DPF(T01) 1.3C-07
Control unit	SEC606-R4 with RS485 communication bus
Pressure sensor	YCQC02L18
Temperature sensor	TP-C5

Figure 4. Expansion device

The dimensions of the valve and corresponding total charge are given in Table 3.

Table 3. Expansion valve dimensions

F [mm]	78
G [mm]	36
H [mm]	30
ϕM [mm]	6,35
Total charge [g]	0.7

The expansion valve was controlled by PropacControl via the RS485 communication bus. The valve open ratio could be set from 0-100% open in 500 steps.

3.3 Connection lines

In Tables 4 and 5 the dimensions of the connection tubes related to the labeling in Figure 3, used in the test rigs are given. There are also calculated pressure drop, expressed as saturated temperature difference and calculated refrigerant hold up at conditions given at the bottom of the tables. As a consequence of short tube length, heat is conducted from adjacent components, influencing the temperatures measured. In order to somewhat reduce that problem, stainless steel tubes were used for line L_4 and L_6 shown in Figure 41. The lines L_1 and L_7 are discussed separately below.

Table 4. Connection lines Propac #1 & #2

	Di mm	Length m	$\Delta T_{sat}(\Delta p_{sat})$ °C	Charge gram
L_2	11	1.2	0.06	1.5
L_3	7.83	1.6	0.1	2.1
L_4	3.0	0,20	0.11	0.7
L_5	4.65	0.10	0.01	0.8
L_6	3.0	0.20	0.11	0.7
Q2=3.5kW T1sat=43°C T2sat=10°C				

Table 5. Connection lines Propac #3

	Di mm	Length m	$\Delta T_{sat}(\Delta p_{sat})$ °C	Charge gram
L_2	11	0.9	0.04	1.2
L_3	7.83	1.2	0.09	2.0
L_4	3.0	0,2	0.11	0.7
$L_5 + L_6$	3	0.2	0.01	0.8
Q2=3.5kW T1sat=43°C T2sat=10°C				

Figure 5. Stainless steel lines Connection lines L_4 (left) and L_6 in Propac #1 and 2#

3.3.1 L_1 Suction line- Evaporator to Indoor unit

A flexible type of refrigeration hose from fastpipe was used as connection line from the evaporator outlet to the outdoor unit (line L_1 in Figure 3). A fastpipe hose with inner diameter 8.4 mm (denominated 3/8”), 3.0 m long was used in prototype #1. In prototype 2 and 3, a fastpipe hose with inner diameter 10.5 mm (denominated 1/2”) and length 6 m was used. It should be noted that the diameter denomination for fastpipe hoses is different from standard copper tubes. A fastpipe hose is illustrated in Figure 6. The calculated pressure drop, expressed as lowering of the saturation temperature, and charge for these hoses are given in Table 6. The last line in Table 6 is for Propac #3 assuming a vapor quality of 0.9 at the suction line inlet (evaporator outlet). The reason for this is discussed in the result chapter for Propac #3. It is assumed that the liquid-vapor mixture is homogenous.

Figure 6. Fastpipe hose

Table 6. Suction line L_1

Prototype	Di mm	Length m	ΔT_{sat} K	Charge gram
#1	8.4	3	0.48	2.2
#2 and #3	10.5	6	0.33	7.0
#3 inlet quality 0.9	10.5	6	0.38	7.8
Q2=3.5kW T1sat=43°C T2sat=10°C				

The dimensions are a compromise between marked need for installation length, pressure drop and refrigerant charge. The charge and pressure drop, expressed as the lowering of the saturation temperature, ΔT_{sat}, as function of the length for different tube diameters are given in Figure 7. The calculation assumes superheated vapor without any liquid. This is a somewhat unrealistic simplification. Some maldistribution in the evaporator is inevitable with so many parallel channels why a mixture of liquid and superheated vapor leaves the evaporator (unless the superheat is high, >10 K). Especially for the ½"-fastpipe suction line (inner diameter 10.5 mm), with low velocities, liquid pools can be formed and captured which increases the charge considerably. Similar pools of circulating oil make the charge estimate even more complicated. For a low charge system, the importance of the good old practice, to have a continuous decline of the suction line, is very important, both for charge and lubrication reasons.

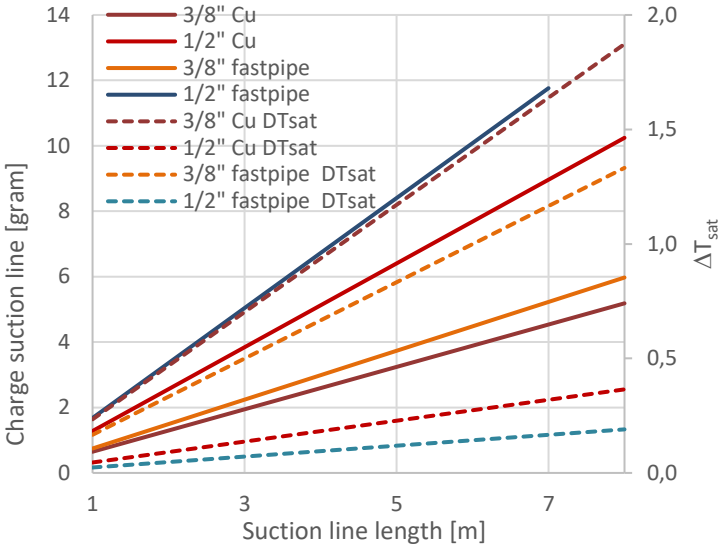

Figure 7. Suction line charge and ΔT_{sat}. T_1= 43°C, T_2= 10°C, Q_2=3.5 kW, internal hex efficiency=0.4, 4 K superheat and 3 K subcooling. 3/8" Cu⇔d_i=7.83 mm, 1/2" Cu ⇔d_i=11mm, 3/8" fastpipe⇔d_i=8.4 mm, 1/2" fastpipe⇔d_i=10.5 mm.

3.3.2 L_7 Two-phase line- Expansion Valve to Evaporator

A fastpipe hose with inner diameter 5.2 mm (denominated ¼") was used as two-phase line, line L_7 in Figure 3. Again, fastpipe diameter denomination is confusing. A large pressure drop limits the operation range of the expansion valve and the refrigerant mass flow, i.e. the system maximum capacity. One way to express this is to calculate the fraction of p_1-p_2 remaining over the expansion valve. An example of charge and remaining pressure drop over the expansion valve for different line alternatives is given in Figure 8. The charge is estimated by stepwise calculation along its length, taking the pressure drop and corresponding increase of the vapor fraction into account (in a similar way as for capillary tube calculations). The calculation was iteratively balanced with the pressure drop over the expansion valve. A complication is the added pressure drop over the distributer which is difficult to calculate. A homogenous mixture of liquid and vapor is assumed in this line. The result for the lines used in the different Propac versions is summarized in Table 7.

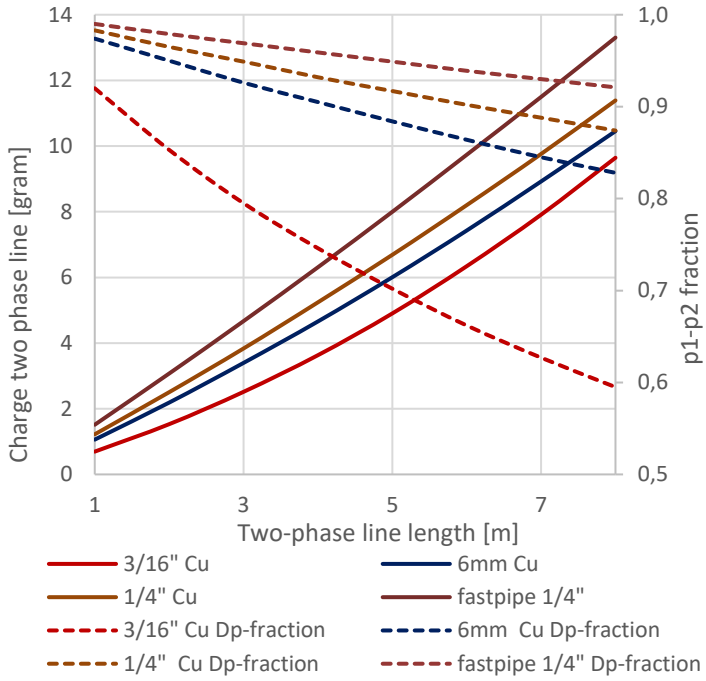

Figure 8. Two-phase line charge and Δp fraction. T_1= 43°C, T_2= 10°C, Q_2=3.5 kW, internal hex efficiency=0.4, 4 K superheat and 4 K subcooling. 3/16"⇔d_i=3.34 mm, 6mm⇔d_i=4.3 mm, 1/4"⇔d_i=4.65 mm, 1/4" fastpipe⇔d_i=5.2 mm.

Table 7. Two-phase lines L_7

Propac	Di mm	Length m	Expansion valve Δp fraction	Charge gram
#1	5.2	3	0.97	4.8
#2 and #3	5.2	6	0.94	10.0
Q2=3.5kW T1sat=43°C T2sat=10°C				

3.4 Internal heat exchanger

In the internal heat exchanger, the cold gas coming from the evaporator is heated by the warm liquid coming from the condenser. The correspondingly lowered liquid temperature reduces the refrigerant enthalpy at the evaporator inlet, experienced as lower vapor quality. The cooling capacity increases in proportion. The temperature increase of the suction gas reduces vapor density at the compressor inlet why the mass flow and cooling capacity is reduced. The net effect on the cooling capacity can be positive or negative depending on the properties of the refrigerant. For propane the net effect for an ideal (no pressure drop or other losses) system is positive with about 0.11%/K superheat.

Increased suction gas temperature increases the compressor work why also the net effect on COP_2 can be either positive or negative. For propane it is positive by about 0.07%/K superheat for an ideal system. For R32 both cooling capacity and COP_2 decreases with approximately 0.2%/K superheat. Increased superheat also increases the discharge temperature after the compressor. For propane this is a minor problem, even if an internal heat exchanger is used whiles it for R32 would be a major problem. This is further discussed in the Refrigerant comparison chapter.

The internal heat exchanger adds charge and pressure drop. For a minimum charge system it is a tricky balance with performance.

3.4.1 System control

An important improvement with external heat exchanger comes from drying the wet vapor after the evaporator before the compressor inlet. This gives an extra safety margin for a small charge system like Propac, with a large refrigerant mass flow (about 12 g/s) in relation to the total charge (<150 g). Maldistribution occurs quickly. The internal heat exchanger reconnects evaporator conditions to the condensed liquid before the expansion valve by extra subcooling. Extra subcooling reduces the pressure drop over the expansion valve why the mass flow increases. This requires a different control strategy for the expansion valve to avoid oscillations.

3.4.2 Evaporator performance

The use of an internal heat exchanger allows less superheat in the evaporator which increases its performance. Heat transfer is improved and pressure drop is reduced. Especially with many parallel channels in the evaporator, where even distribution is a challenge, one benefits from low superheat. Unevaporated liquid, without an internal heat exchanger, gives a proportional decrease of the system performance.

3.4.3 Compressor

Even though a superheat is measured there is always some droplets left which dissolves in the oil and makes optimum lubrication and oil circulation in the system more difficult to maintain. Large superheat increases compressor life. Increased temperature of the suction gas increases the compressor and oil temperature. This reduces the amount of refrigerant dissolved in the oil and somewhat reduces the vapor density which to some extend make up for the extra charge hold up by the internal heat exchanger. Compared to no superheat, the isentropic efficiency of compressors generally increases with superheat.

3.4.4 The internal heat exchanger in Propac

The internal heat exchanger was made by pressing copper tubes into a flat shape and solder them together, including connections as illustrated in Figure 9.

Figure 9. Internal heat exchanger in Propac

A disadvantage is the 90° turn from the connections into the flat vapor channels where uneven distribution of oil and refrigerant mist occurs.

The dimensions and calculated theoretical characteristics are given in Tables 8 and 9 where the temperature effectiveness is

$$\eta_{T,eff} = \frac{T_{gas,out} - T_{gas,in}}{T_{liq,in} - T_{gas,in}}$$

The characteristics are calculated at the conditions given in the tables. The measured effectiveness was considerably lower than the theoretical. The thermal contact in-between the gas and suction tubes might not be as good as assumed in the calculation due to uneven wetting of the solder during brazing. Another explanation is maldistribution and blocking oil. A temperature effectiveness of no better than 0.4 was achieved during the tests.

Table 8.

Q_2=3.5 kW T_1=43°C T_2=10°C ΔT_{sup}=4K ΔT_{sub}=4K	Vapor side	Liquid side
Charge hold up [g]	1.0	4,1
Pressure drop [Pa]	1200	6700
Temp. effectiveness	0.58	
Arrangement	counterflow	

Table 9.

	Vapor side	Liquid side
Height [mm]	1.2	0.6
Width [mm]	10	10
Length [mm]	300	260
Number of channels	16	3
Connection diameter [mm]	11	4.65

The heat balance over the internal heat exchanger was used to calculate the vapor quality (mass fraction in vapor phase) at the evaporator outlet.

In prototypes #1 and #2 the internal heat exchanger was oriented with the connection lines in vertical direction. In prototype 3 it was laying flat with the connection in horizontal direction. This is illustrated in Figure 10.

When dissembling the system, it was noticed that quite some oil was accumulated in the vapor headers of the heat exchanger, especially the inlet header. One then has to assume that also liquid pools of refrigerant can be trapped at the same place during operation.

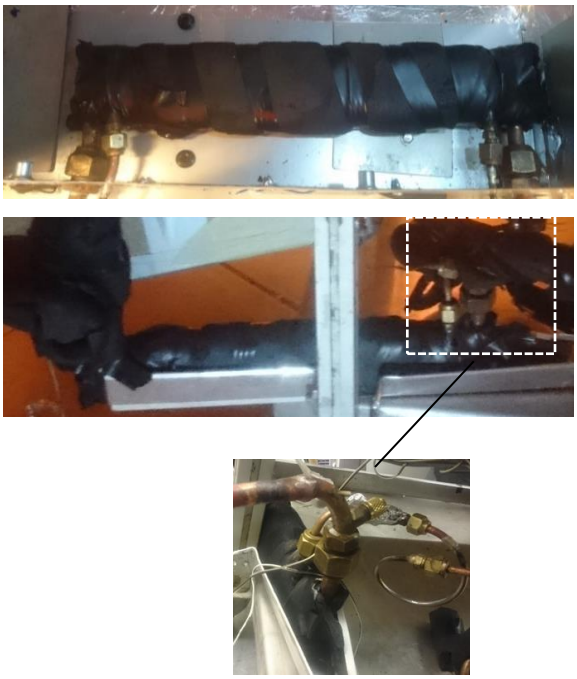

Figure 10. Internal heat exchanger orientation. Horizontal in Propac #3 (top) and vertical in Propac #1 and #2 (lower).

3.4.5 Internal heat exchanger development

A new type of internal heat exchanger was developed during the project. It was developed in cooperation with Gränges and the team running the Ecopac* project at the Royal Institute of Technology in Stockholm, studying a high temperature heat pump with R600a. The main objective with this development was to demonstrate a more commercial and industrial feasible technique than the internal heat exchanger described above. It was also an attempt to take a step forward in terms of performance in relation to refrigerant charge. The prototype is shown in Figure 11. Unfortunately, the first working prototype (after many attempts) was completed at the very end of this project, with no time to introduce it in the Propac prototype. Its performance could though be confirmed by measurements with water on the liquid side and air at the vapor side.

Figure 11. New internal heat exchanger

* The Ecopac project studies a minimum charge heat pump with isobutane as refrigerant aimed for small temperature lift from high evaporating temperatures, typically 20°C.

3.5 Compressor

The compressor, shown in Figure 12, is a semi hermetic Sanden SHS33 scroll type with permanent magnet DC motor. The inverter drive and control electronics are integrated within the compressor and the motor is cooled by the suction gas. It has sealed ball bearings with permanent lubrication. The oil is mainly for sealing and lubrication of the scroll wheel. It is developed for climatization in electric vehicles with R134a or R1234yf as refrigerant. It is controlled and read from with the LIN-bus communication protocol with PropacControl.

The required lifetime in vehicle AC-applications is normally much shorter than for residential air conditioners. Another issue is the O-ring sealed connections that might be a problem in terms of approvals of a “hermetic” system with flammable refrigerant. In cooperation with Shievre, Sanden has made life span tests to find suitable oils with propane. One such oil candidate was provided for the project. Sanden has supported serval research projects with natural refrigerants and has developed technique for a stationary version for use with natural refrigerants. Some characteristics are given in Table 10. The total amount of oil in the system was approximately 120 ml.

This compressor is a major utilizer of the project target by its small interior volumes and small oil charge.

Table 10. Compressor characteristics

Swept volume [cm^3/turn]	33
Speed range [rpm]	800-8500
Suction side volume [cm^3]	500
Discharge side volume [cm^3]	260
Oil charge [cm^3]	120
Oil type	PAG II
Weight [kg]	6.85
Charge Suction/Discharge/Oil [g]	4.9/7.1/5.8

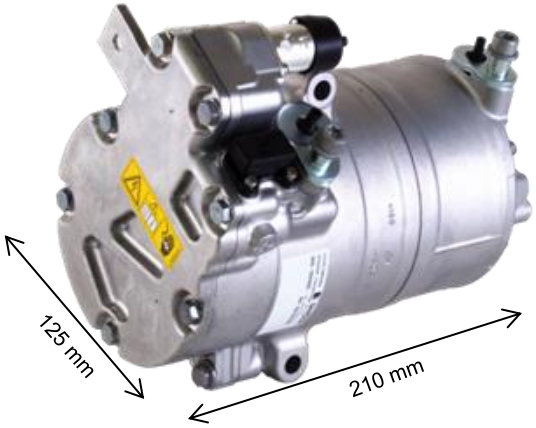

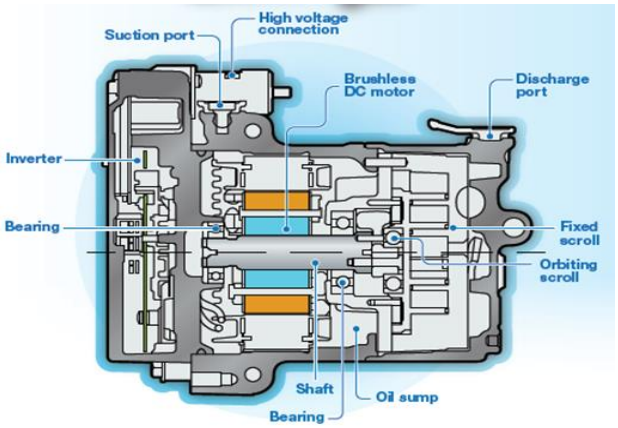

Figure 12. Sanden SHS33 compressor

3.6 Filter/Dryer

A rebuilt household type filter/dryer with reduced internal voids was used in Propac #1 and #2. The filter/dryer and its assembly are illustrated in Figure 13. The refrigerant charge is estimated to be 2.5 gram. In Propac #3 there was no filter/dryer.

Figure 13. Filter/dryer used in Propac #1 and #2.

3.7 Fans

ebmpapst provided the project with fans that were selected to fit the heat exchangers and supported with calculations on fan performance and specifications of Modbus communication used by PropacControl. They also provided fan-heat exchanger assembly units. A benchmark study set the nominal flows at which the project target should be reached to maximum 15 m^3/min (900 m^3/h) for evaporator air flow and 30 m^3/min (1800 m^3/h) for the condenser air flow.

3.7.1 Fans in Propac #1

The condenser (ebmpapst K3G280-PR04-I2) and evaporator (ebmpapst K3G250-PR04-H2) fan and inlet nozzle units in are shown in Figure 14. These fans were selected for test purposes to ensure sufficient air flow for any prototype arrangement despite the pressure drop and was not intended to be the most efficient. The inlet nozzles had a pressure connection (marked with arrows in Figure 14) for air flow calculation from a given K-factor with an equation on the form $Flow \sim K \cdot \Delta p^{0.5}$,

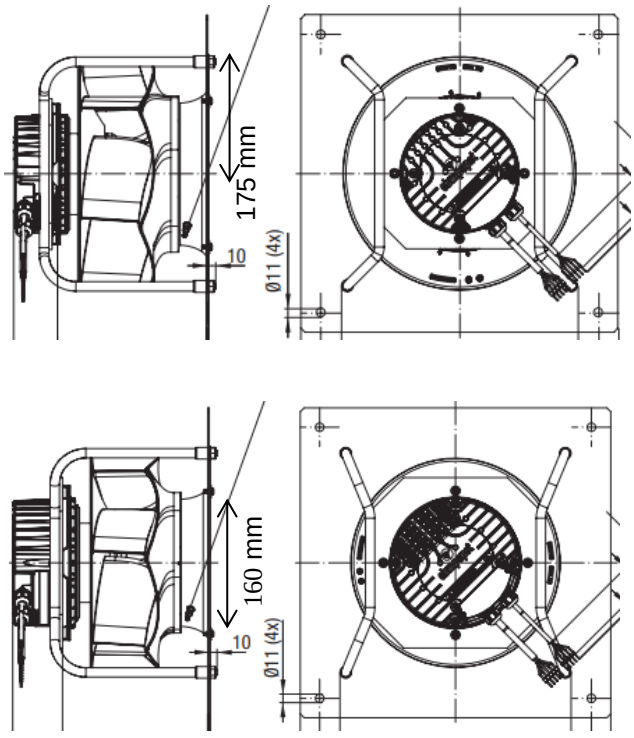

Figure 14. Condenser (top) and evaporator fan (lower) in prototype #1.

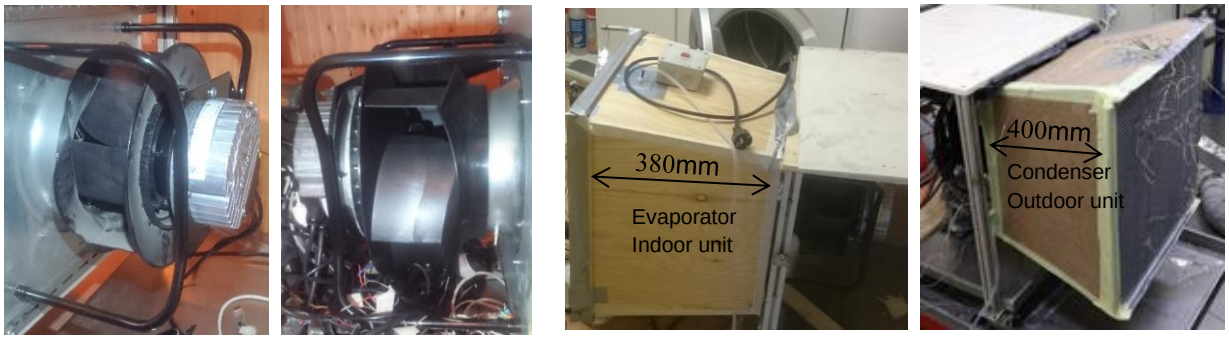

Figure 15. Mounting of radial fans in the prototype with conic ducts to the evaporator and condenser. The evaporator and condenser active flow dimensions were 500x495 mm.

where Δp is the pressure drop over the inlet nozzle. The fan units were assembled with a conic duct with the evaporator and condenser as illustrated in Figure 15. At the tests at Electrolux this arrangement was used for the condenser with fan but the evaporator fan was replaced with the fan integrated in Electrolux test system.

3.7.2 Fans in Propac #2

In Propac #2 the condenser fan and assembly were unchanged compared to Propac #1. A new evaporator (rebuilt SD12 described in the evaporator chapter) was introduced and also a new fan and fan assembly unit. The model was ebmpapst axial fan W3G350CA5801 shown in Figure 16 . Figure 17 shows the fan characteristics.

Figure 18 shows the fan and evaporator assembly with the distance from the evaporator outlet to the fan inlet (left) and the active evaporator flow dimensions (right).

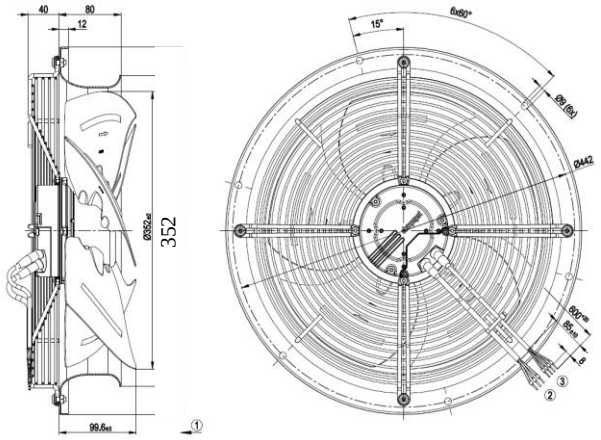

Figure 16. Axial fan W3G350CA5801

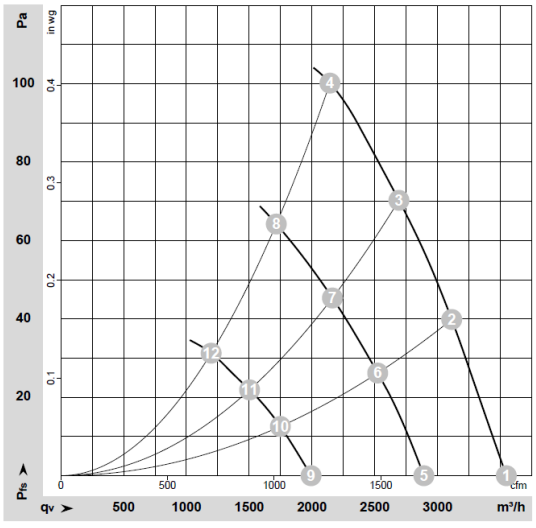

Figure 17. W3G350CA5801 characteristics

Figure 18. Axial fan and evaporator SD12 assembly in prototype #2.

3.7.3 Fans in Propac #3

In Propac #3 the radial condenser fan was replaced with the same axial fan as used for the evaporator. The condenser was the same but with a new fan assembly illustrated in Figure 19. The distance, condenser outlet – fan inlet, was 160 mm and the active condenser flow dimensions were 500x495 mm.

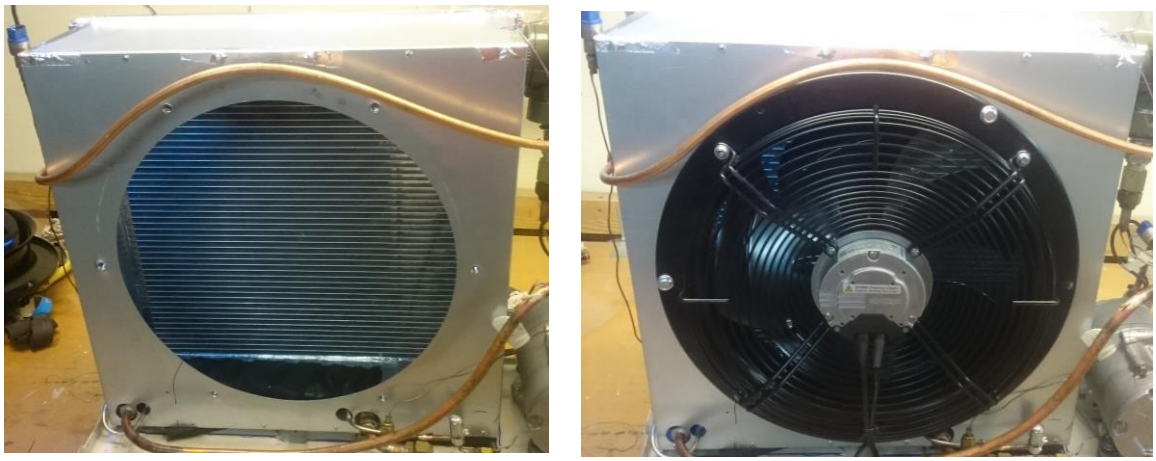

Figure 19. Axial fan and condenser SD13 assembly in Propac #3.

The evaporator fan was the same as in Propac #2 but the SD12 evaporator was replaced with the Z021 and a new assembly unit shown in Figure 20.

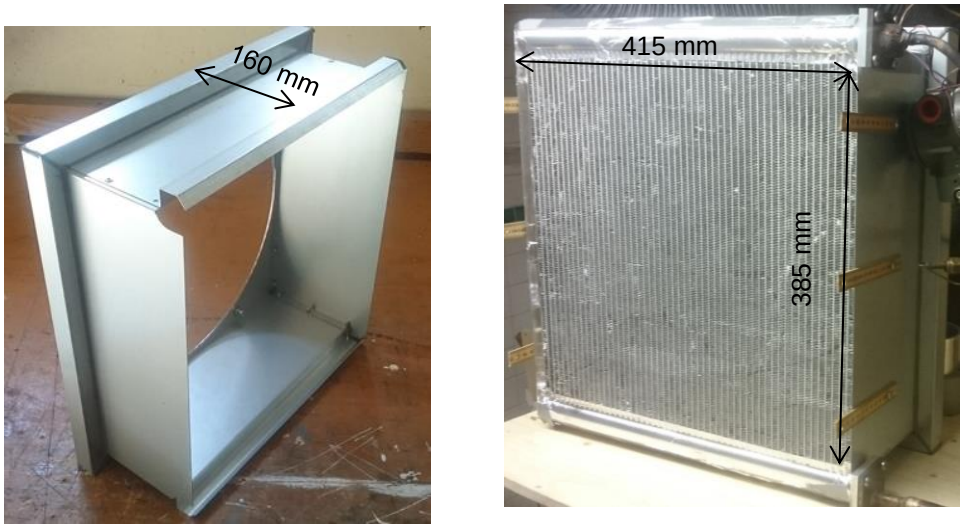

Figure 20. Evaporator Z021 fan assembly in Propac #3.

.

3.7.4 Fan - heat exchanger interaction

There were three different heat exchangers (described in condenser and evaporator chapters) used with the same axial fan, SD13 as evaporator and condenser, SD12 evaporator and Z021 evaporator. The measured load curves for these heat exchangers at dry conditions are illustrate in Figure 21. The corresponding fan power and fan efficiency is shown in Figure 22. When water condensates at the evaporator during operation at wet, humid conditions the pressure drop increases. Examples of how the pressure drop changes with water condensation are given in the Result chapter.

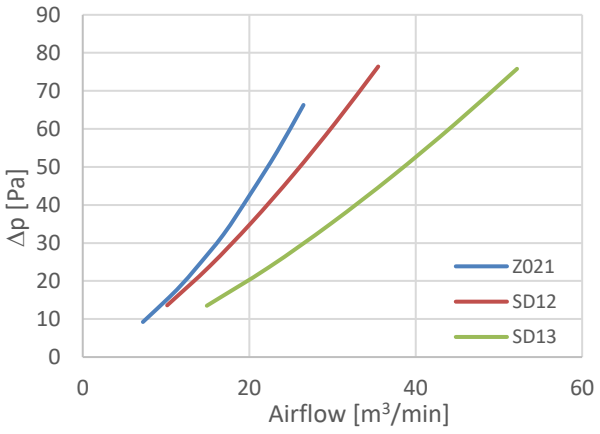

Figure 21. Load curves for the three heat exchangers at dry conditions.

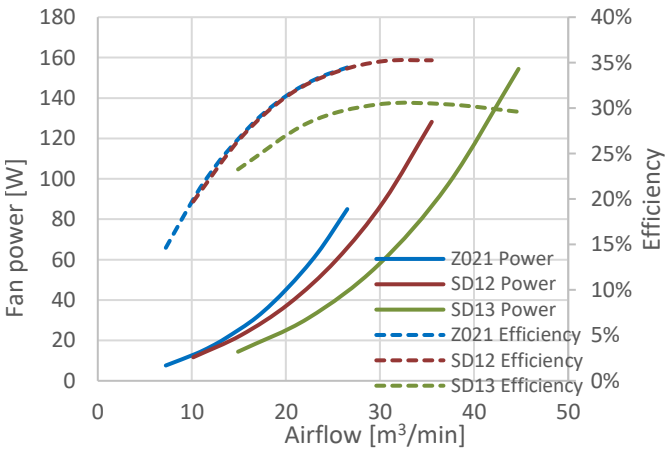

Figure 22. Fan power and efficiency for the axial fan operating with the three different heat exchangers at dry conditions.

3.8 Condenser

The condenser was a standard Sanhua microchannel model SD13 with two passes as illustrated in Figure 23. The geometry is given in Table 11. The total number of channels is 16·28 = 448 in the first pass and 16·24 = 384 in the second. Figure 24 shows the principle for how the header, tubes and fins are arranged. The tube and fin depth in direction of air flow is 16 mm.

The refrigerant outlet is about 10 mm above the bottom of the header (inner diameter 17 mm) representing an internal volume of 2.7 cm^3 holding about 1.2 gram of propane. To reduce this amount, a tube with 3.4 mm inner diameter was inserted through the outlet connection in a bend towards the bottom of the header as illustrated in Figure 25Figure 25. Sanhua condenser SD13 .

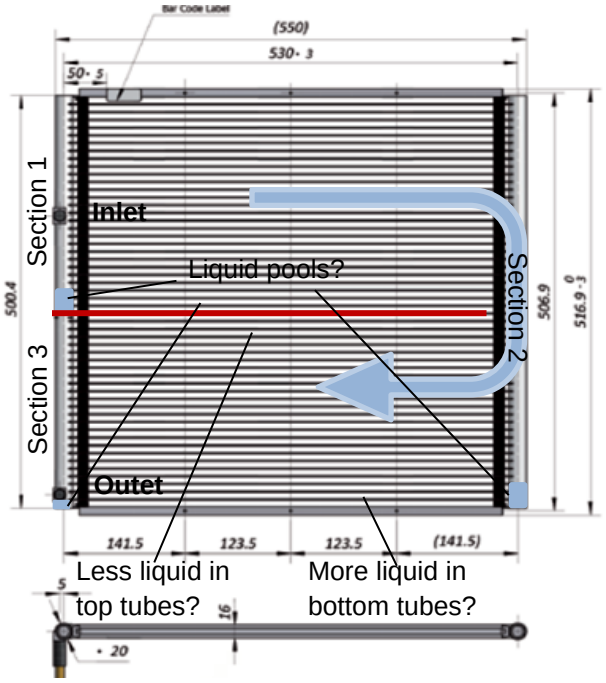

Figure 23. Sanhua condenser SD13

Table 11. Condenser SD13 geometry

Heat exchanging length [mm]	500
Heat exchanging height [mm]	495
Fin distance [mm]	1.1
Fin height [mm]	8.1
Fin depth [mm]	16
Tube height [mm]	1.3
Channels internal volume [cm^3]	197.8
Header internal volume [cm^3]	202.2
No. of flat tubes pass 1 / 2	28 /24
No. of channels in each tube	16
Channel dimensions [mm]	0.63 x 0.74

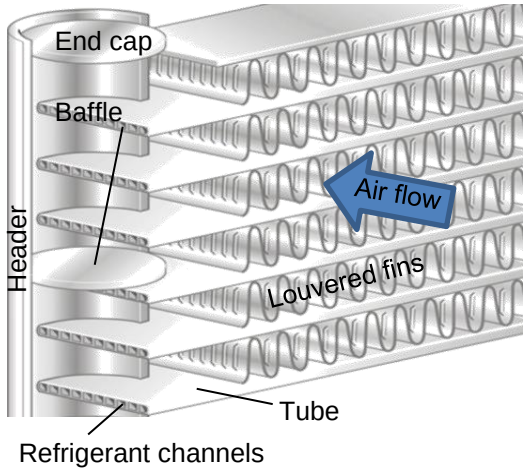

Figure 24. Sanhua microchannel condenser and evaporator principal arrangement.

This assumes that there is some vapor left at some of the tube outlets into the outlet Section 3 of the headers. Otherwise, the complete outlet Section 3 would be filled with liquid. It is hard to know how liquid and vapor refrigerant is distributed along the passage through the condenser and correspondingly difficult to calculate the charge. It might be that liquid is separated and falls down towards the bottom of the headers as indicated in Figure 23. Tubes at the bottom would then be filled with liquid and tubes at the top would have higher vapor

fraction. One can also assume a liquid film covering the inside of the headers and the tubes insertion in the headers. In the outlet Section 3, the velocities are low and at many of the channel outlets the refrigerant is subcooled liquid. This gives a high separated liquid fraction.

An estimate of the charge is made by assuming that a fraction of the total header volumes is filled with separated liquid and the rest has an assumed homogenous mixture vapor quality. The tube channels are assumed to have a vapor quality represented by the average of the adjacent header's quality. The result of such an estimate is given in Table 12. The total charge would then be 49 gram. The estimates for the different components are adopted to sum up with the total charge required in the prototypes. The purpose is to give a rough picture of a potential distribution of the refrigerant in the system.

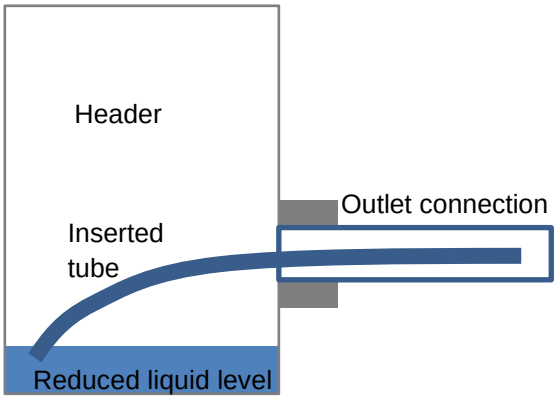

Figure 25. Sanhua condenser SD13 outlet arrangement.

Table 12. Estimated charge in the SD13 condenser

Header Section	Number of tubes	V_{header} [cm^3]	Liq sep fraction	m_{header} [gram]	Vapor Quality	V_{tubes} [cm^3]	m_{tubes} [gram]	m_{tot} [gram]
1	28	54.4	0.1	4.1	1	106.5	4.5	
2	24	101.1	0.2	14.3	0.5	91.3	9.1	
3		46.7	0.5	17.3	0.05			
Tot	52	202.2		35.6		197.8	13.6	49.2

3.9 Evaporator

Three different evaporators were used in the project. Each operated and rebuilt in different ways which is described in the following.

3.9.1 Evaporator 1 - SD13

The evaporator used in Propac #1 was a Sanhua SD13 condenser as described in the Condenser chapter but with the refrigerant flow in the opposite direction, with the inlet at the bottom and outlet at the top, as illustrated in Figure 26. Initially the SD13 was tested as evaporator with the headers vertically as in Figure 26. In that position, the drainage of condensate water from the fins was pore. Water blocked the air flow and reduced air side heat transfer. The evaporator was therefore turned 90°C with

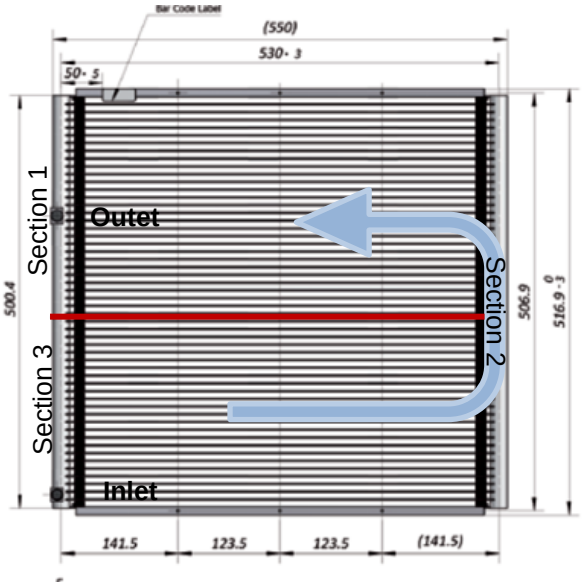

Figure 26. SD13 as evaporator

the inlet and outlet at the bottom as illustrated in Figure 27 which improved water drainage and heat transfer performance considerably.

This arrangement has a major drawback though, since liquid refrigerant most likely separates from the vapor in the second, top header Section 2, forming liquid pools in-between the tubes. In general, liquid separation must be assumed also in the inlet header Section 1. See Figure 27.

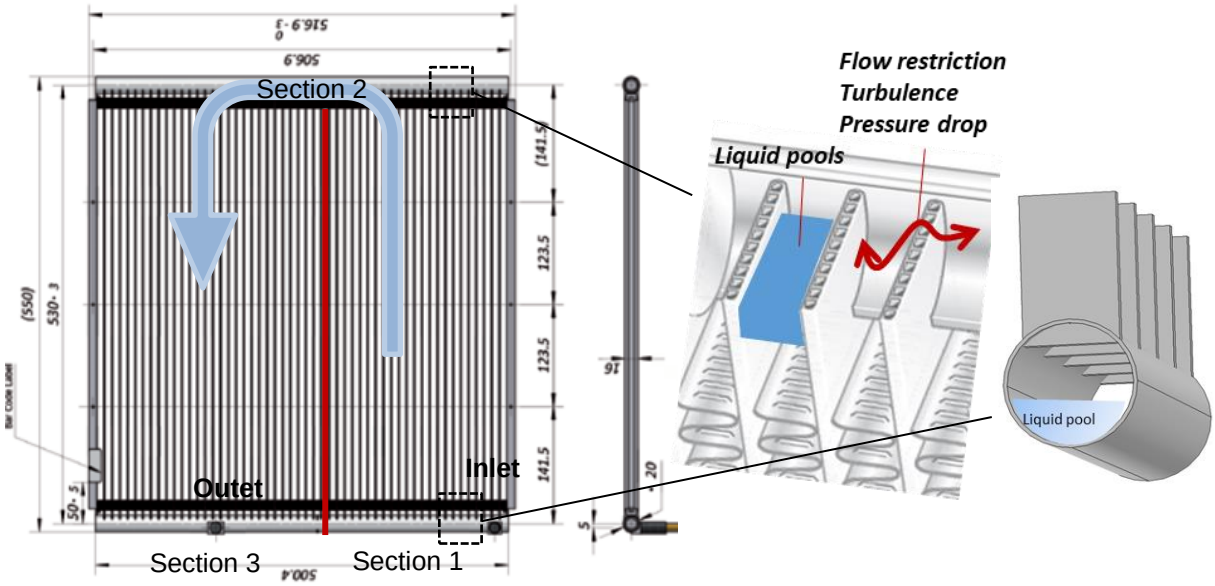

Figure 27. Liquid pools in SD13 used as evaporator

As for the condenser it is hard to know how the refrigerant is distributed. Liquid droplets could separate in any of the three header sections and form liquid pools. An estimate of the charge for the SD13 as evaporator with headers in horizontal position, made in a similar way as for the condenser is shown in Table 13. Here the separated liquid fraction of 0,4 is used. It assumes that liquid is filled up in level with tube height inside the header in Section 2 and to a similar height in Section 1 and 3 as illustrated in Figure 27. The tubes also cause turbulence, increasing pressure drop.

Table 13. Charge in the SD13 evaporator

Header Section	Number of tubes	V_{header} [cm^3]	Liq sep fraction	m_{header} [gram]	Vapor Quality	V_{coil} [cm^3]	m_{coil} [gram]	m_{tot} [gram]
1	28	54.4	0.4	13.2	0.2	106.5	3.5	
2	24	101.1	0.4	22.2	0.6	91.3	1.6	
3		46.7	0.4	10.0	1	0.0	0.0	
Tot	52	202.2		45.4		197.8	5.1	50.5

3.9.2 Evaporator 2 - Rebuilt Sanhua SD12

The evaporator in Propac #2 was based on the smaller Sanhua condenser model SD12. The dimensions are given in Figure 28 and Table 14. SD12 is more suitable in size for an indoor unit than SD13. For the same air flow as for SD13, the velocity would be increased for the SD12 in proportion to the area ratios. The air side heat transfer performance (hA-value) is therefore approximately the same. Originally it had four refrigerant passes, illustrated with the red lines in Figure 28. This is suitable for a condenser with decreasing vapor fraction along the passes with corresponding decrease of the refrigerant velocity. As evaporator the pressure drop would be too high. The baffles in the headers (see Figure 29), dividing them in to sections and directing the refrigerant flow into the respective passes, therefore had to be removed to get only one pass. One pass would give a reasonable combination of heat transfer and pressure drop. To avoid the risk for liquid pools in-between the tubes as discussed earlier, also the part of the tubes inserted into the header need to be removed. Both the baffles and the tubes were therefore cut, using wire sparking technique. For sparking, the header end caps were removed and a brass wire was introduced all along the header length. The wire is connected to high voltage in relation to the heat exchanger base material and sparks occur when the wire comes close to the base material. The sparks burn base material away as the wire is moved along the wanted pathway. The inside of the header before and after this operation is shown in Figure 30. About 1 mm of the tube was left to avoid to remove too much of the brazed joint. Both headers were sparked. The SD12 has 43 tubes, each with 16 channels, 0.63 x 0.74 mm in size. Screw connections with O-ring sealing and new endcaps were manufactured and brazed to both headers as illustrated in Figure 31. The screw connection facilitates easy exchange of different distributors. The original in- and outlet connections were blocked. The SD12 evaporator was tested with injection at the bottom and at the top as illustrated in Figure 32. By injecting the refrigerant at the top, a reduction of required charge was experienced, probably related to reduced amount of separated liquid at the inlet for top injection. An estimate of the charge for the respective injection alternatives is given in Table 14. A separated liquid fraction (by volume) of 0.05 is assumed to correspond to liquid between the remaining's of the sparked tubes and

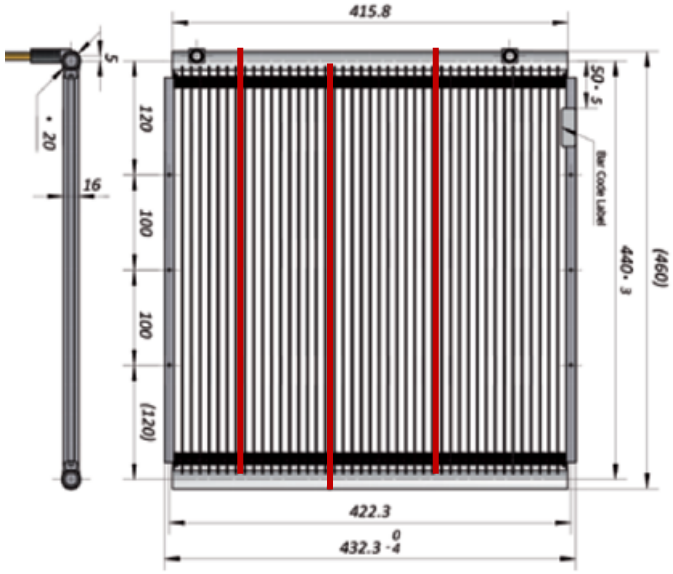

Figure 28. Rebuild SD12 to use as evaporator

0.02 to a smooth tube interior with only a thin liquid film at the bottom. Again, the real refrigerant distribution is unknown and the estimate is intended only as an illustration of the order–of-magnitude potential to reduce charge. It is evident that the main potential for charge reduction is in the headers.

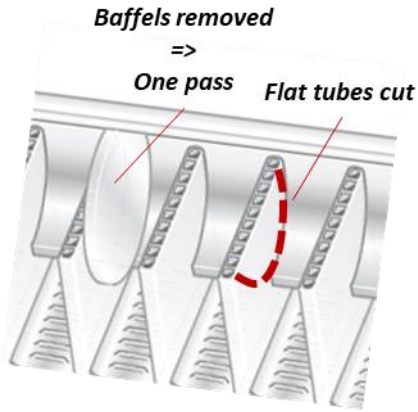

Figure 29. Removed baffles in SD12

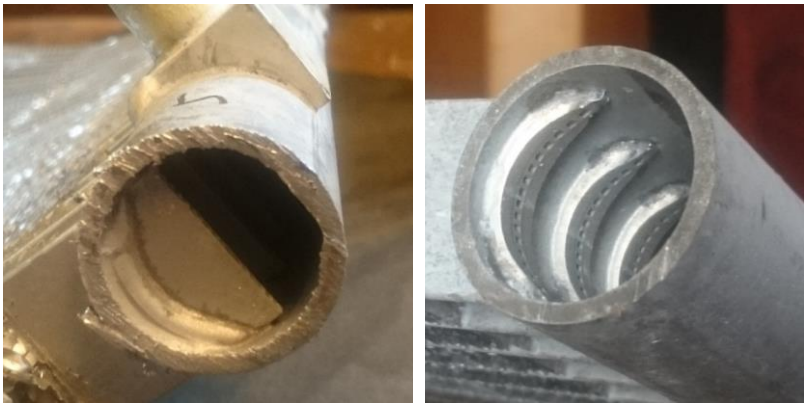

Figure 30. SD12 before and after sparking

Figure 31. New screw connections and endcaps

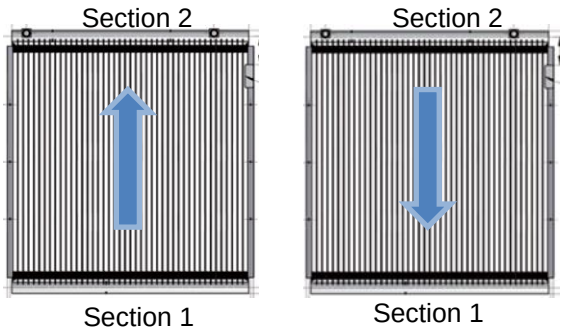

Figure 32. SD12 bottom and top injection.

The large charge for the bottom injection is related to an assumed liquid pool at the bottom inlet header and a corresponding but smaller amount of liquid between the remaining solder of the tube inserts at the top Section 2. With top injection the amount in Section 2 is approximately the same but the amount at the bottom outlet Section 1 is assumed to be much smaller. These assumptions are adopted to what was measured for Propac #2.

Table 14. Charge in rebuilt SD12 evaporator

Header Section	Number of tubes	V_{header} [cm^3]	Liq sep fraction	m_{header} [gram]	Vapor Quality	V_{tubes} [cm^3]	m_{tubes} [gram]	m_{tot} [gram]
Bottom injection								
1 bot	43	86.2	0.6	28.8	0.2	141.1	3.3	
2 top		86.2	0.4	18.5	0.95			
Tot	43	172.4		47.3		141.1	3.3	50.6
Top injection								
1 bot	43	86.2	0.15	7.7	0.95	141.1	3.3	
2 top		86.2	0.4	21	0.2			
Tot	43	172.4		28.7		141.1	3.3	32

3.9.3 Evaporator 3 - Sanhua evaporator prototype Z021

Sanhua provided a unique prototype evaporator, Z021, for the Propac project designed for the project target 3.5 kW cooling capacity at 15 m^3/min air flow at the condition 27°C and relative humidity 47%. The prototype included a refrigerant distributor inserted into the inlet header.

The evaporator dimensions are illustrated in Figure 33 and with geometry details given in Table 15. It has 52 tubes each with 20 channels, 0.74 x 0.675 mm in size. In total 1040 channels in parallel over one pass. The depth of the tubes and fins in direction of air flow were 20.6 mm compared to 16 mm for SD12 and SD13. The header inner diameter was 27 mm compared to 17 mm for SD12 and SD13.

The evaporator was first tested in its original version, without any changes. In that version the tubes were inserted into the headers as illustrated in Figure 29. During tests it was experienced that the evaporator held too much charge. It

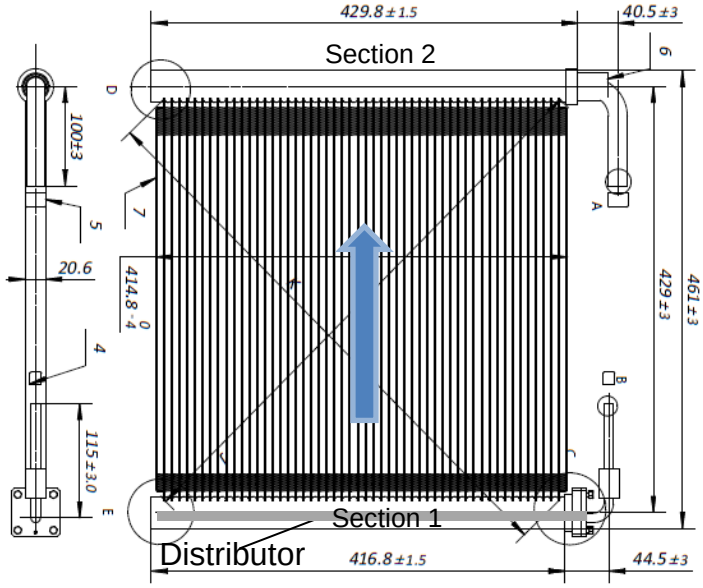

Figure 33. Z021 evaporator

Table 15.

Tube Geometry		Fin Geometry	
Tube Number	52	Fin Type	Louver Fin
Tube Length [mm]	398		
Tube Height [mm]	1.3	Fin Height [mm]	6.5
Tube Width [mm]	20.6	Fin Depth [mm]	20.6
Port Type	Rectangular	Fin Thickness [mm]	0.08
Port Num	20	Louver Count	12
Port Height [mm]	0.74	Louver Length [mm]	5.6
Port Width [mm]	0.675	Louver Angle [°]	45
		Louver Pitch [mm]	1.5

was therefore rebuilt in a similar way as the SD12, removing the tube insertion into the header and introducing O-ring connections as illustrated in Figure 30. This time the remaining tube/solder sticking in was about 0.5 mm.

The distributor, shown in Figure 34 has eight outlet holes oriented horizontally. The distributor was evaluated with air-water mixture as described in the Evaporator inlet distributor chapter. The main experience from the distributor test was that it worked quite well with the outlet holes horizontally but not very well in vertical position. Especially the last hole from the inlet was poorly fed in vertical direction upwards. All tests where therefore done with the distributor outlet holes in horizontal direction.

An estimate of the charge for the original Z021 with bottom injection and for Z021 with the insert of tubes removed and top injection is given in Table 16. Again, this is more or less a guess work adopted to what was measured in the protype.

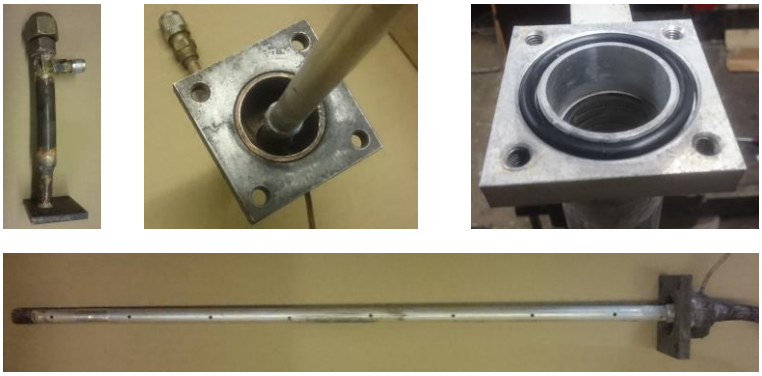

Figure 34. Z021 distributor and screw connection. Outlet (left), inlet (mid) and O-ring sealing (right).

Table 16. Charge in Z021 evaporator

Header Section	Number of tubes	V_{header} [cm^3]	Liq sep fraction	m_{header} [gram]	Vapor Quality	V_{tubes} [cm^3]	m_{tubes} [gram]	m_{tot} [gram]
Original, bottom injection								
1	52	207.6	0.3	41.4	0.2	207	4.9	
2		207.6	0.3	34.2	0.95			
Tot	52	415.2		75.6		207	4.9	80.5
Removed insert, top injection								
1	52	224	0.1	24.1	0.95	207	4.8	
2		224	0.1	14.5	0.2			
Tot	52	448		38.5		207	4.8	43.4

3.9.4 Evaporator charge considerations

The amount of liquid refrigerant that can be captured in the headers for a standard arrangement, with inlet at the bottom, of microchannel evaporator is illustrated in Figure 36. It is based on an assumed liquid level at the bottom of the header as illustrated in Figure 35, with dimensions from Table 17. The inlet case represents refrigerant inlet at the bottom where the tubes are inserted from above. At the top outlet case, the tubes are inserted from below and liquid pools are formed in-between the tubes. The assumed vapor fraction above the liquid, 0.2 at the inlet and 0.96 at the outlet, explains the charge difference for the same liquid level for the inlet and outlet header respectively.

Table 17. Example header dimensions

Header outer diameter [mm]	20	30
Header inner diameter [mm]	17	27
Header length [mm]	410	420
Tube width [mm]	16	20
Number of tubes	43	52

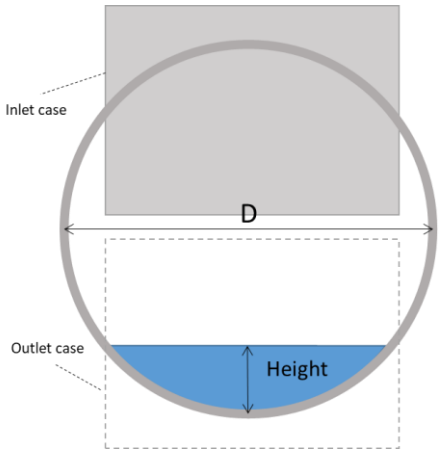

Figure 35. Liquid in bottom of header.

During operation it is likely to be quite turbulent and there are probably waves in the liquid why this calculation is a large simplification. Still, as an order of magnitude estimate, it illustrates that only a few millimeters capture quite some charge. 3 mm in the 30 mm headers capture 21 gram. For a Propac system this is devastating.

A summary of the estimated charges for the respective evaporators tested is given in Figure 37.

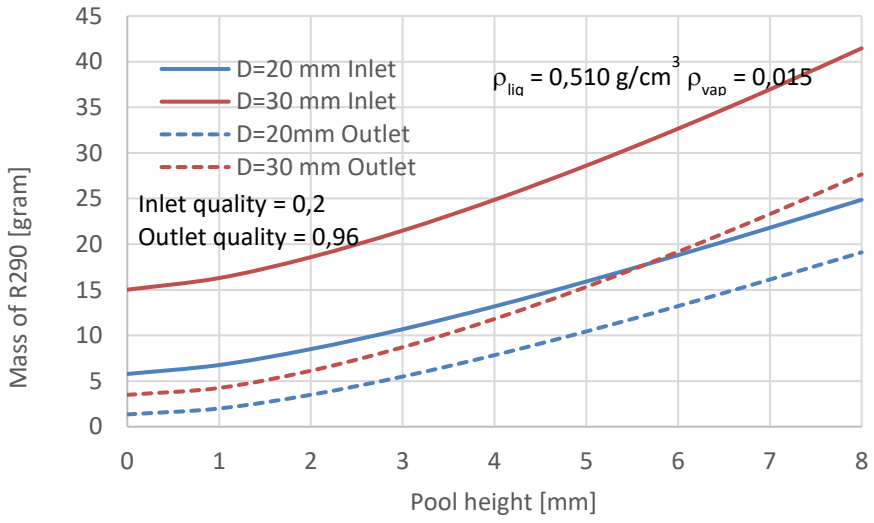

Figure 36. Estimated charges for different evaporators depending on liquid pool height

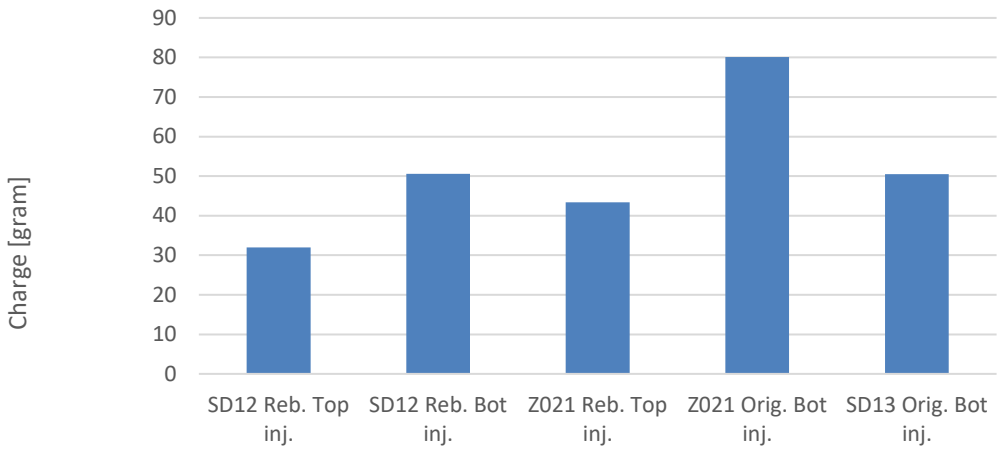

Figure 37. Estimated charges for tested evaporators

3.9.5 Evaporator inlet distributor

The evaporators tested in the Propac project have up to 1040 parallel refrigerant channels. It is of major importance and a great challenge to get the refrigerant evenly distributed over the channels. Maldistribution results in high superheat, related to low heat transfer and high pressure drop for channels poorly fed. In overfed channels the refrigerant is not fully evaporated, introducing liquid into the suction line which increases charge considerably. The liquid and superheated vapor at the evaporator outlet is not in thermodynamic equilibrium why superheat can be measured despite remaining liquid. In the Propac evaporators with bottom outlet, it seems like remaining liquid is separated from the vapor and pours out along the bottom of the outlet connection. It has been experienced that a sensor measuring the superheat in a pocket at the center of the outlet, measures a higher superheat than a sensor placed towards the outside bottom. See Figure 38. In the Propac system remaining liquid can be tracked from a heat balance over the internal heat exchanger. If pure liquid is ensured at the internal heat exchanger liquid side, missing heat at the gas side, from the heat given off from the liquid, can be assumed to relate to vaporization of remaining liquid. In this way the heat balance over the internal heat exchanger is an indicator of maldistribution in the evaporator. Another way to evaluate maldistribution is to measure the temperature distribution over the evaporator with infrared camera. A shortcoming with the IR-camera is that only the front channel in the tubes is visible. Channels further inwards are hidden and maldistribution in-between them can not be seen. The front temperature you see is though, probably an average of the distribution along the channels which depends on the conductivity in the tube walls in relation to the local air heat transfer.

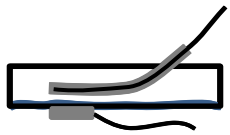

Figure 38. Different superheat measurement positions

A test was set up with pressurized water and air that were mixed before entering a distributor to be evaluated. The arrangement was very simple and neither the flow nor vapor fraction was measured. The density of water is twice of liquid propane. Vapor density and viscosity also differ. Flow regimes and separation phenomena can therefore be expected to differ a lot in this setup compared to the real conditions. Still, the air-water tests could be performed with a great variety of flows and vapor qualities. That gave at least a qualitative hint of what could not work. The tests also gave some interesting experience in how sensitive the distributor could be for changes of the flow and vapor quality. Also changing the orientation relative gravity could have a great impact on the distribution. A number of different distributors were evaluated. Two examples are shown in Figure 39. A Propac (top) and the Sanhua distributor (lower) evaluated with water-air mixture. for a case with relatively low vapor fraction and high flow. The lower picture shows the Sanhua distributor with higher vapor fraction and lower flow. The concept with one large tube with small holes along, was experienced to be sensitive to liquid separation. If the velocities are low (large diameter and low flow rate) the vapor fraction could differ a lot between outlets. Another observation was that the inlet distribution seemed to influence the outlet distribution. A straight inlet with assumed homogenous mixture could give a quite different result than the same conditions with a 90° turn close before the inlet, where more liquid could be assumed to be separated and forming a thicker film on the inside wall of the distributor.

The distributor adds quite some pressure drop that has to be considered together with the pressure drop over the two-phase line between the in- and outdoor units. This limits the operation range of the expansion valve. Depending on the distributor arrangement some extra charge can also be expected.

Figure 39. A Propac (top) and the Sanhua distributor (lower) evaluated with water-air mixture.

The first heat exchanger used as evaporator was the Sanhua SD13 which had no distributor. In the rebuilt SD12 evaporator the best sample from the evaluation described above was used. The Z021 was tested with the Sanhua distributor.

3.10 Propac versions

The component described in the previous chapters were put together in different versions of system. The main configurations are summarized in Table 18 and described in the following chapters.

Table 18. Main Propac prototyes

Propac	#1	#2	#3
Evaporator	Condenser SD13	SD12	Z021
Evaporator arrangement variants	Original with tube insert Two passes Horizontal headers Bottom inlet No distributor	Tube insert removed One pass Horizontal headers Top inlet Propac distributor	Tube insert removed One pass Horizontal headers Top inlet Sanhua distributor
Evaporator fan	Electrolux test site built-in fan	W3G350 axial type	W3G350 axial type
Condenser fan	K3G280 radial type	K3G280 radial type	W3G350 axial type
Indoor-Outdoor connection lines	3 m 8.4 / 5.2 mm	6 m 10.5 / 5.2 mm	6 m 10.5 / 5.2 mm
Filter / Dryer	After internal hex	After internal hex	No Filter/Dryer

3.10.1 Propac #1

Propac #1 had the SD13 as both condenser and evaporator. As condenser the headers were vertically oriented. As evaporator it was tested with the headers both vertical and horizontal. The in- and outdoor units were connected with 3 m long, flexible hoses approved for refrigerants. The inner diameter was 10.5 mm for the suction hose and 5.2 mm for the two-phase hose. The outdoor unit is shown in Figure 40 - Figure 42. The radial fan used at KAE with the evaporator was removed at tests at Electrolux where the built in fan was used.

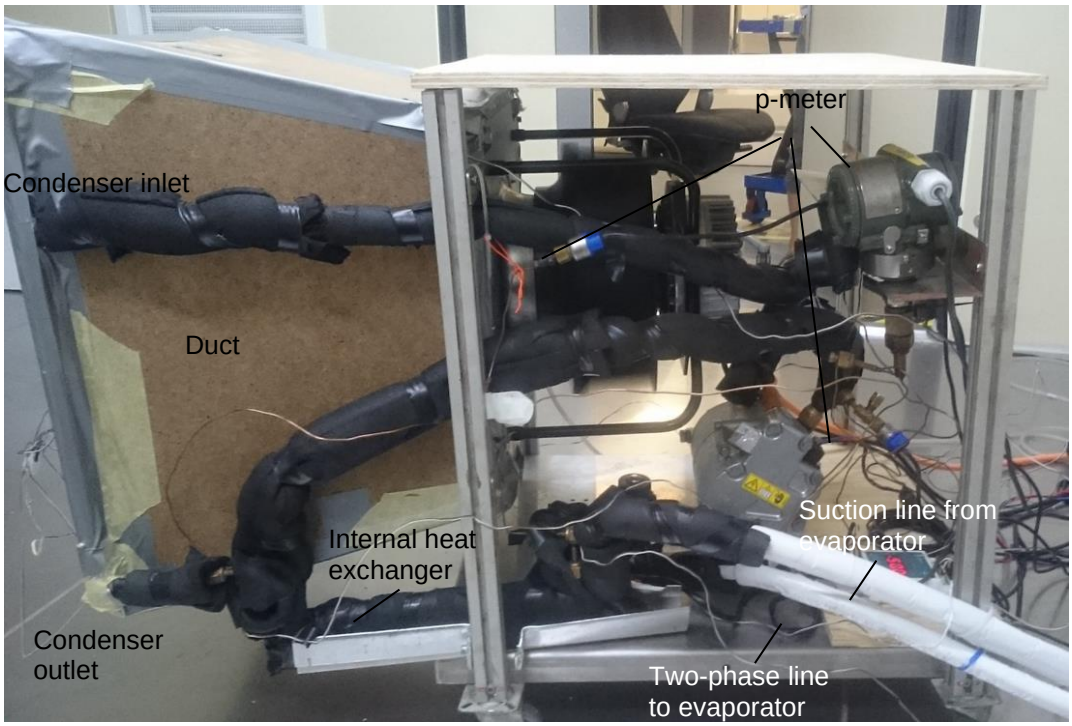

Figure 40. Propac #1. Outdoor unit left side

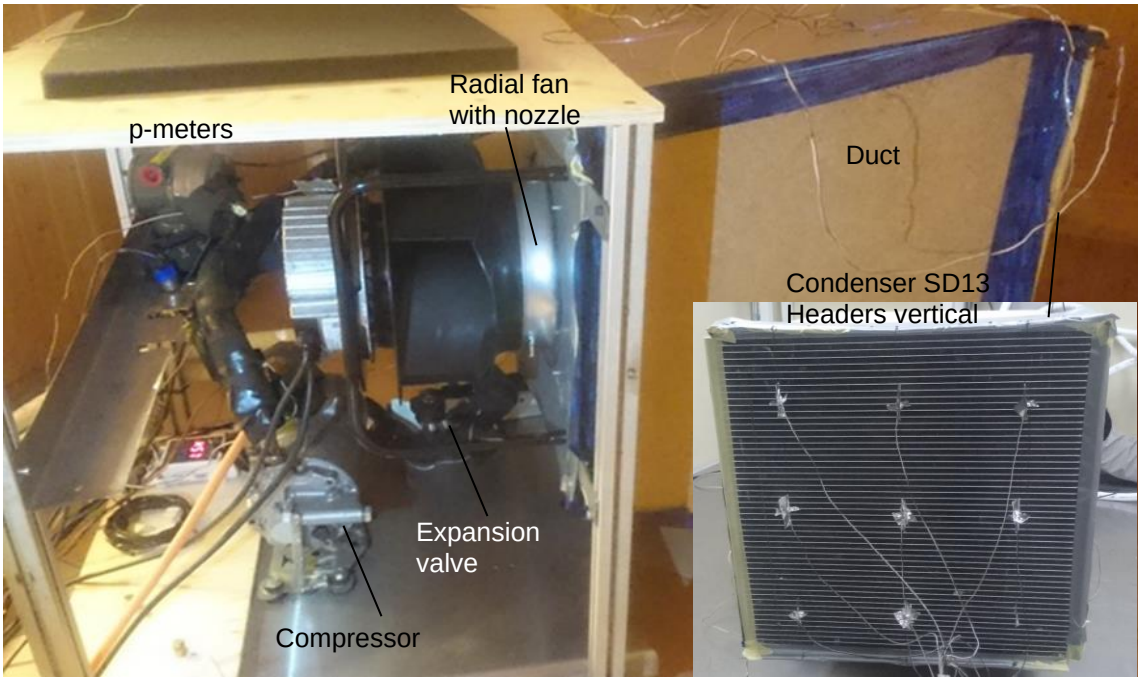

Figure 41. Propac #1. Outdoor unit right side with the condenser from the front embedded.

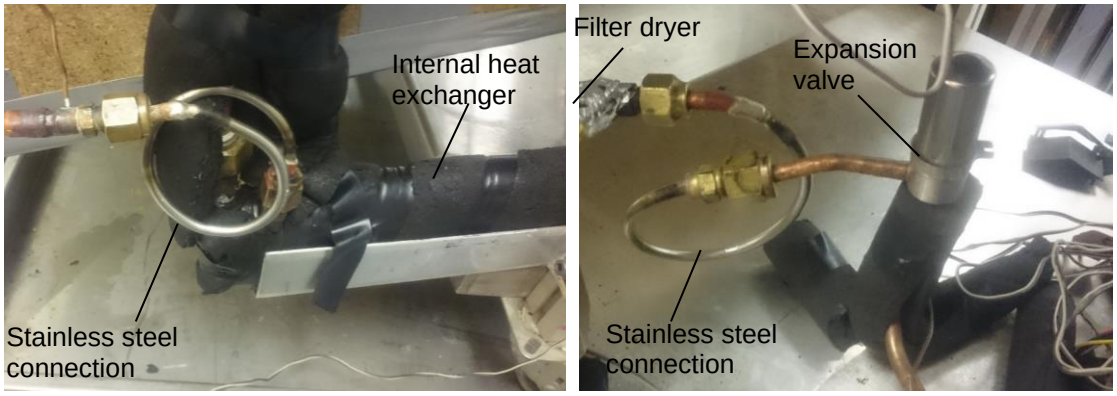

Figure 42. Propac #1. Condenser outlet and expansion valve inlet with stainless steel tube connections

3.10.2 Propac #2

The difference between Propac #1 and #2 was that the evaporator and fan was replaced to an assembly with the rebuilt SD12 evaporator and an axial fan as illustrated in Figure 43. Also, the hoses were replaced to 6 m long with 10.5 mm inner diameter of the suction line hose and 5.2 mm inner diameter of the two-phase line. The outdoor unit in Propac #2 was the same as in Propac #1.

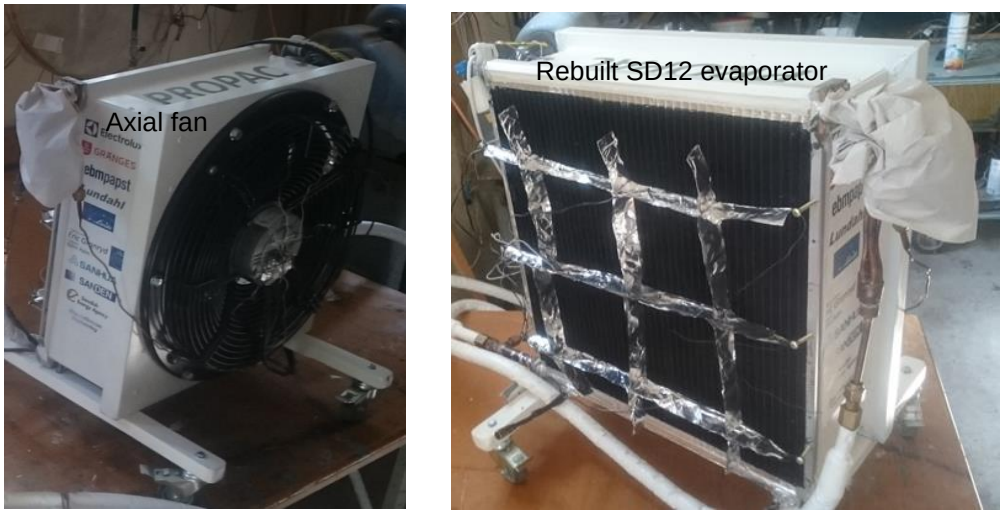

Figure 43. Propac #2. Indoor unit from two sides

3.10.3 Propac #3

Propac #3 was a major rebuilt of the outdoor unit into a standard architecture as shown in Figure 44. The fan was replaced by an axial fan which was mounted together with the SD13 condenser in the assembly unit. The internal heat exchanger was placed horizontally (instead of vertically as in Propac #1 and #2) at the bottom of the fan-condenser assembly. See Figure 45. A new assembly unit with the Z021 evaporator replaced SD12 and its assembly unit but with the same axial fan as in Propac #2 as illustrated in Figure 46.The connection hoses were the same as in Propac #2. The filter dryer was removed.

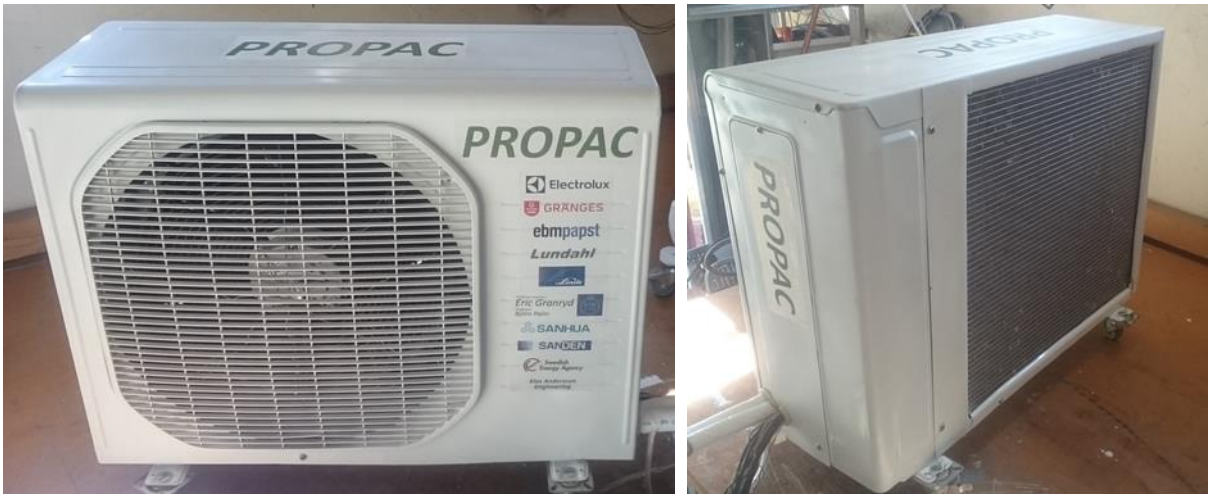

Figure 44. Propac #3 Outdoor unit.

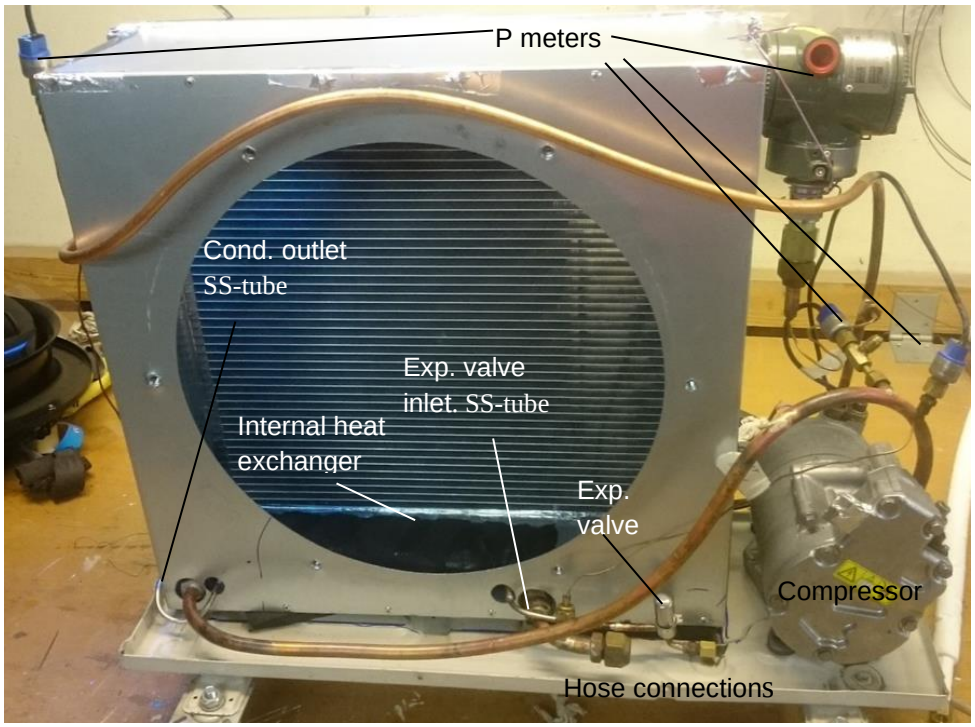

Figure 45. Propac #3 outdoor unit uncovered without the fan.

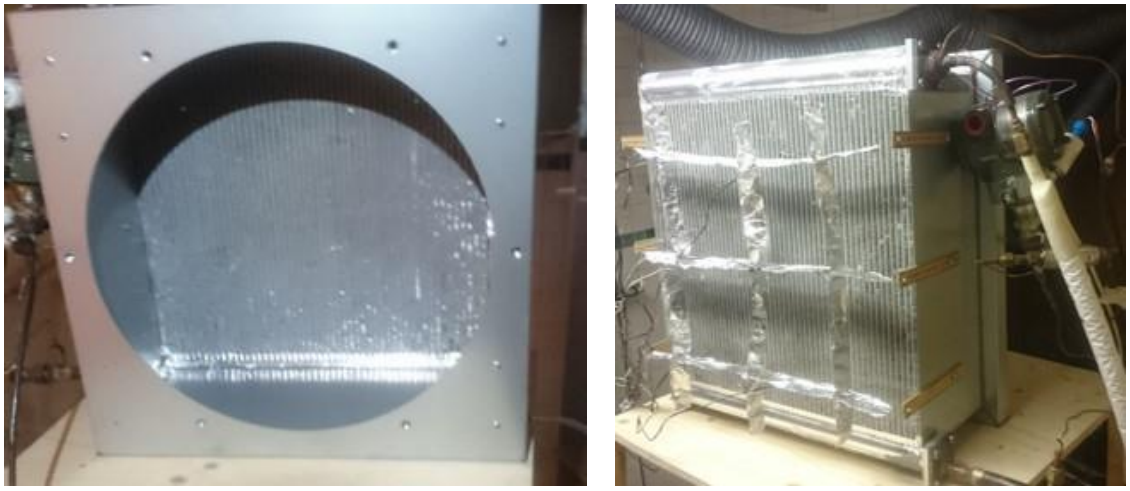

Figure 46. Propac #3 Indoor unit assembly with the Z021 evaporator without the fan.

4 Test setup

4.1 Measurement

The components and the measurement system used different communication protocols. To control and acquire data from the different parts, a special data system was developed allowing for setting fan and compressor speeds, expansion valve opening ratio and real time plotting of data from these components, merged with output from the measurement system. The data system used Coolprop for calculations and EasyView for real-time presentation. PropacControl is further described in a separate chapter.

Temperatures were measured with type T thermocouples (TC). The TC zero compensation was related to a precision PT100 sensor (with a PReasy 4114 transmitter) to which the TC cold junctions were thermally connected. The accuracy of the temperature measurements was estimated to ±0.3°C. The refrigerant temperatures were measured in pockets at the center of the tube interior except for the liquid lines.

The evaporator outlet pressure, determining the evaporating temperature and the condenser inlet pressure, determining the condensing temperature were measured with Yokogawa EJA510E pressure transmitters. Their accuracy is 0.01 bar. The pressure was also measured with standard pressure meters provided by Sanhua at the inlet to the internal heat exchanger vapor side, the compressor inlet and the condenser outlet. The Sanhua pressure meters were surprisingly accurate. At calibration measurements over a wide pressure range the differences from the Yokogawa meters were less than 0.05 bar. The corresponding accuracy of the saturation temperatures from pressures is within ±0.2°C.

Differential air pressure over the evaporator and condenser was measured with a HK Instrument DPT-Dual-2500 with an accuracy of ±2 Pa. Also, differential air pressure for flow calculation with inlet nozzle with K-factor was measured with this instrument. The air flow based on this method is only approximate and hard to estimate since the flow conditions at the nozzle inlet were not ideal. The compressor power was measured with a Voltech PM100 power meter with an accuracy of ±10 W at 1-2 kW reading.

The above-mentioned temperatures, pressures and power were connected to an AAC-2 data logger with 16 bit resolution. The values from the logger were read by PropacControl.

The fan powers were measured with DIZ-W1E4 meters within ±3 W and read by PropacControl via M-bus communication.

4.2 Tests at Electrolux

At the Electrolux laboratory the indoor unit is connected to a measurement chamber measuring the air flow and outlet enthalpy, calculated from a dry and wet bulb temperature. The outlet air from the evaporator is connected via a ducting to the inlet of the Electrolux measurement chamber. The ducting has to be individually built and adopted to the shape of the evaporator outlet and the measurement chamber inlet. This was done according to standard ANSI-ASHRAE 41-1.
The air inlet enthalpy is defined by a dry and wet bulb temperature measured with fork of tubes with openings. Air is sucked through the array of openings and blown over the dry and wet bulb. There were routines for changing the wick keeping the bulbs wet. The air flow was calculated from the pressure drop over calibrated nozzels. There were a number of nozzles for different air flow ranges that should be selected in accordance with the air flow through the evaporator. The pressure drop over the ducting, from the evaporator to the measurement position for the air flow, was compensated with a built in compensation fan. All lab temperatures measurement used RTD sensors.

The state of the inlet air to the condenser was measured with a fork in in a similar way as for the evaporator. The air flow and its outlet state for the condenser were not measured by the Electrolux equipment. It was determined from either the differential pressure over the nozzle for the radial fan or the pressure drop over condenser and fan data for the axial fan.

The indoor and outdoor units were placed in separate test chambers where the air temperature and humidity could be set and controlled accurately (according to EU standard tests EN-14511-2:2018). All tests were performed at the conditions given in Table 19.

Table 19. Air test conditions

	$T_{dry,bulb}$ °C	$T_{wet,bulb}$ °C	RH %	Dew point °C
Outdoor	35	24	40	19.5
Indoor	27	19.4	49	15.5

Dry air temperatures, air pressure drop, refrigerant temperatures, refrigerant pressures and fan electric power were measured with PropacControl. Compressor power was measured with both the Electrolux system and PropacControl. The Electrolux system provided data on evaporator air inlet and outlet enthalpy's, sensible and latent heat capacity separately and corresponding drain rate of water condensed on the evaporator surfaces. The cooling capacity (Q_2) was calculated from the enthalpy change (Δh) of the air over the evaporator, the air flow (V) and air density (ρ) as: $Q_2 = \Delta h \cdot V \cdot \rho$. The test setup at Electrolux with Propac #1 is illustrate in Figure 47 and with Propac #3 in Figure 48.

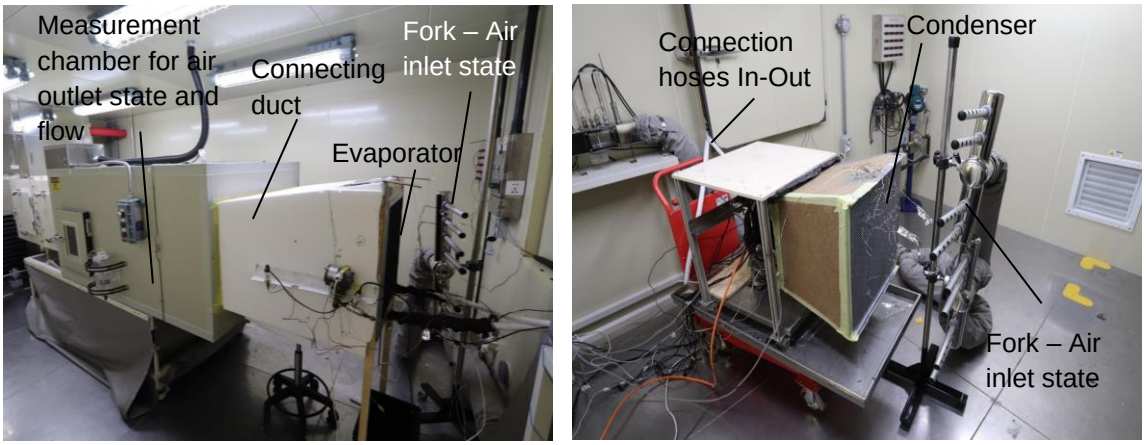

Figure 47. Test setup at Electrolux, Propac #1. Indoor unit at the left and the outdoor unit to the right.

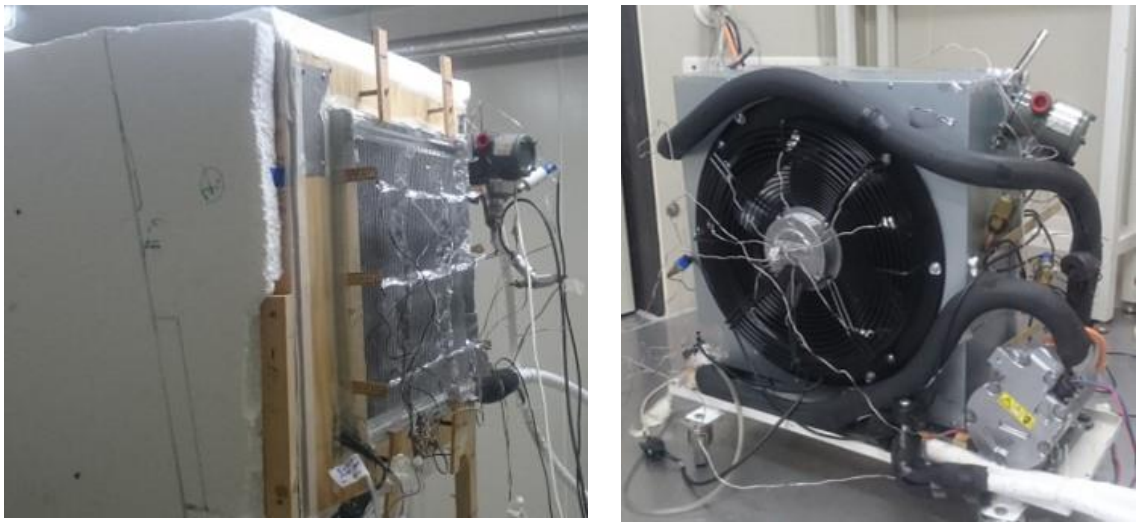

Figure 48. Test setup at Electrolux, Propac #3. Indoor unit at the left and the outdoor unit to the right.

4.3 Tests at Klas Andersson Engineering

The tests at the facility of Klas Andersson Engineering (KAE) were only approximate. Here the air flows and enthalpies of the air could not be measured accurately enough to define a sufficient accurate cooling capacity. Still, all other parameters were measured accurately so that rough estimates of the performance could be done. Test rooms were built in which the indoor (27°C) and outdoor (35°C) temperatures could be approximately set. The humidity was not controlled why the conditions mostly became dry, with little or no condensation on the evaporator. At KAE the refrigeration distribution was evaluated with infra-red camera and some comparisons of required charge for different system configurations was performed.

4.4 Charging

The system was filled from a small, 400 g, bottle connected to the filling station via a capillary tube winded into spiral spring to avoid any forces to influence the scale reading. The capillary tube also lowers the filling flow rate, facilitating accurate filling. The scale had a resolution of 0.1 g. See Figure 49. The charge was determined by filling during operation at nominal conditions (Q_2~3.5 kW T_1~43°C, T_2~10°C) until a combination of about 4 K subcooling and superheat was achieved. At higher capacities, when T_1 increases and T_2 decreases, less charge is required and the opposite for lower capacities. There are two reasons for that. 1) The internal volumes of the low-pressure side (mainly suction lines and compressor) are much larger than on the high-pressure side. 2) Higher T_1 and lower T_2 increase the vapor fraction in the long two-phase line and at the evaporator inlet. It is an interesting challenge to design a minimum charge system for a wide range of operation conditions. In this project mainly the nominal conditions were considered.

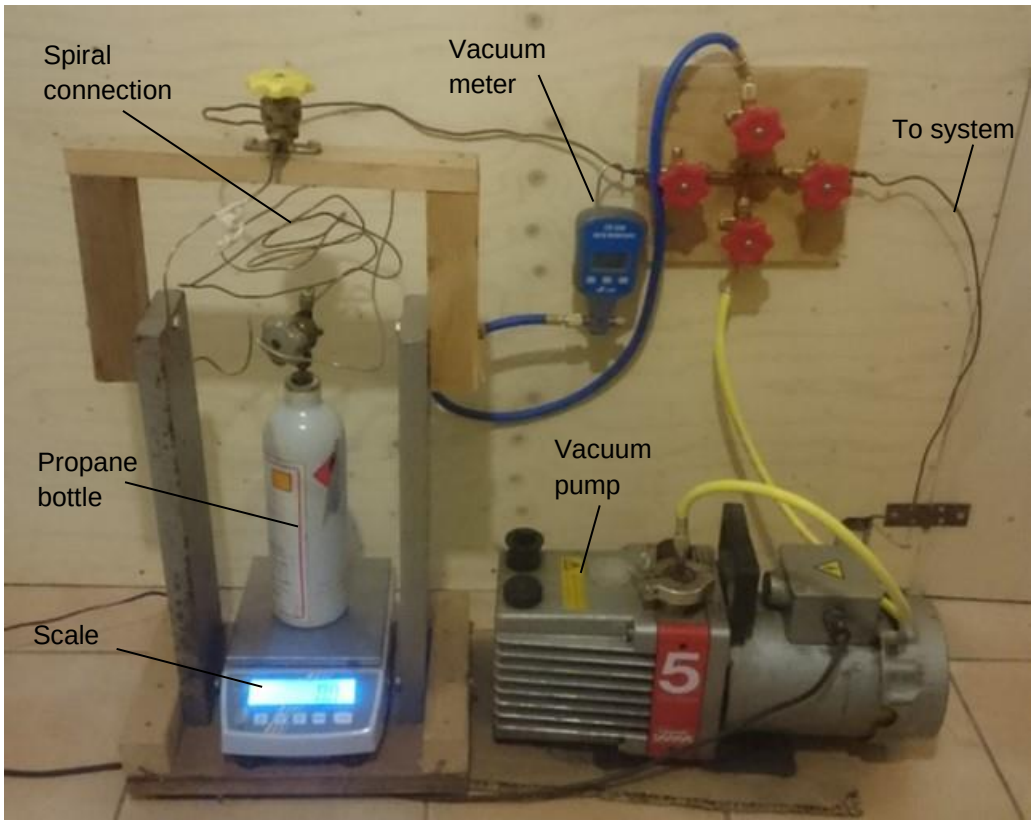

Figure 49. Filling station with spiral connection to the refrigerant bottle.

5 PropacControl - Control and Measurement System

5.1 Overview

The Propac control and measurement system, PropacControl, includes devices and applications for controlling the main components in Propac and to measure vital parameters for evaluating function and performance.

The main components; compressor, expansion valve and fans, have in addition to control functionality also the option to provide data that define the state of the item and internal signals such as temperature, speed etc. See Figure 50 for overview of Propac main components with control and read options.

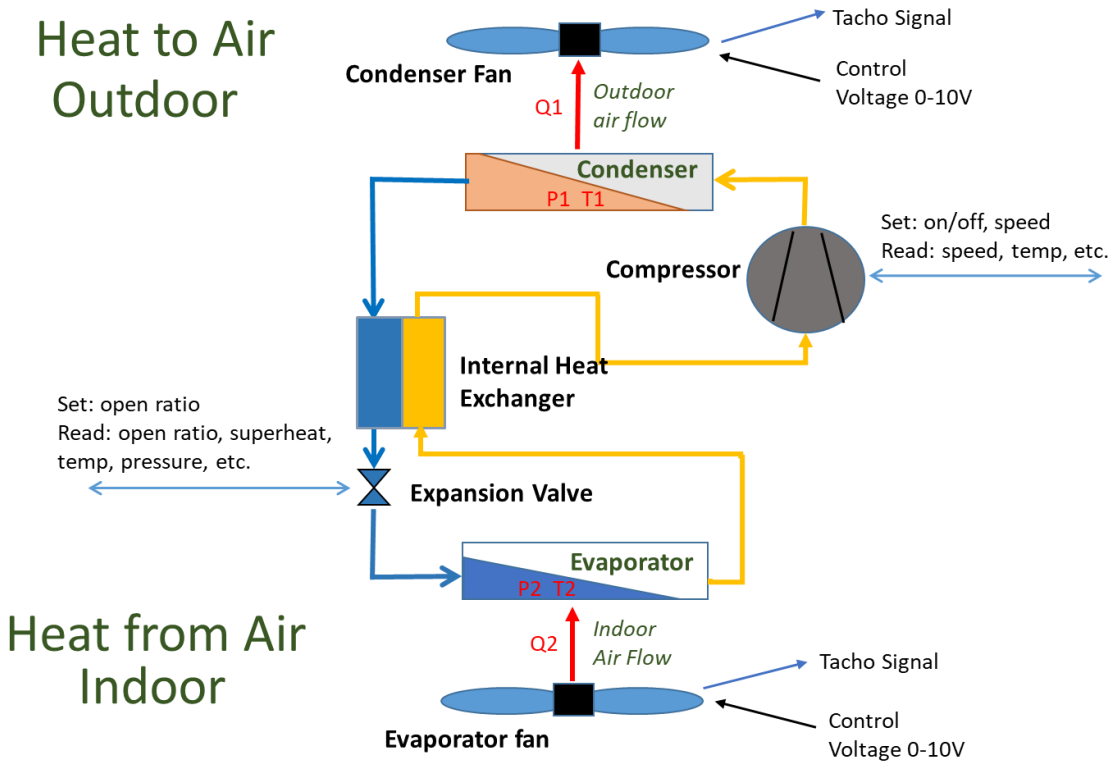

Figure 50. Main components in Propac with control and read options

PropacControl is implemented with a VBA application with Excel as user interface on a standard Windows PC. For the different communication methods, interfacing devices and applications are used. The data analyzing and visualization application EasyView is used for on-line monitoring and data evaluation.

Since thermodynamic properties and performance parameters are evaluated while running the system, they are calculated immediately at data collection using Coolprop and displayed on-line with EasyView. See Figure 53 for illustration of software components in PropacControl.

5.2 Communication methods

The devices and parameters to control in the system are:

- Compressor speed
- Expansion valve open ratio
- Evaporator fan speed
- Condenser fan speed

There is no automation built into PropacControl, so all changes are done manually through controls in PropacControl Excel interface except for fans used during the project (Protypes #2 and #3) that had voltage input as control signal. These were manually controlled from power supplies.

Since the components used in Propac origin from different use applications, they have different communication methods that suit their normal usage. The **compressor** is used in electric cars and has LIN bus communication. In most vehicles CAN bus is used for communication between a control computer and devices such as gearbox, climate and security alarm devices. LIN bus was developed as a cost-efficient alternative to CAN bus for devices where speed and fault tolerance is not critical.

The **electronic expansion valve (EEV)** and the test **fans** (Prototypes #1 and #2) have Modbus communication which is a serial communication protocol widely used in industry for connecting electronic devices.

For measurements, the **PC logger AAC-2** from Intab, designed for long term recordings of process signals and temperatures, is used. It provides on-line measurements via the RS-232 port of the PC. RS-232 was introduced in 1960´s and used for serial communication transmission of data between teletypewriters and modems. Due to its simplicity, it is still used in industry and scientific instruments for short range point-to-point connections.

Power consumption of the **fans** (Protypes #2 and #3) is measured with **energy meters** which have M-Bus communication. M-Bus is used for remote reading of utility meters such as consumption of gas, water and electricity in homes. We chose to convert the M-Bus signal to Modbus using a Modbus Slave – M-Bus Gateway which acts as an M-Bus Master and Modbus RTU slave.

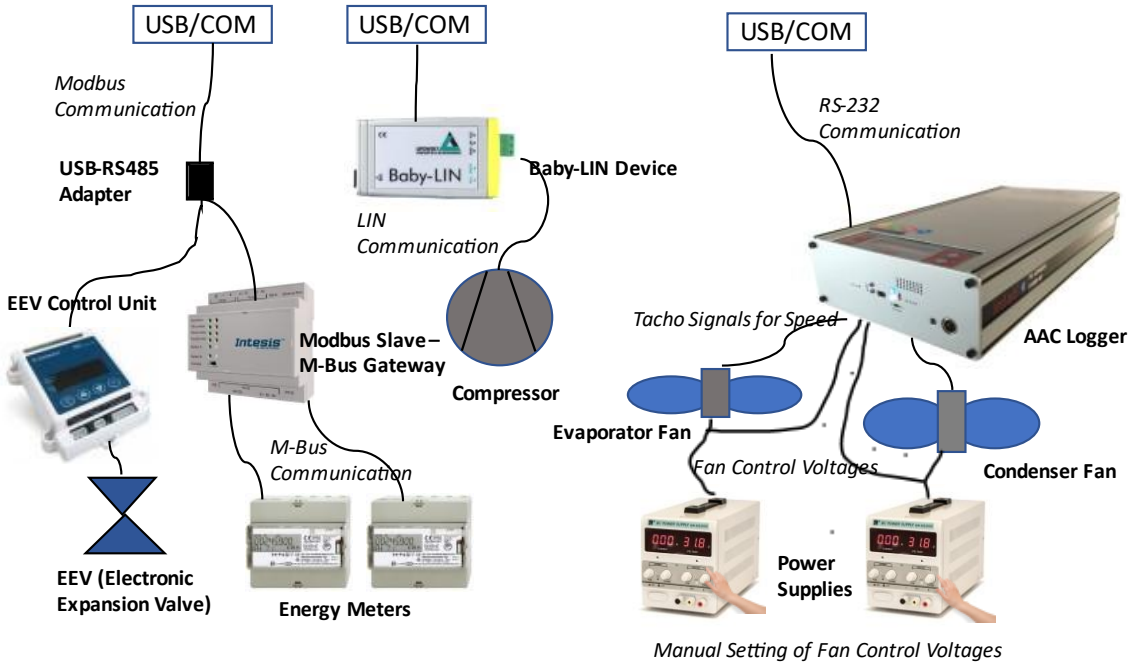

Figure 51. Communication methods between devices and control PC

5.3 PropacControl software components

The software architecture used for control and measurement utilizes off-the-shelf applications; an efficient and cost-effective approach to implement a test site in short time with limited resources.

The system is managed from Excel/VBA that interfaces communication applications and Coolprop with different methods.

5.3.1 PropacControl main application – Excel and VBA

The Excel sheet includes the interface to:

- Configure which devices to run in the test
- Configure communication settings

- Configure which parameters to write to text file during logging
- Configure text file name and period between logged samples
- Configure AAC-logger channels
- Start communication applications and initiate data transfer from them
- Set compressor speed, EEV open ratio and early test fan speed
- Read out data from compressor and EEV such as speed, open ration, temperatures, alarms
- Start/stop logging

During logging all the parameters selected to be written to text file and displayed in EasyView are measured and calculated and sampled every 5:th second.

The VBA scripts implements all the underlying functionality.

The flowchart for a test sequence is described in Figure 54.

5.3.2 Modbus Poll

Modbus Poll from Witte Software is a Modbus Master simulator that monitors several Modbus slaves. It has OLE Automation to interface to Excel acting as the “server” while the VBA application is the automation controller and the “client”. From VBA you may create Modbus Poll windows which are configured to execute Modbus commands such as “ReadHoldingRegisters” from a slave at defined time interval. You may also write registers to be send to the slave.

Once initiated, Modbus Poll keeps polling the slaves for data and from VBA the data is read from Modbus Poll very efficiently.

In PropacControl, Modbus Poll is initiated to

1) establish connection with EEV and read Holding Registers with open ratio and overheat and set register for Open Ratio at manual operation.
2) establish connection with M-bus gateway and read Holding Registers with power measurements from energy meters
3) in first prototype, establish connection with fans and read Holding Registers with speed and power and set registers for fan speeds

5.3.3 WinWedge

For communication with AAC logger and RS-232, the application WinWedge from TAL Technologies is used. It provides serial communication capabilities to any Windows application using DDE (Dynamic Data Exchange) acting as a DDE server. Although OLE automation is the recommended method for communication with Excel, VBA still supports DDE.

WinWedge needs to be configured with the communication parameters for the AAC logger and the commands to send to AAC logger during logging. This configuration is done in an interface of the application and stored in a configuration file. From PropacControl main application WinWedge is started with the configuration filename as a parameter. With the “Timer-on” command, WinWedge starts polling the AAC logger according to the configuration file settings. During logging, data is read from WinWedge every 5:th second.

5.3.4 Baby-LIN

The Baby-LIN device from Lipowsky comes with the Baby-LIN DLL which is a native C/C++ DLL with wrappers for .NET, Python and VB6, neither of these works with VBA.

To control Baby-LIN from VBA we ordered a COM Wrapper to the Baby-Lin DLL which was developed by Lipowsky according to our requests on functionality. In the implementation the COM Wrapper uses the .NET Wrapper as illustrated to the right, Figure 52.

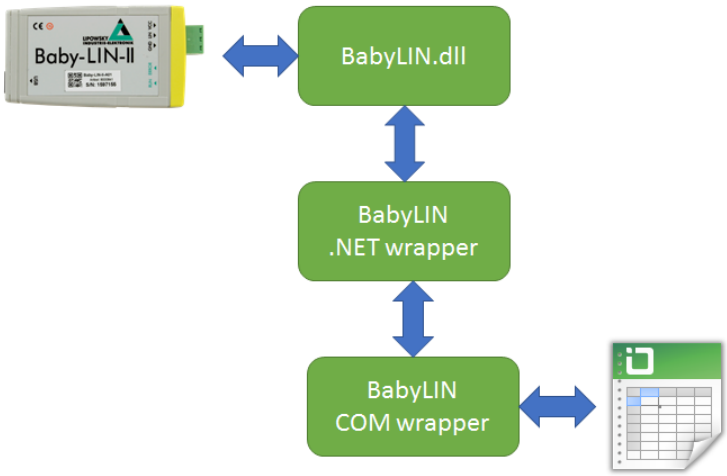

Figure 52. BabyLin COM wrapper design

LIN bus communication requires that the device to control, the compressor, states which LIN-bus functionality it has in a so called LDF file. We got the LDF file for the compressor from Sanden. This file is the specification on how to communicate with the compressor and it is downloaded to the Baby-LIN device and the DLL.

In PropacControl, communication with Baby-LIN is done according to the API specification for the DLL enabling setting values on speed and reading compressor status, speed, temperature, current and voltage, etc.

5.3.5 CoolProp (www.coolprop.org)

CoolProp is a freeware C++ library that implements fluid equations of state and transport properties for many components including propane and humid air and it has an interface to Microsoft Excel. CoolProp functions are used during logging to enable immediate evaluation of system performance based on measured parameters.

5.3.6 EasyView

EasyView from Intab is a powerful tool for visualizing data. During data logging, all measured values and all calculated parameters are written to a text file which is continuously read by EasyView and displayed in graphs.

EasyView is also used for data evaluation after completed recordings to select and preprocess data which is exported to Excel for final assembly of test series.

Figure 53 displays an overview of applications and software tools in PropacControl. The control interface is an Excel application and the monitoring display is provided by EasyView.

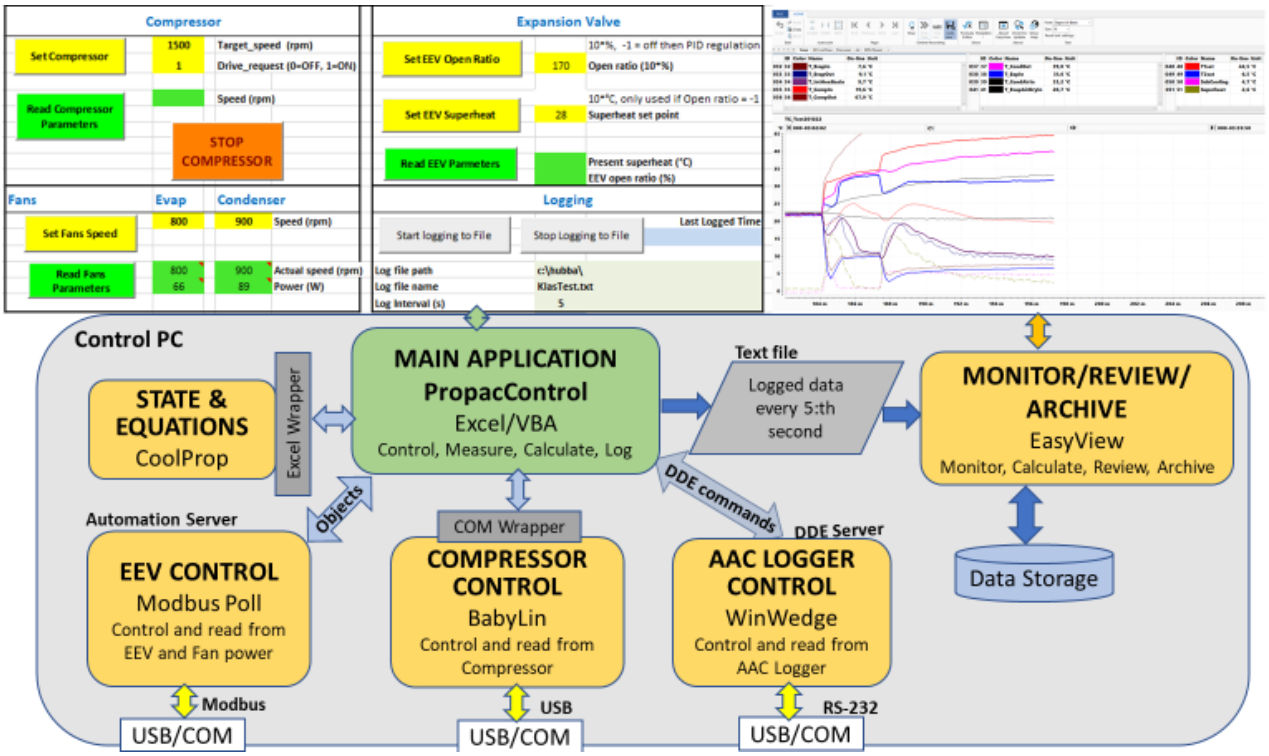

Figure 53. PropacControl – software components

5.4 Operate PropacControl Main Application

When started, PropacControl main application needs to be cleared and reset and configured for the actual test. Once the test procedure is established, only the name of the text file used during logging is changed between tests.
The next two steps to reach Control Mode are to 1) start the communication applications; Modbus Poll, Baby LIN and WinWedge and 2) to establish communication between the applications and the devices to control.

In Control Mode, you can set parameters and read extensive information from all connected devices. To get on-line monitoring logging needs to be started which creates the text file and start logging selected parameters to this text file every 5:th second (configurable). EasyView is then started to continuously read and monitor data from the text file.

5.4.1 PropacControl Main Application Flow Chart

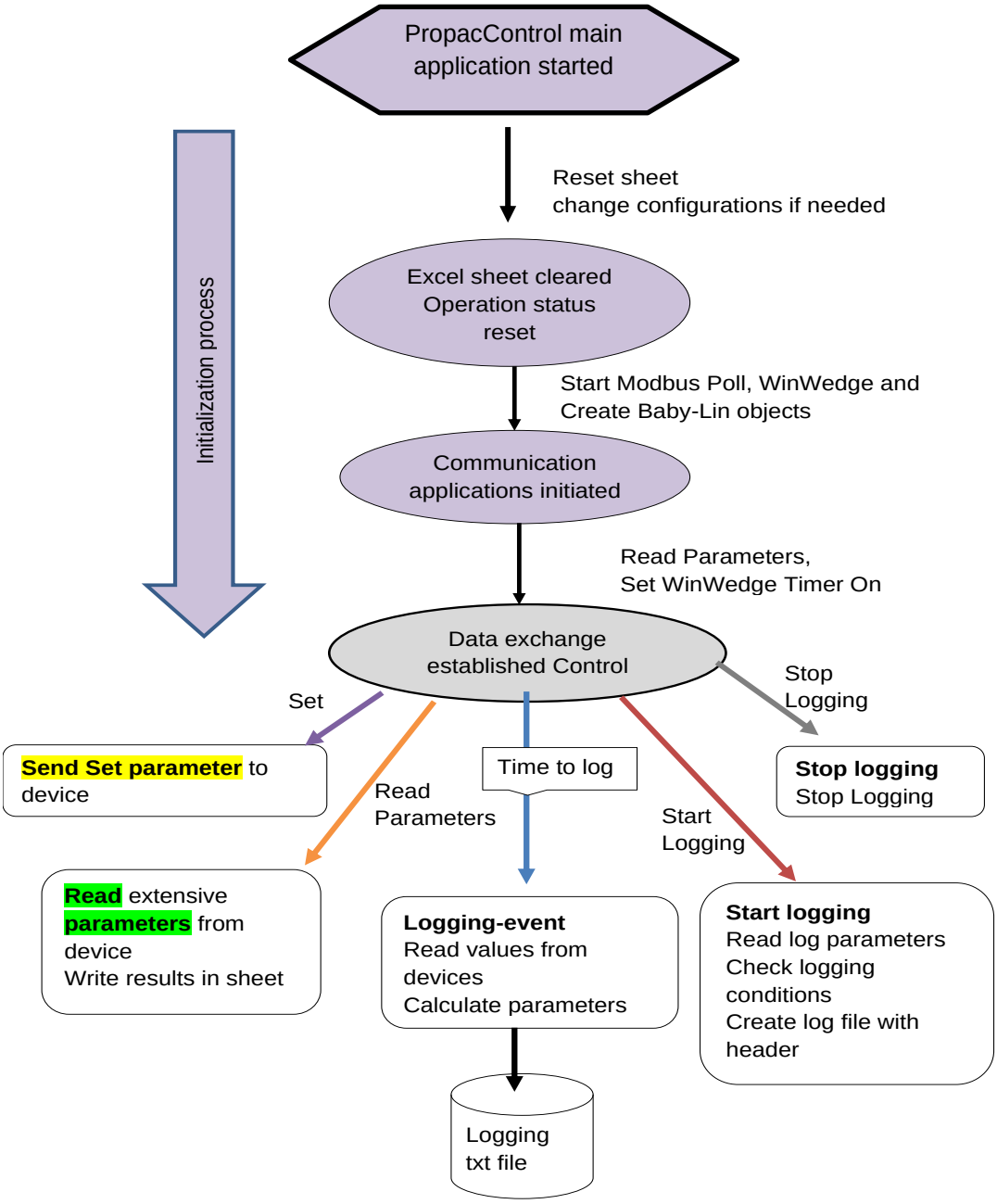

Figure 54. PropacControl – Main application flowchart

6 Results

Most tests were performed at standard conditions according to Table 20. Some test was performed at dry conditions, meaning that the humidity of the indoor air was lowered below the dew point of the evaporator surface, other conditions being the same as in the table.

Table 20. Standard conditions

	T_{dry} °C	T_{wet} °C	RH %	Dew point °C
Outdoor air	35	24	40	19.5
Indoor air	27	19.4	49	15.5

6.1 System charge summary

A major topic of the project was the charge. During the project a lot of configuration combinations were tested and some interesting differences in the charge was experienced. The learning from this quite extensive trial and error process is summarized in Table 21 in which the charge and performance are given for the respective variants. All are using the same condenser and operated at similar conditions. This does not tell the full story but gives a base for discussion of charge considerations.

Table 21. Result summary

Evaporator				In-Outdoor lines		Charge	Q_2 /COP_2	Propac
Type	Header orient.	Inlet	Distrib.	Two-phase L / di	Suction L / di	gram	kW / -	
SD13	Vert.	Bot	non	fastpipe 3m/5.2mm	fastpipe 3m/8.4mm	150	3.5 / < 3	
SD13	Horiz.	Bot	non	fastpipe 3m/5.2mm	fastpipe 3m/8.4mm	150	3.5 / 3.3	#1
SD12 Rebuilt	Horiz.	Bot	A	fastpipe 3m/5.2mm	fastpipe 3m/8.4mm	140		
SD12 Rebuilt	Horiz.	Top	A	fastpipe 3m/5.2mm	fastpipe 3m/8.4mm	122		
SD12 Rebuilt	Horiz.	Top	B	fastpipe 3m/5.2mm	fastpipe 3m/8.4mm	120		
SD12 Rebuilt	Horiz.	Top	B	fastpipe 6m/5.2mm	fastpipe 6m/10.5mm	143	3.5 / 3.5	#2
Z021 Original	Horiz.	Bot	Sanhua	fastpipe 3m/5.2mm	fastpipe 3m/8.4mm	180		
Z021 Rebuilt	Horiz.	Top	Sanhua	fastpipe 6m/5.2mm	fastpipe 6m/10.5mm	155	3.5 / 3.5	#3

The system with evaporator SD13, being the same as the condenser, took 150 g despite the smaller lines. The performance with vertical header was very poor due to the insufficient water drainage. With vertical headers the performance improved, but

despite its large dimensions it didn’t reach the efficiency target, mainly because of the pressure drop and uneven refrigerant distribution.

The tests with evaporator SD12 resulted in a charge decrease of about 20 g by injecting at the top instead of the bottom. The switch to the larger connection lines added about 20 g.

Evaporator Z021 with remaining tube insert, the small lines and injection at the bottom took 180 g and was therefore not further tested. The test with removed tube insert, injection from the top and the larger lines almost reached the target but took 155 g. The reason for the charge being higher than for evaporator SD12 is partly the larger headers (30 vs. 20 mm diameter). The main explanation is though poor distribution resulting in large amounts of liquid entering the suction line and even passing the internal heat exchanger vapor side into the compressor. This also reduces the system performance. It is likely that evaporator Z021 will perform better than SD12, within 150 g of charge, with improved distribution.

6.2 Propac #1

All results presented below are achieved with a refrigerant charge of 150 gram and the 3-meter fastpipe hoses with 5.2 mm and 8.4 mm inner diameter for the two phase and suction line respectively.

6.2.1 Evaporator orientation – Water drainage

Propac #1 had a Sanhua SD13 as both evaporator and condenser. In the first test series both the evaporator and condenser were tested at standard conditions with the headers in vertical orientation. In a second test series the evaporator was turned 90° so that the headers were horizontal with the inlet and outlet at the bottom (two passes).

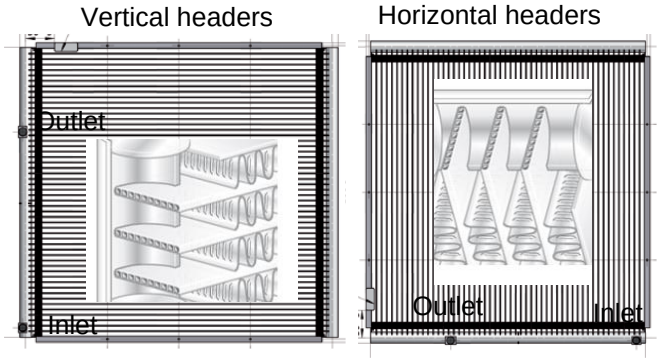

Figure 55. Evaporator orientations with corresponding tube and fin orientations

Figure 56 shows how the air pressure drop over the evaporator gradually increases with vertical headers, compressor and fan speed being constant. Figure 57 shows the corresponding gradually reduction of the cooling capacity. The explanation to this is gradual accumulation of condensed water on the evaporator surfaces, reducing heat transfer and blocking the air flow. With horizontal headers and vertical tubes, the drainage is more efficient. The capacity changes until 100 min. for both cases are mainly caused by changing the expansion valve setting and thereby the superheat. The conclusion is clearly that the headers should be horizontal (tubes vertical).

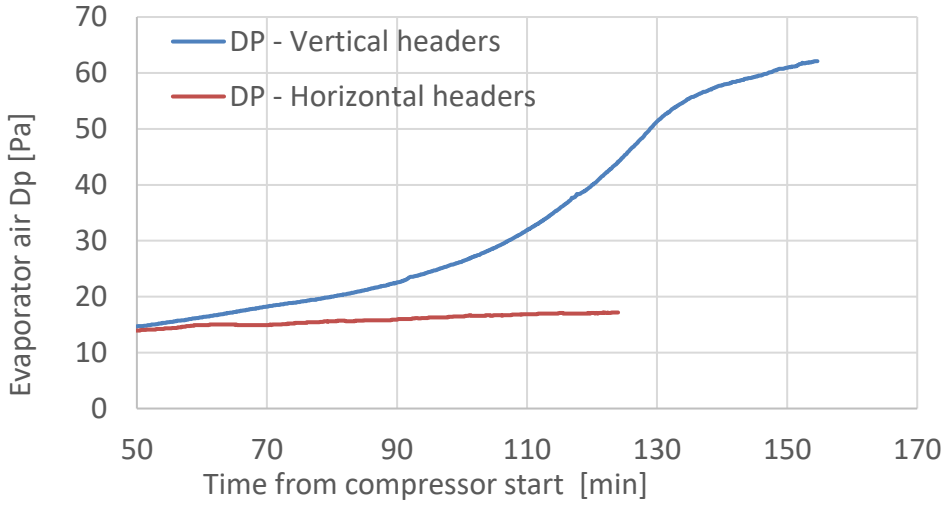

Figure 56. Increase of pressure drop with accumulating water

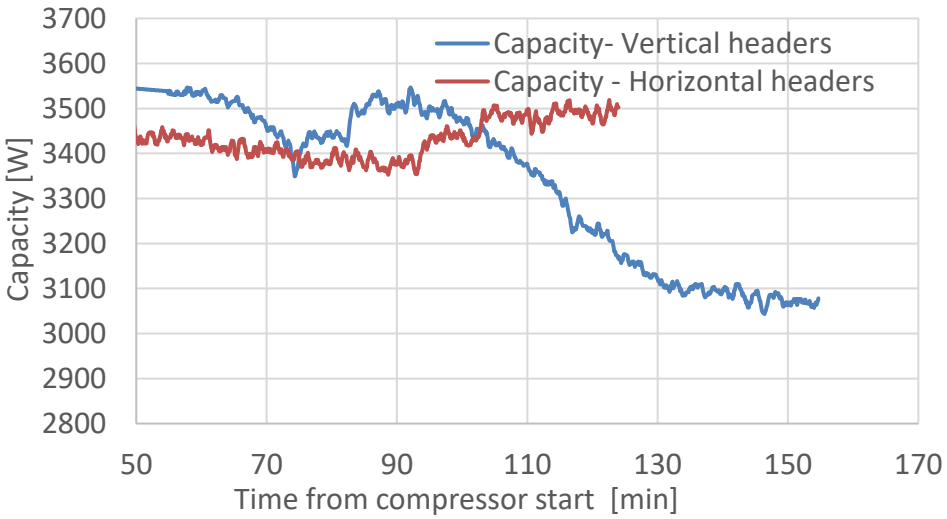

Figure 57. Capacity decrease with accumulating water

Figure 58 shows the development of evaporating temperature and sensible heat ratio for the same tests. If drainage is insufficient, the heat transfer is reduced causing the evaporating temperature to decrease correspondingly. Lower evaporating temperature increases the rate of condensation that further reduces heat transfer and so on. Another aspect of the orientation is illustrated in Figure 59 showing the relation between superheat and subcooling. With vertical headers the subcooling is larger than for horizontal at the same superheat. This indicates that there is more liquid available in the condenser with vertical headers. This can partly be explained by the lower evaporating pressure with vertical headers, increasing evaporator inlet vapor quality and reducing the vapor density in all suction side volumes. In addition, it might be that liquid pools of refrigerant are formed at stagnant sections in-between the flat tubes in the horizontal, upper header as discussed in the Evaporator chapter.

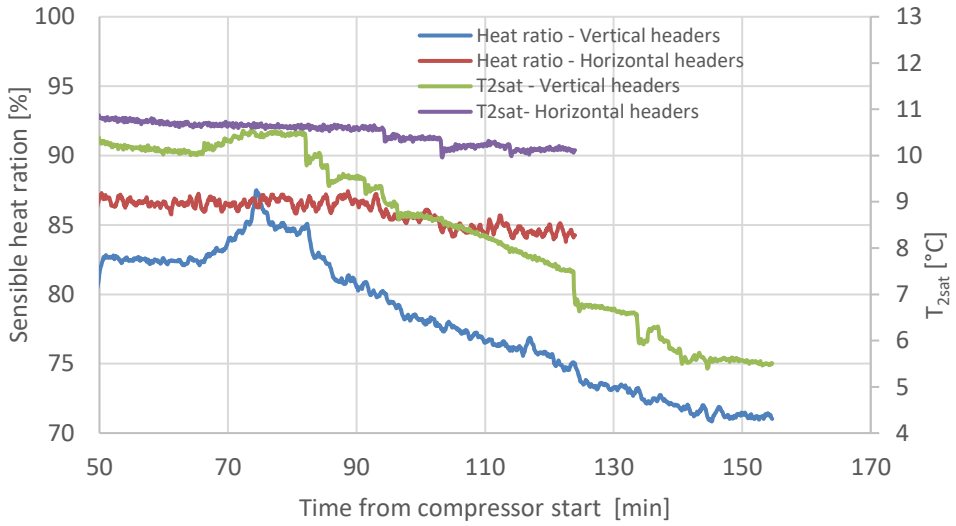

Figure 58. Sensible heat ratio and evaporating temperatures

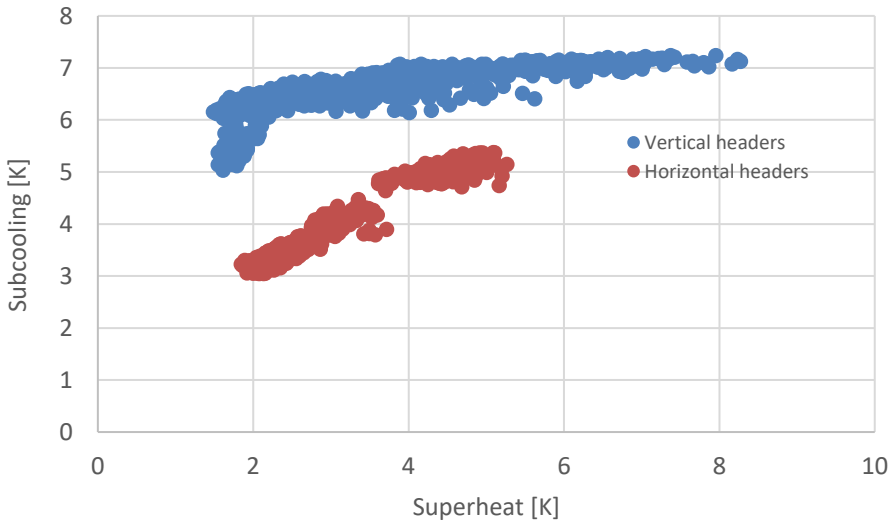

Figure 59. Superheat and subcooling

6.2.2 Superheat variation

The cooling capacity and COP_2 as a function of the superheat at standard conditions and horizontal headers are illustrated in Figure 60. There is a flat maximum of the performance in the range 4-8 K superheat. It seems like too little superheat is more harmful than too much.

In the Evaporator chapter the possibility to calculate the outlet vapor quality from the evaporator by a heat balance over the internal heat exchanger was discussed. Such an example for Propac #1 is illustrated in Figure 61. The important implication of the fact that liquid remains, even though a sufficient superheat is measured, is that liquid pools can be formed in the suction line, increasing the charge.

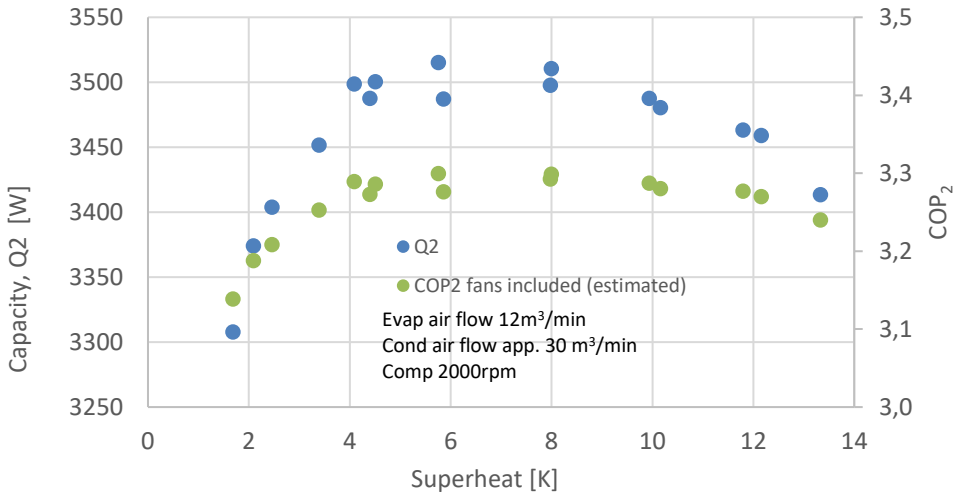

Figure 60. Optimum superheat

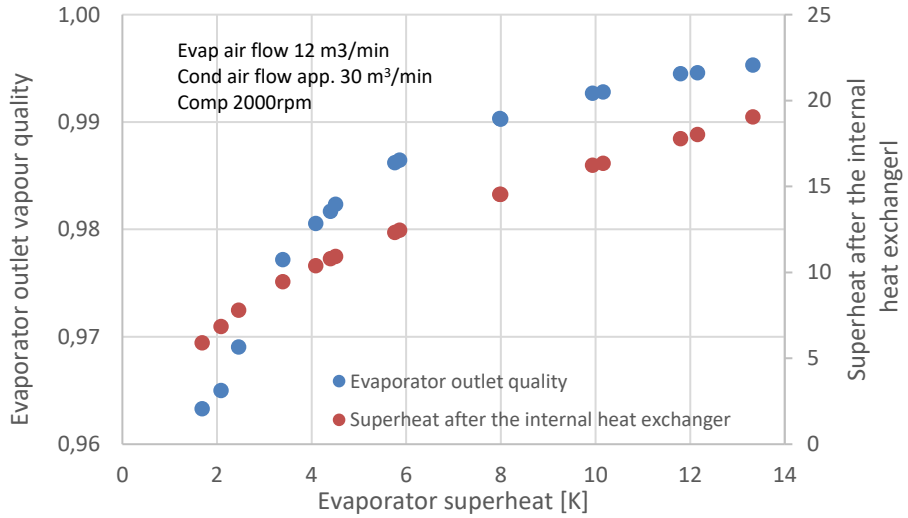

Figure 61. Evaporator outlet vapor quality

Figure 62 shows the evaporating temperature (T_{2sat}) and subcooling as a function of the superheat. The evaporating temperature decreases somewhat with the superheat. The increase of the subcooling with superheat changes inclination at 5 K superheat. This might be related to liquid beginning to fill up the bottom of the vertical outlet header of the condenser, acting as a receiver. This liquid is not cooled as efficiently as in the tubes.

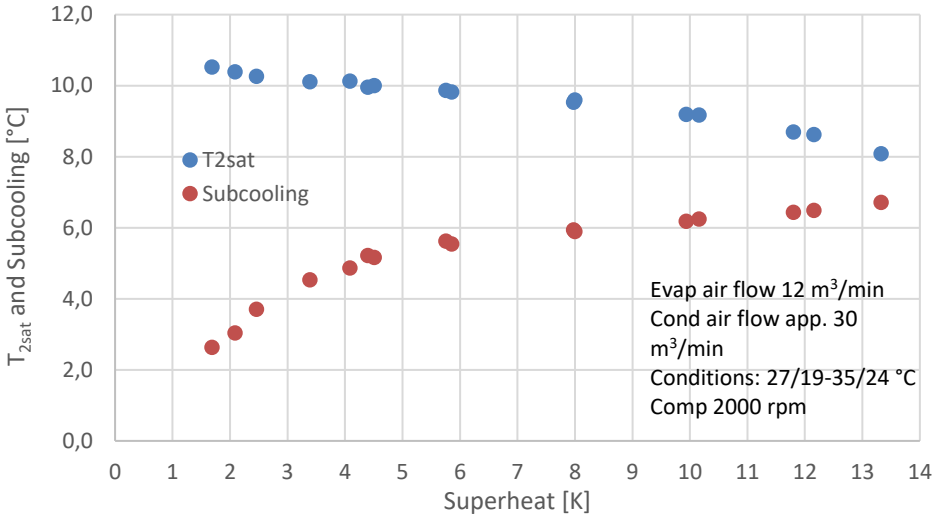

Figure 62. Evaporating temperature and subcooling change with superheat

Figure 63 shows the evaporator heat transfer performance (UA-value), referred to the inlet temperature difference to the evaporator, as a function of the superheat. Even if the tendency is weak, it seems like there is an increase of the UA-value up to 4 K superheat. The increase corresponds to the relatively steep increase of the latent heat (decrease of sensible heat ratio), increasing the thermal load from water condensation. Thereafter the UA-value decreases with increased superheat.

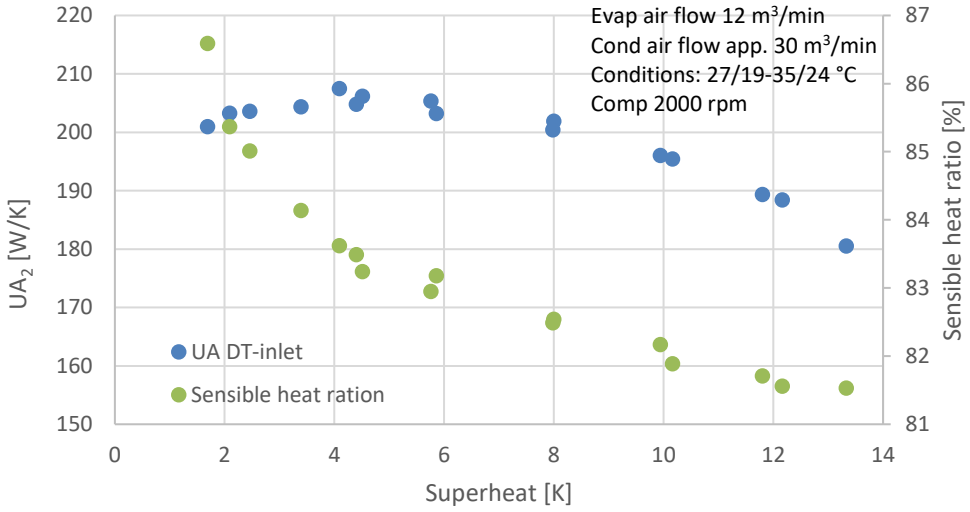

Figure 63. UA value and sensible heat change with superheat

The compressor efficiencies as a function of the compressor inlet temperature are shown in Figure 64 together with the pressure ratio. The compressor performance increases with the inlet temperature and the corresponding increase in the pressure ratio. The pressure ratio is also shown in the graph and it is varying in a quite narrow range, indicating that the influence on the performance from the inlet temperature is positive.

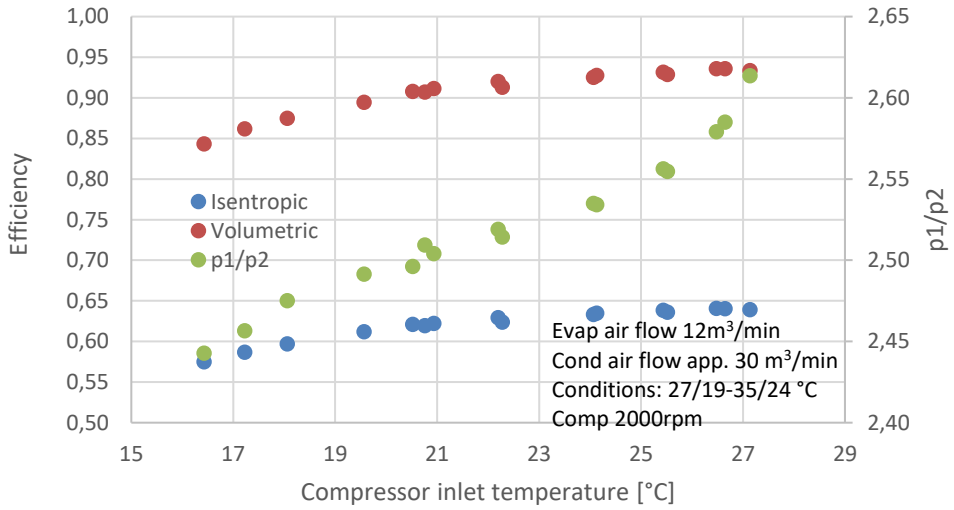

Figure 64. Compressor performance for varying inlet temperatures

6.2.3 Air flow variation

The evaporator heat transfer performance as a function of the air flow is illustrated in Figure 65. The evaporator influence on the system performance is given in Figure 66. COP_2 seems to approach a maximum just above 15 m^3/min. The project goal, 3.5 kW cooling capacity (Q_2) is reached at about 12 m^3/min evaporator air flow, 2000 rpm compressor speed and 30 m^3/min condenser air flow where the system efficiency is 3.3.

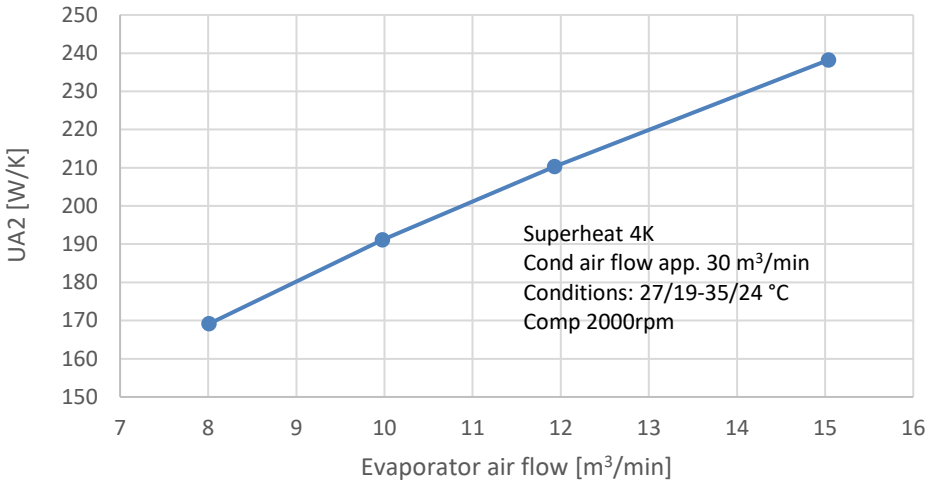

Figure 65. Evaporator heat transfer performance for varying air flow

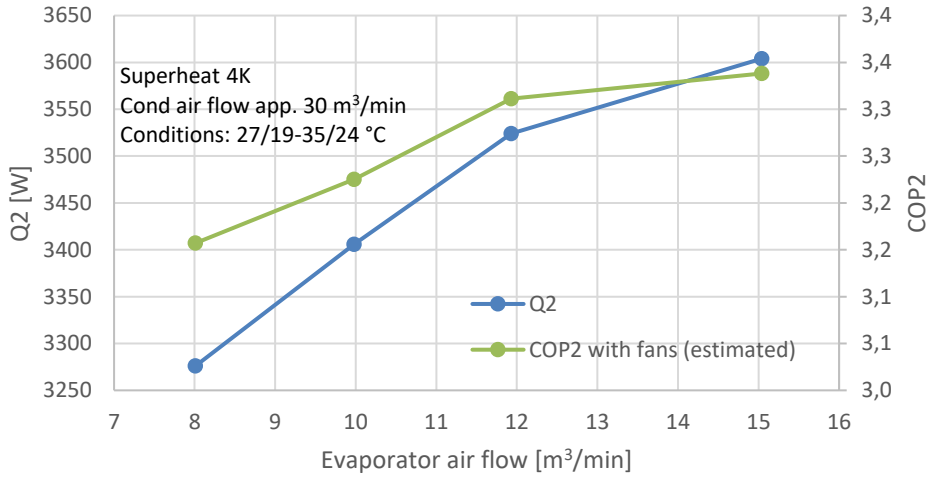

Figure 66. System performance for varying air flow

Figure 67, showing the system performance, indicates that optimum condenser air flow is above 30 m^3/min. The condenser is treated in more detail in the Propac #2 chapter.

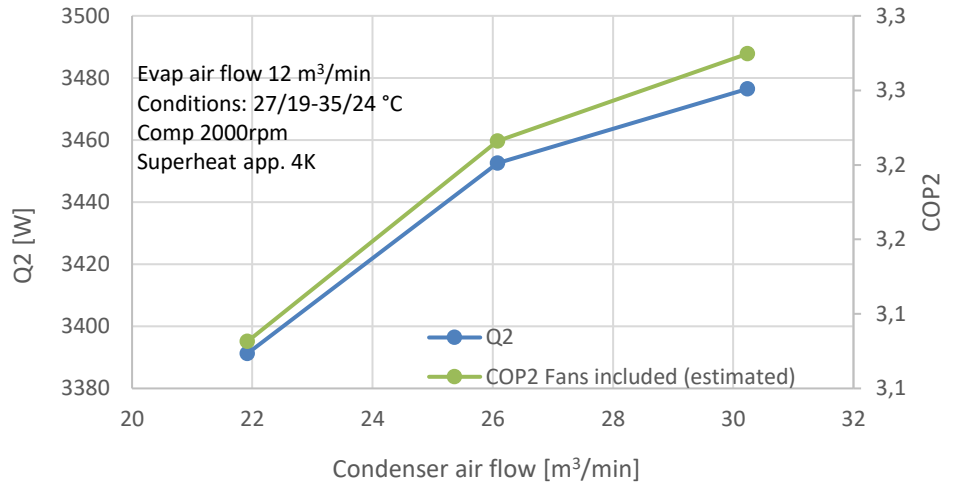

Figure 67. System performance for varying condenser air flow

6.2.4 Compressor speed variation

Figure 68 shows the system performance at different compressor speeds. Keeping in mind that the maximum compressor speed is 8500 rpm the system seems quite powerful in terms of cooling capacity. Especially if the evaporator and condenser fans could be allowed to speed up with the compressor in a high-capacity operation mode, where high noise levels could be accepted.

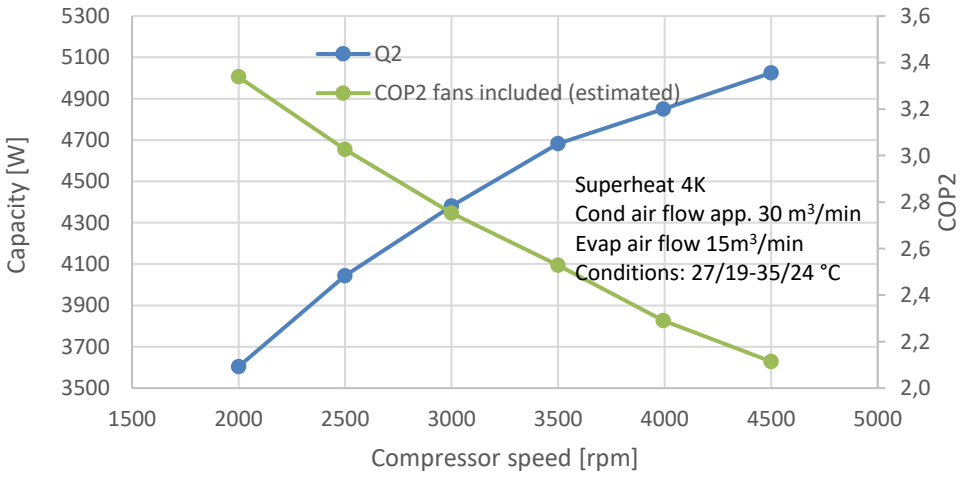

Figure 68. System performance for varying compressor speed

The compressor efficiencies are given in Figure 69 together with the pressure ratios. The volumetric efficiency seems slightly lower than expected. It might be that more oil should be added.

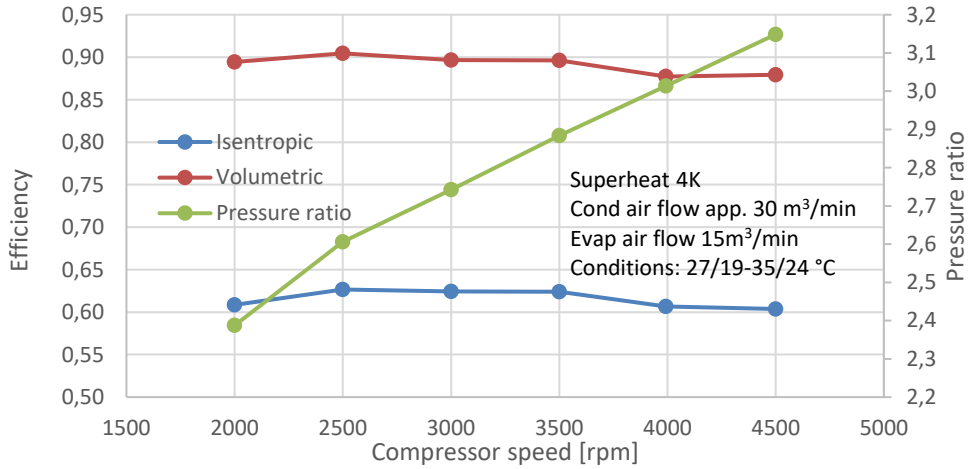

Figure 69. Compressor efficiency for varying compressor speed

The refrigerant side pressure drop and the corresponding saturated temperature drop over the evaporator are shown in Figure 70. The pressure drop is too high. It should be less than 1 K. In addition, the pressure drop over the suction line, from the evaporator to the internal heat exchanger inlet, was about 0.5 bar at 2000 rpm compressor speed, corresponding to 3 K reduction in the saturation temperature. This is also far too much and has a strong negative influence on the performance. There is probably some blockage in addition to the normal frictional pressure drop.

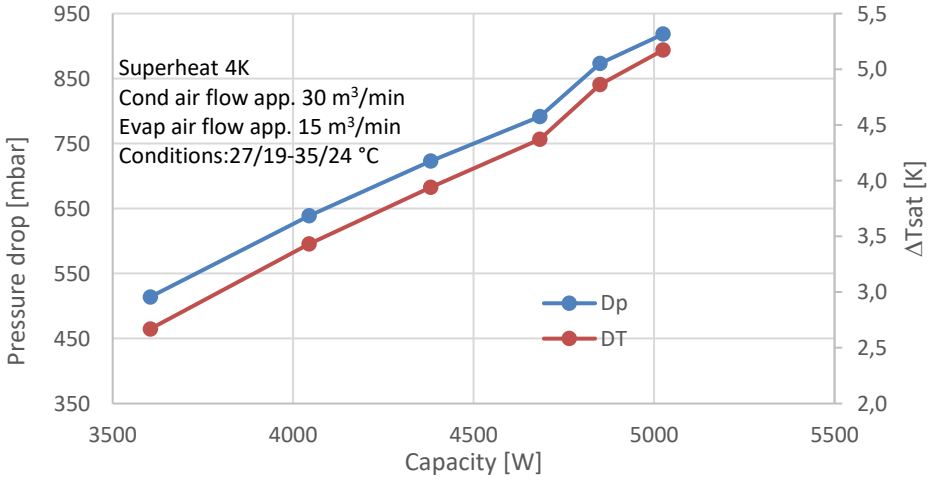

Figure 70. Evaporator pressure drop for different capacities

6.2.5 Seasonal COP_2 - SEER

The seasonal COP_2 (SEER) was measured according to EN14825-2018 at four conditions A, B, C and D with part load ratio ranging from 100 to 21% and outdoor temperature from 35 to 20 °C. The indoor temperature was 27(19) in all conditions. The results of the tests where Propac #1 is compared to Electrolux benchmarked products available on the EU-market are shown in Figure 71.

It can be concluded that at high load conditions (A and B) Propac performs in level with products on the EU-market. In low part-load condition C, Propac prototype has higher input power requirement, thus reducing total SEER. In low part-load condition D, Propac is limited by the minimum set compressor frequency. The evaporator fan power, 22 W, was not included for Propac calculations. With the later prototypes, #2 and #3, Propac would have come out better.

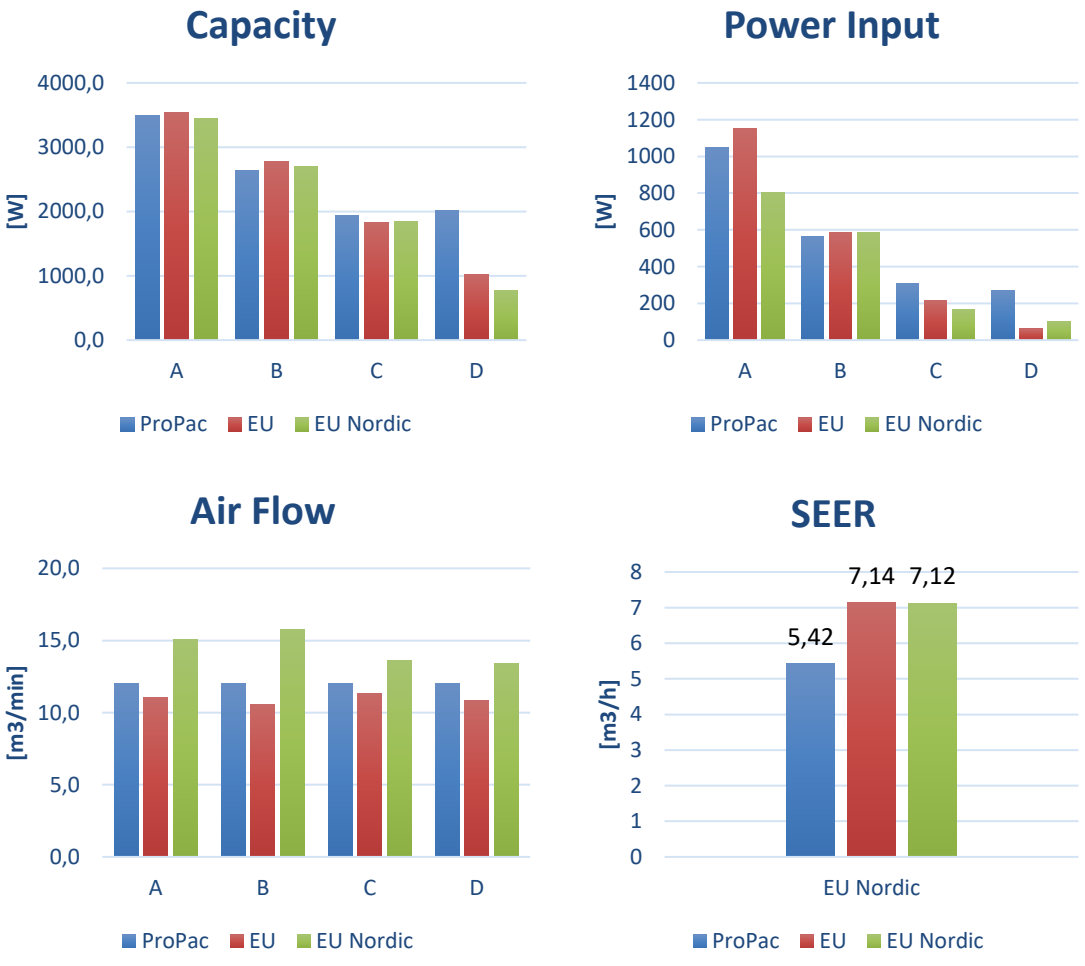

Figure 71. Benchmark Propac #1 to Electrolux EU products

6.2.6 Competitor comparison

Figure 72 shows a comparison between Propac #1 and a competitor in a similar operating condition. Propac #1 has the same blowing conditions (temperature and dehumidification) as the competitor. However, Propac needs more compressor power to achieve similar cooling performance, thus the lower EER in this condition. For this test scenario, Propac prototype used a higher airflow amount (12 compared to 10.8 [m^3/min]). The competitor uses 1100 [g] of R32 with a GWP of 675 [CO_{2eq}]. Total GWP: 742 [$kgCO_2$]. Propac uses 150 [g] of R290 with a GWP of 3 [CO_{2eq}]. Total GWP: 0.5 [$kgCO_2$]. Propac pipe length is 3 [m] compared to 5 [m] for the competitor.

Figure 72. Propac #1 and competitor performance

6.2.1 Summary of Propac #1 results

The project target was close to be met but failed on the COP_2. The refrigerant pressure drop over the SD13 evaporator was too high. It is not suitable as evaporator. It was concluded that this type of microchannel heat exchanger should be operated with horizontal headers to drain condensed water properly. There is a potential for increased performance with reduced the pressure drop over the evaporator and suction line.

6.3 Propac #2

In relation to Propac #1, Propac #2 used the rebuilt SD12 evaporator with horizontal headers, inlet at the top and with an inlet distributor. The suction line between the indoor and outdoor units was 6 m ½" fastpipe hose (inner diameter 10.5 mm) and the corresponding two-phase line was 6 m ¼" (inner diameter 5.2 mm) fast pipe hose. The SD12 evaporator and axial fan were mounted in the assembly provided by ebmpapst.

The outdoor unit was unchanged compared to Propac #1. The condenser fan power was calculated as if the axial fan was used.

All results in this chapter are with a refrigerant charge of 143±3 gram.

Initially, tests with injection also at the bottom of the rebuilt SD12 were performed. Depending on the conditions, bottom injection required about 20 gram more charge than the top injection but with no performance advantages.

6.3.1 Compressor speed variation

Figure 73 shows the cooling capacity and COP_2 (fan powers included) as a function of the compressor speed. The fan control setting was kept constant and therefore the evaporator air flow varied with the compressor speed from 11 to 15 m^3/min. This is due to reduced evaporating temperature with increased capacity and corresponding increase of water condensation on the evaporator, which restricts the air flow. The related air flow and air pressure drop are shown in Figure 74.

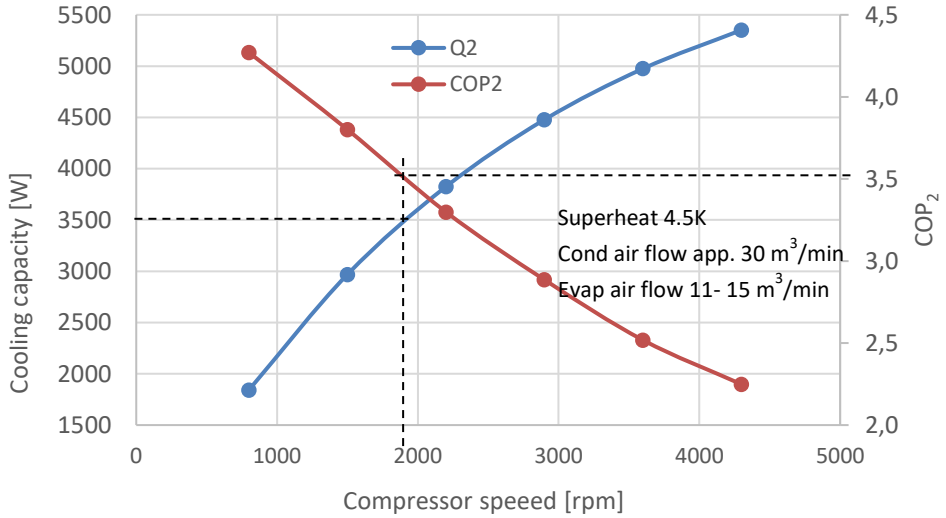

Figure 73. System performance with varying compressor speed

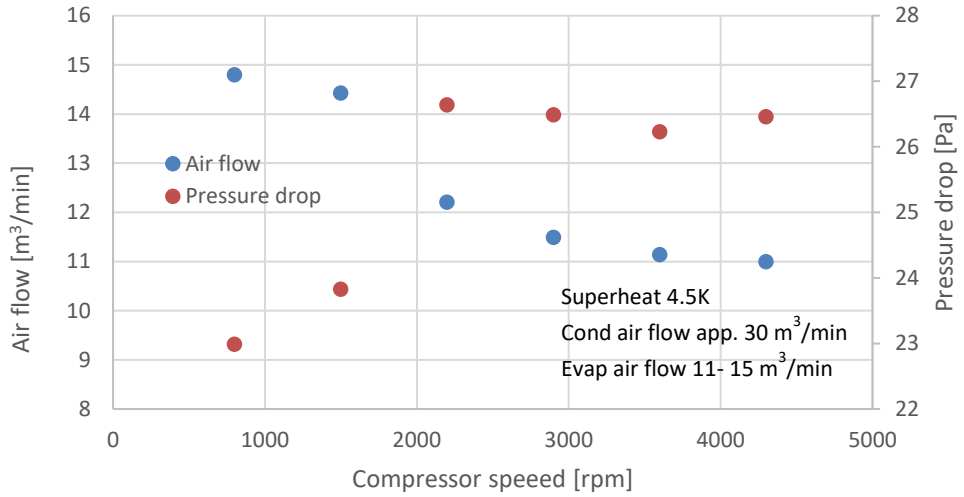

Figure 74. Evaporator air flow and pressure drop with varying compressor speed

The project target, 3.5 kW cooling capacity and COP_2=3.5, is met at the compressor speed 1900 rpm, condenser air flow 30 m^3/min and evaporator air flow 13 m^3/min with 143 gram of propane.

As the compressor speed is increased the evaporating temperature is lowered and the rate of condensation of water (drain rate) on the evaporator is increased in proportion. This is illustrated in Figure 75. Just above 1000 rpm the evaporator temperature passes the dew point, 15°C, which can be seen as change of the inclination of the drain rate curve. The same phenomenon explains the jump in pressure drop and air flow in Figure 74.

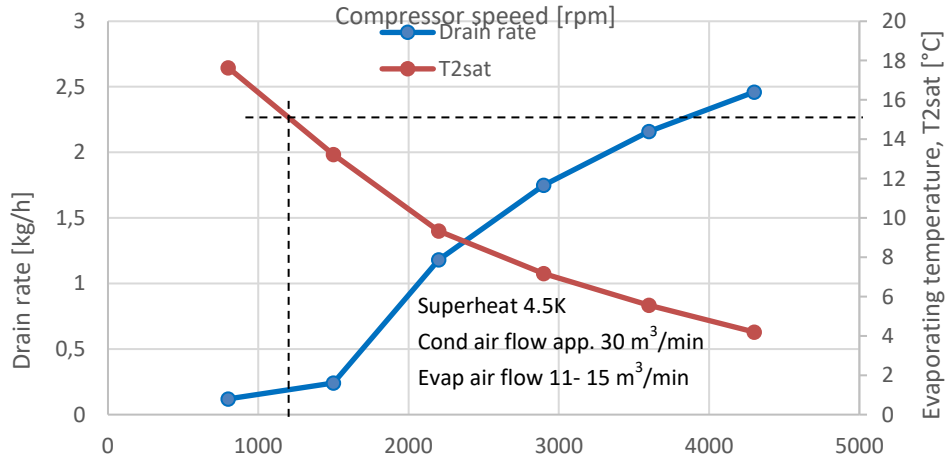

Figure 75. Drain rate and evaporator temperature with varying compressor speed

The refrigerant mass flow for the compressor speeds in this test series and related cooling capacity is shown in Figure 76. The mass flow is about 13 g/s at the target capacity, 3.5 kW. With a total charge of 143 g the refrigerant makes one lap through the system in app. 11 sec. This allows the system to respond quickly on changes.

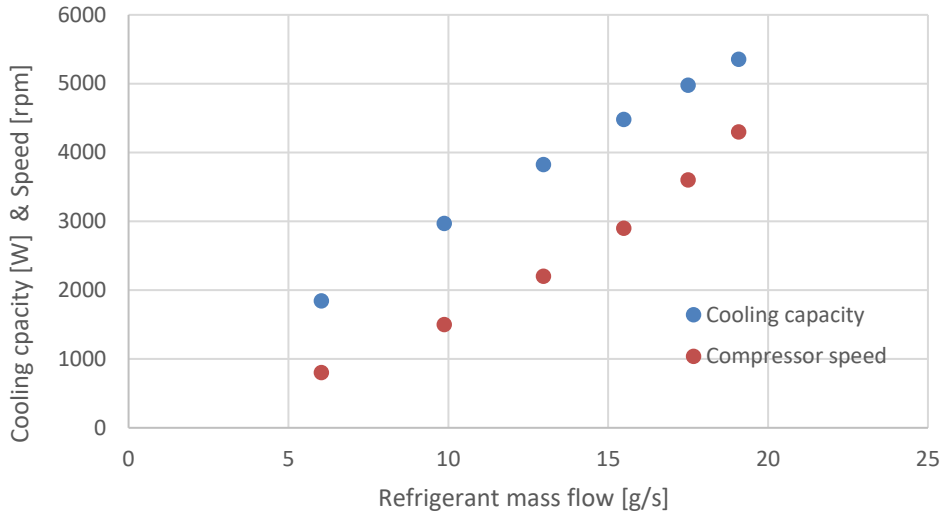

Figure 76. Cooling capacity and compressor speed with varying refrigerant mass flow

Figure 77 shows the evaporator heat transfer performance (UA_2-value), referred to inlet temperature difference, variation with the compressor speed (i.e. capacity). The red dot represents the performance of the SD13 evaporator at the same conditions and 12 m^3/min air flow. The heat transfer performance in this test is mainly influenced by the increase of latent heat load with increased speed (reduced T_{2sat}), rather than increased heat transfer on the refrigerant side.

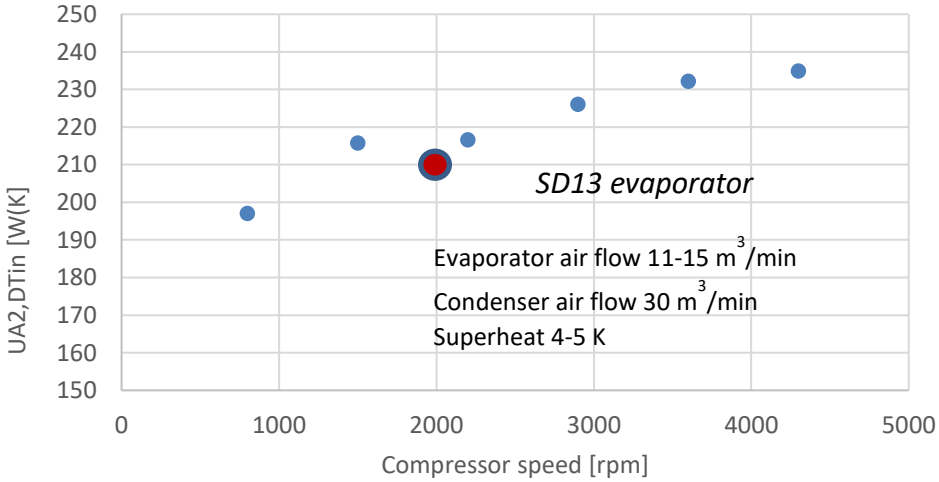

Figure 77. UA_2 value for the rebuilt SD12 evaporator with varying compressor speed

Figure 78 shows the heat transfer performance for the condenser as a function of the condenser capacity, corresponding to the compressor speed in earlier figures. Also the subcooling is given. The condenser performance dependence of the capacity is very weak (watch the scale) which indicates that the UA_1-value is dominated by thermal resistance on the air side. Still, there seems to be a minimum just below 6 kW. The highest UA_1-value is measured for low load and low subcooling, that might be explained by the related low heat flux maximum free surface for condensation. In contradiction, the shear stress in-between liquid and vapor is lower at low mass flux, increasing film thickness which reduces heat transfer. As both capacity and subcooling increase, the UA_1 performance decreases until a minimum is reached. This might be the net result of the negative influence from more subcooling (lower average vapor fraction along the tube) by less free surface and the positive influence from increased shear stress with mass flux, reducing film thickness. Thereafter the shear stress effect increases more with mass flux than the vapor fraction effect with superheat which may explain the increasing UA_1-value recorded at high capacities.

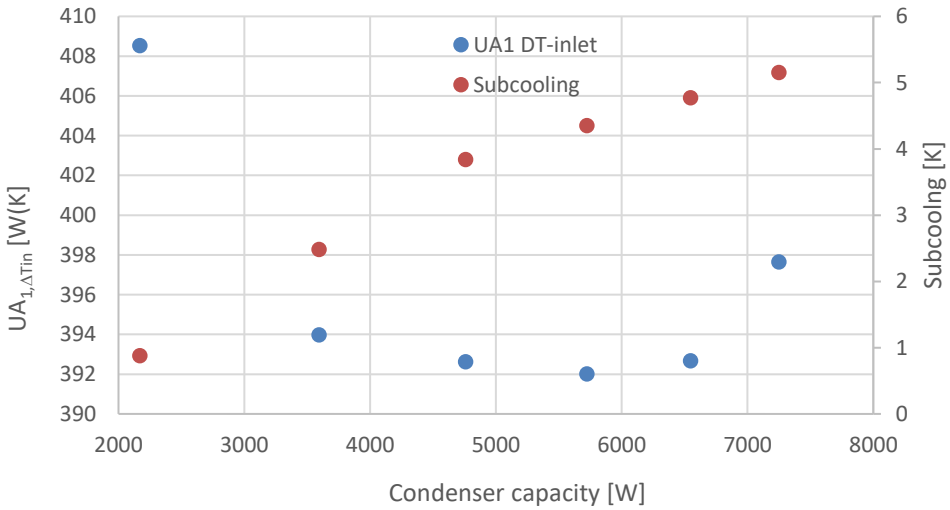

Figure 78. UA_1 value and subcooling with varying condenser capacity

The efficiency of the compressor at different speeds is illustrated in Figure 79. The efficiency is relatively low. A possible explanation is that too much oil was captured in the 6 m long suction line with large inner diameter (12.6 mm) causing insufficient lubrication of the scroll wheels.

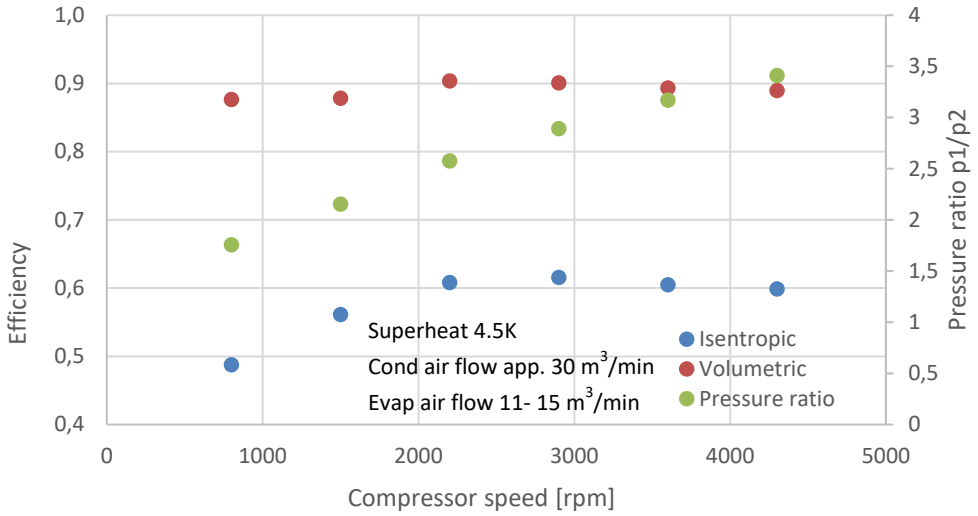

Figure 79. Efficiency of compressor with varying compressor speed

Figure 80 shows an increase of subcooling with increased compressor speed. This illustrates redistribution of refrigerant from the low to the high-pressure side of the system. The charge on the low-pressure side decreases with decreasing evaporating temperature due to lower vapor density and lower vapor fraction at the evaporator inlet.

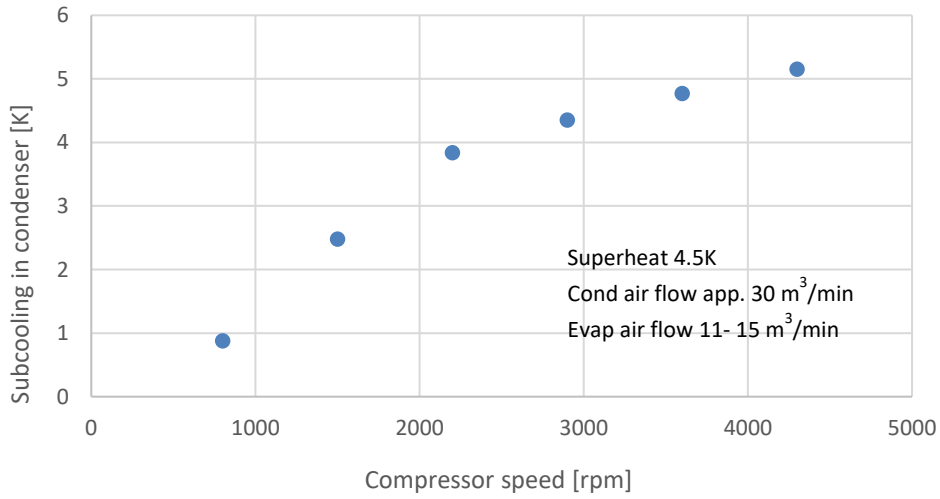

Figure 80. Subcooling increases with increased compressor speed

Figure 81 shows the pressure drop over the evaporator and the corresponding saturated temperature drop as a function of the cooling capacity. Figure 82 is the corresponding pressure drop over the suction line from the evaporator to the internal heat exchanger inlet. The pressure drops are acceptable.

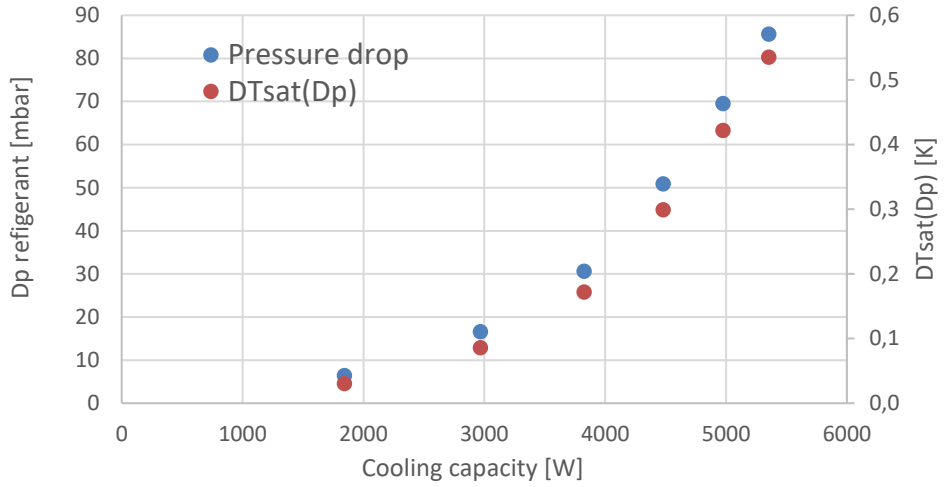

Figure 81. Refrigerant side pressure drop over the evaporator

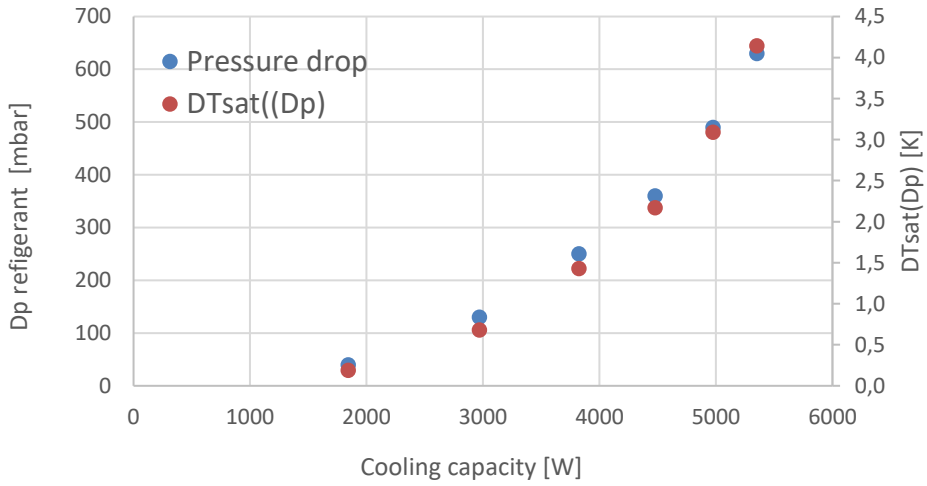

Figure 82. Refrigerant side pressure drop over the suction line

6.3.2 Superheat variation

All superheat values are based on an evaporator outlet temperature measured in a pocket at the center of the outlet connection unless otherwise is stated.

An interesting phenomenon was experienced regarding the evaporator outlet temperature. There was one sensor in a pocket in center of the outlet and another at the outside surface of the tube, thoroughly attached with aluminum tape and insulted (see the Evaporator chapter for illustration). The two sensors measured different outlet temperatures and the difference varied with the conditions. Figure 83 shows the difference in the superheat, defined from the two sensors, when the compressor speed was varied and the superheat defined by the pocket sensor was kept constant. As discussed in the Evaporator chapter one explanation could be that the maldistribution increases with the mass flow and vapor fraction (i.e. higher inlet velocities) at the inlet so that more liquid hits the bottom surface of the outlet header. The saturated liquid keeps the tube surface cold whiles superheated vapor influences the pocket sensor. Figure 84 shows the superheat based on the pocket sensor and tube surface sensor. At 8 K superheat and above they measure similar values. For lower values the difference is larger until they become equal again at 2 K. It seems like the midrange superheat allows liquid overflow in some channels which cools the outside sensor more than the pocket sensor. At the lowest superheat, the amount of liquid droplets at the outlet is large enough to wet also the pocket. The calculated vapor quality at the inlet to the internal heat exchanger was one for all points in these measurements. This can be interpreted as if the maldistribution in the evaporator was not too bad after all. The lesson learned is that superheat is not easily defined

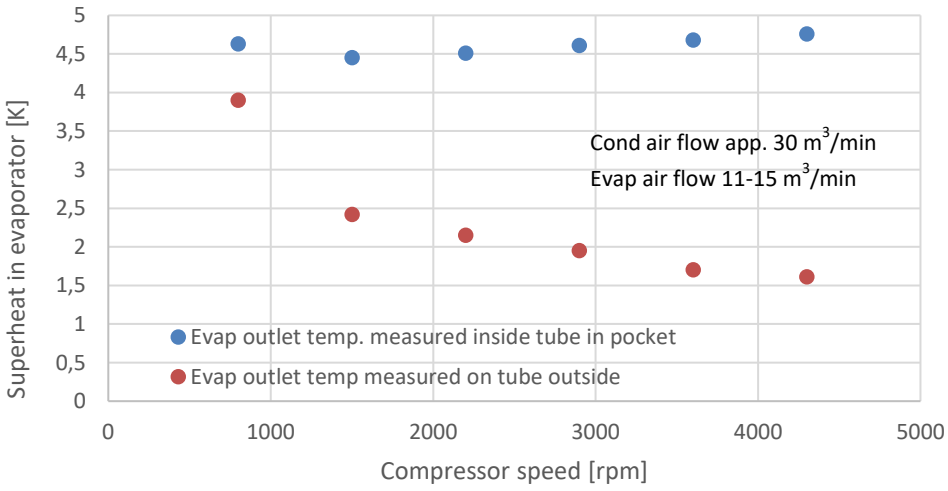

Figure 83. Superheat mesured with two methods at varied compressor speed

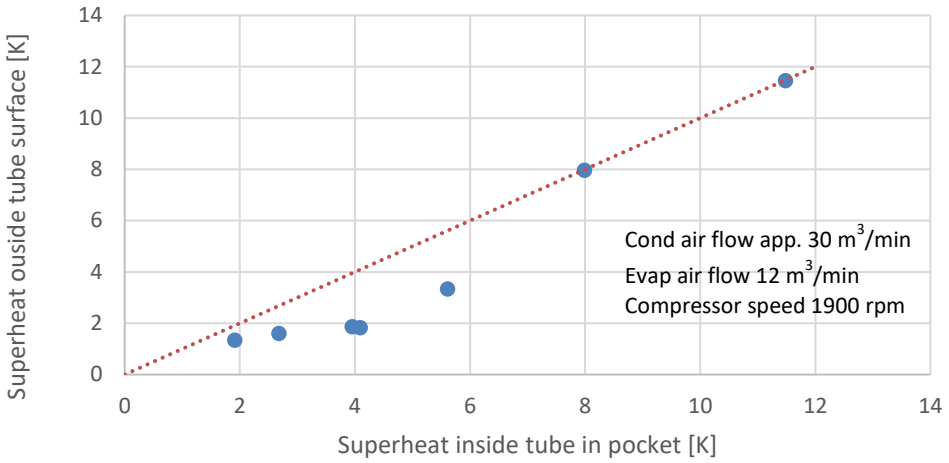

Figure 84. Superheat as recorded outside tube surface versus superheat measured in pocket

Figure 85 shows the change in subcooling with superheat. As discussed earlier, increase of superheat moves refrigerant to the condenser side of the system. Below 6 K superheat, the amount of liquid is increasing mainly at the end of the condenser tubes, providing good heat transfer for subcooling. Above 6 K, the change in inclination of the relation can be interpreted as that liquid starts to fill up the vertical outlet section of the condenser header, acting as a receiver, where the heat transfer is low. This happens in combination with continued decrease of available temperature difference for further subcooling.

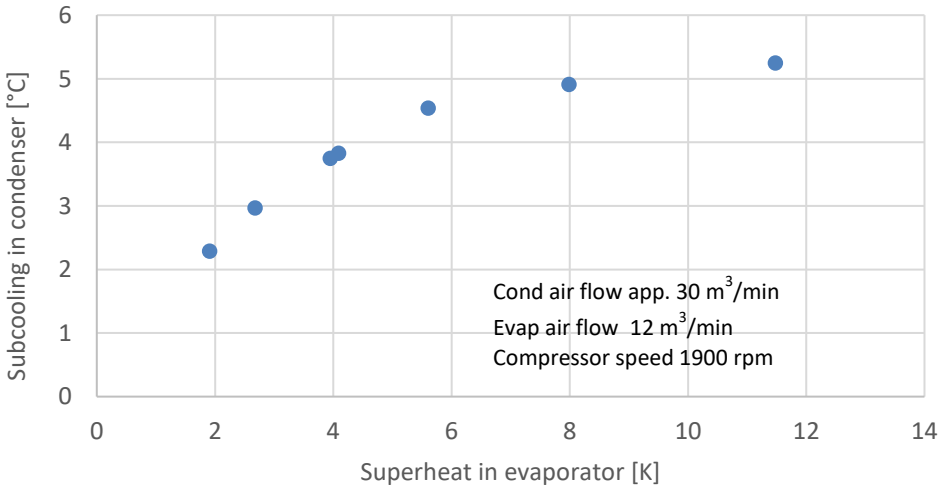

Figure 85. Change of subcooling with changed superheat

Figure 86 shows the influence on the evaporator UA-value, related to inlet temperature difference, from superheat. The continuity of the relation indicates (with reservation for the risk that you see what you want to see) that the distribution in the evaporator is even and that reduced superheat moves the liquid front evenly forward in the tubes.

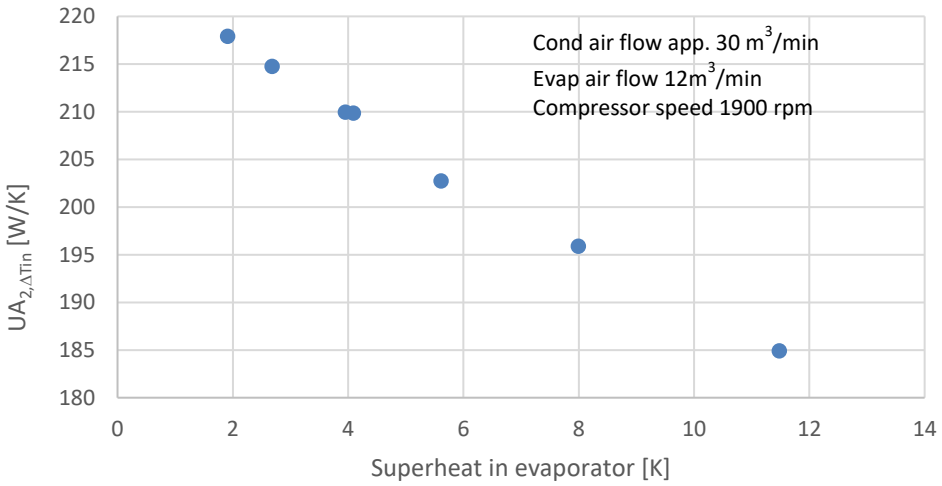

Figure 86. Change of subcooling with changed superheat

Figure 87 shows the influence from superheat on cooling capacity and COP_2. There is a continuous increase of performance with reduced superheat with no maximum.

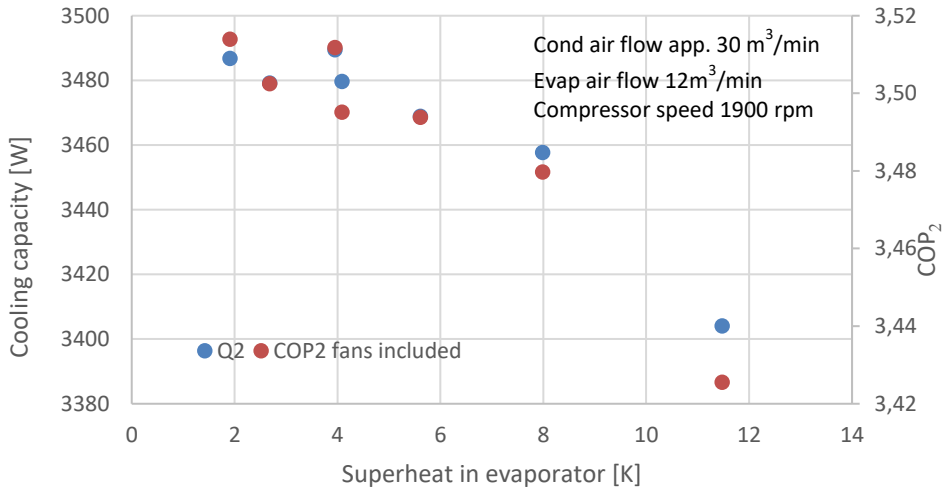

Figure 87. Cooling capacity and COP_2 with varying superheat

6.3.3 Air flow variation

Evaporator air flow variation

Figure 88 shows the evaporator heat transfer performance (UA_2-value) and the temperature difference between the evaporating and air inlet temperatures when the air flow is varied. UA_2 is referred to the inlet temperature difference. One should keep in mind that the evaporating temperature is increasing with higher air flows, lowering the latent heat load. Simultaneously the sensible heat (air side dry heat transfer) increases.

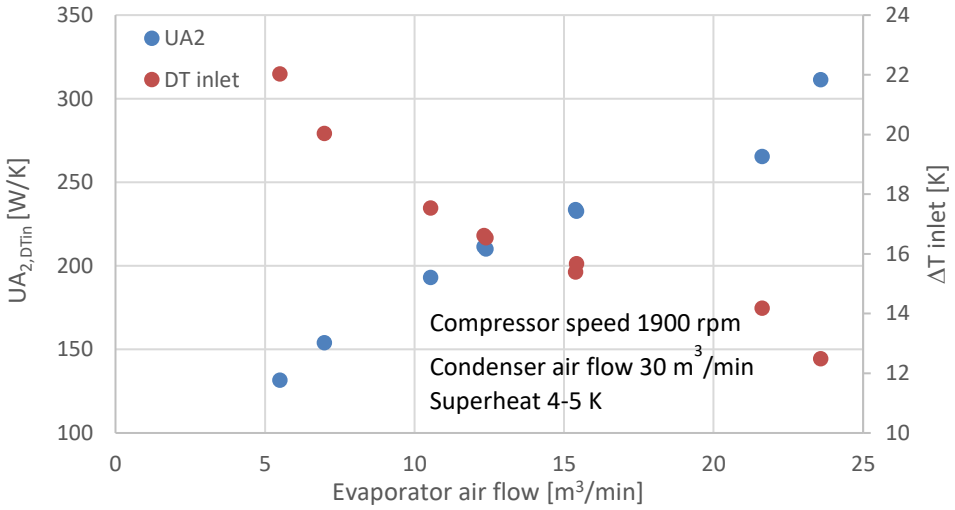

Figure 88. UA_2 and $\Delta T_{inlet}=T_{air,inlet}-T_{2sat}$ with varying evaporator air flow

Figure 89 shows the cooling capacity and COP_2 with evaporator air flow variation. It is a continuous increase and the optimum is for higher air flows.

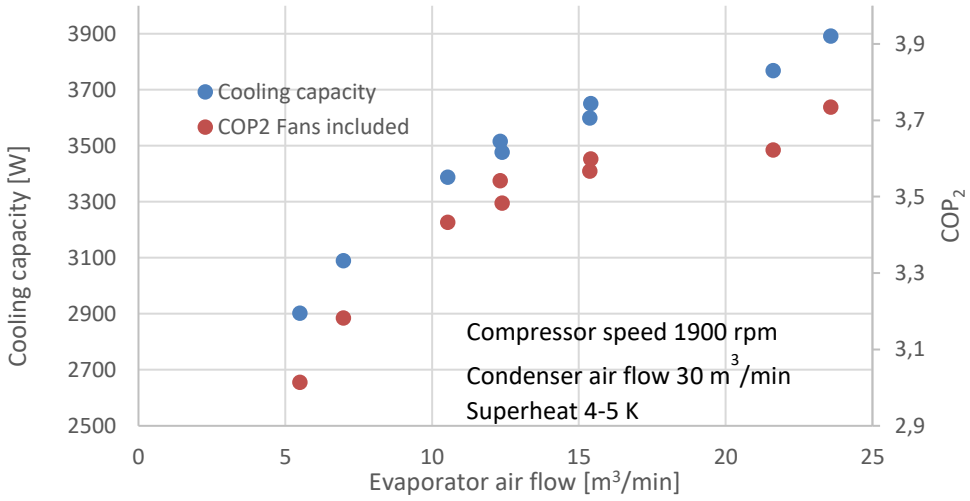

Figure 89. Cooling capacity and COP_2 with varying evaporator air flow

Figure 90 shows the evaporator electric fan power and the air side pressure drop over the evaporator. The lower fan power at maximum air flow can be explained by the fact that at the highest air flow, the evaporator temperature is passing the dew point, 14.9°C. The evaporator surfaces are dried.

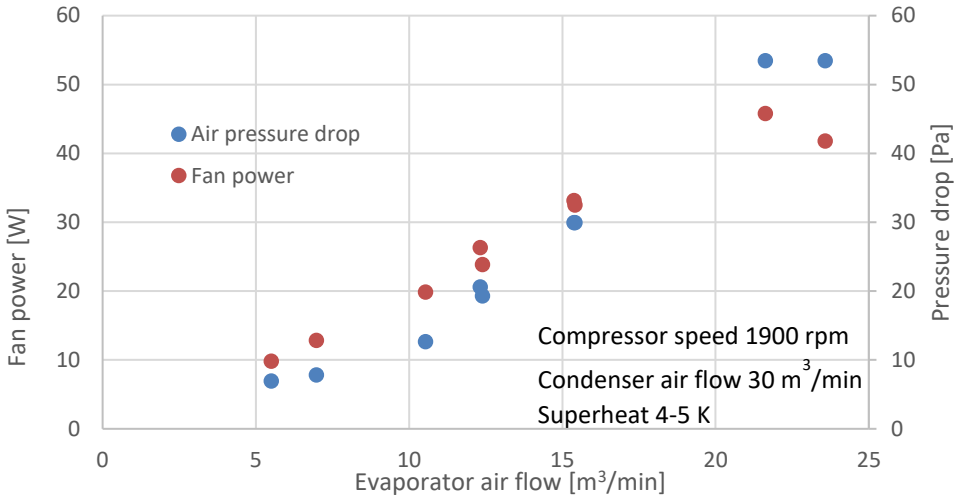

Figure 90. Evaporator fan power and air side pressure drop over evpaporator with varying evaporator air flow

Condenser air flow variation

Figure 91 shows the condenser heat transfer performance (UA_1-value) and the temperature difference between the condensing and air inlet temperatures when the condenser air flow is varied. UA_1 is referred to the inlet temperature difference.

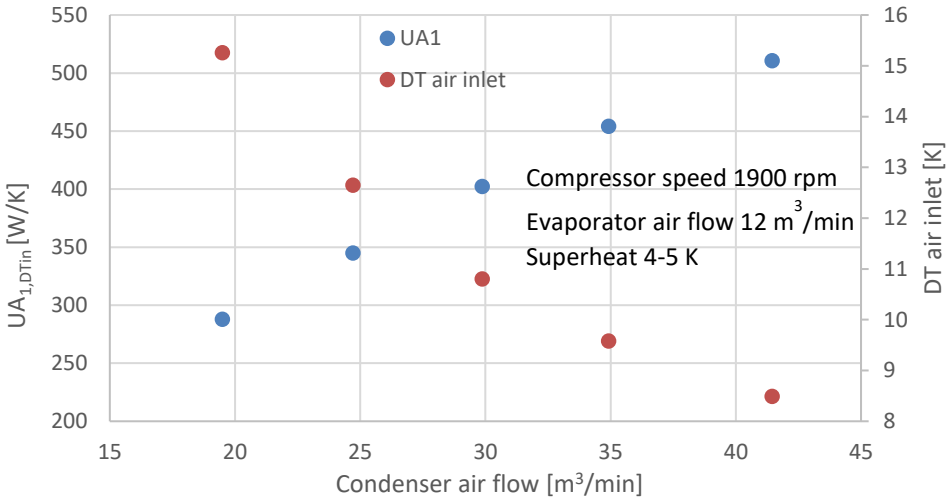

Figure 91. UA_1 and temperature difference between condensing temperature and air inlet temperature over condenser with varying condenser air flow

Figure 92 shows cooling capacity and COP_2 variation with condenser air flow. There is very little influence on the cooling capacity and the efficiency has an optimum at about 35 m^3/min which is close to the nominal air flow used, 30 m^3/min.

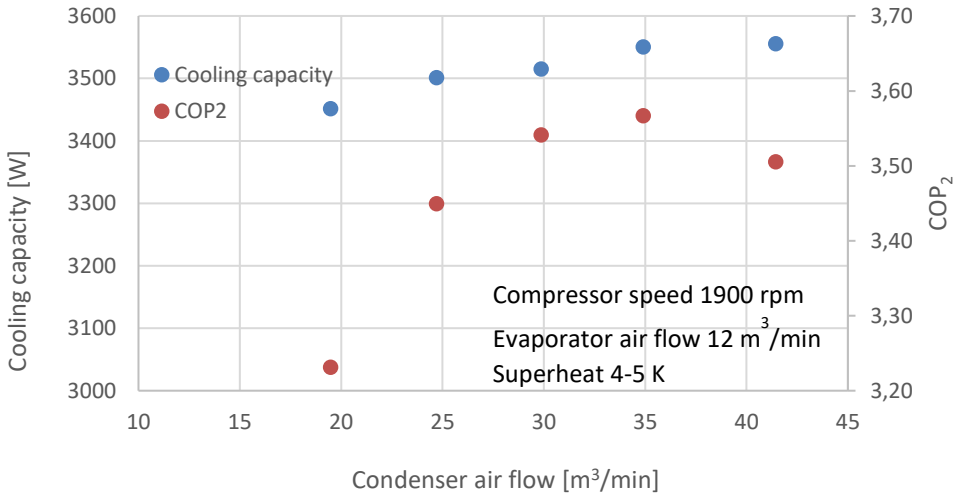

Figure 92. Cooling capacity and COP_2 with varying condenser air flow

6.3.1 Summary of Propac #2 results

The project target was met at 1900 rpm compressor speed, 13 m^3/min evaporator air flow and 30 m^3/min condenser air flow. The connection line in-between the indoor and outdoor unit was 6 m and the total refrigerant charge was 143 gram. The refrigerant side pressure drops were acceptable.

6.4 Internal heat exchanger performance

Figure 93 shows the performance of the internal heat exchanger, expressed as temperature effectiveness and UA-value related to the logarithmic mean temperature difference (LMTD), as function of the refrigerant mass flow. The data is taken from the test series where the compressor speed was varied keeping the superheat in the evaporator constant whiles the subcooling is increased with increased compressor speed. The corresponding capacity and superheat over the internal hex are given in Figure 94.

The temperature effectiveness is approximately 0.37 at 11.8 g/s, corresponding to 3.5 kW cooling capacity. This is much lower than the theoretical value, 0.57 calculated for an ideal case. At the lowest mass flow, the subcooling is below 1 K and it could be vapor condensation at the liquid side of the internal heat exchanger. This can possibly explain the high temperature effectiveness at the lowest mass flow.

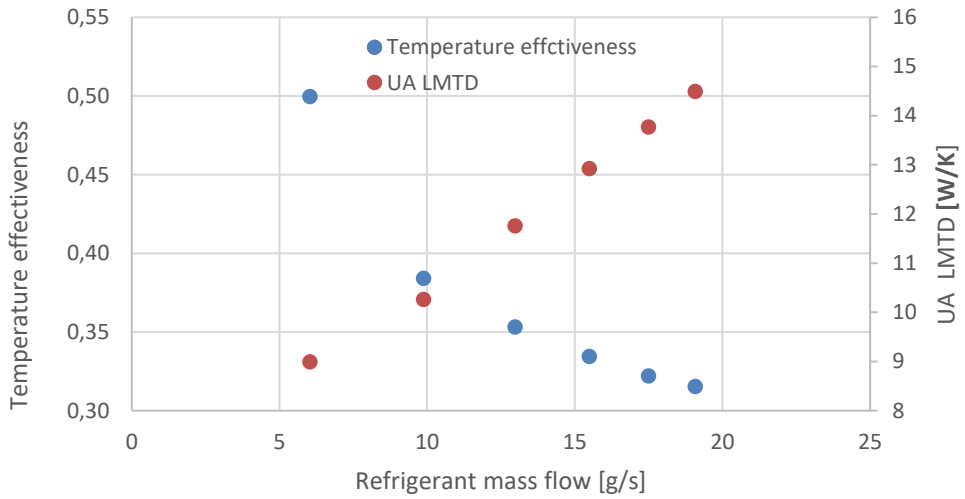

Figure 93. Performance of internal heat exchanger at varying refrigerant mass flow

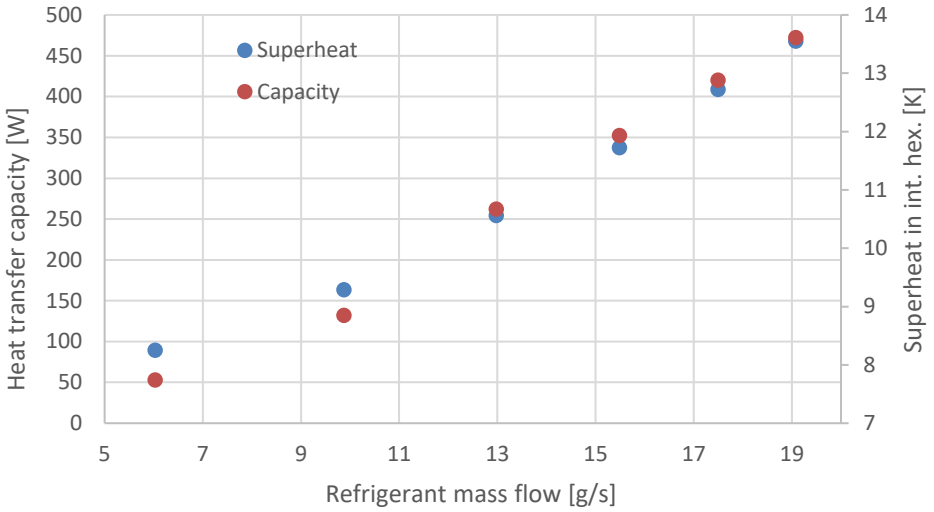

Figure 94. Internal heat exchanger capacity and superheat over internal heat exchanger at varying refrigerant mass flow

The pressure drop over the internal heat exchanger vapor side and corresponding decrease in saturation temperature is show in Figure 95. The pressure drop is acceptable.

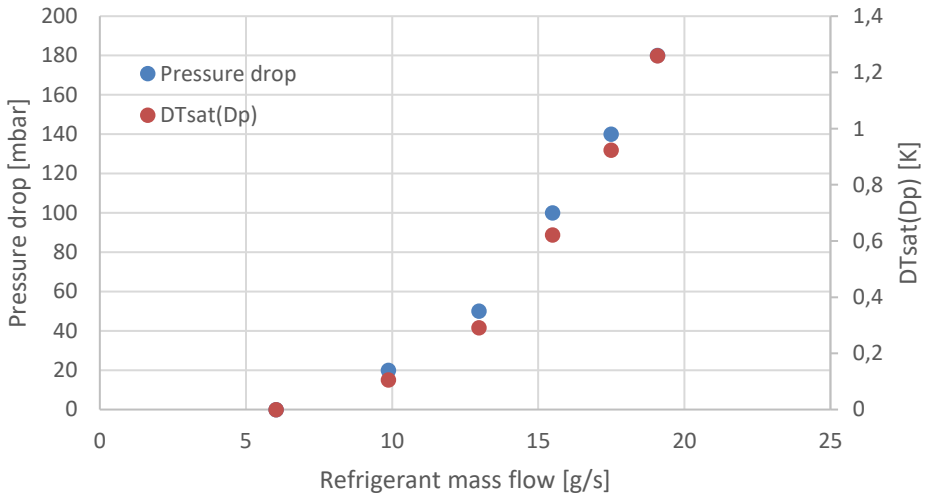

Figure 95. Pressure drop and corresponding reduction in sturation temperature over the internal heat excanger vapor side

6.5 Refrigerant distribution in evaporators

6.5.1 SD13 evaporator

The refrigerant distribution in the evaporator was estimated by using an infrared camera. The evaporator was painted black and the measurement was performed at dry conditions with the headers vertically. The compressor and fan speeds were both 1400 rpm and the measured superheat about 2 K. The temperature distribution over the evaporator is shown in Figure 96 and the corresponding sections of the evaporator are illustrated in Figure 97.

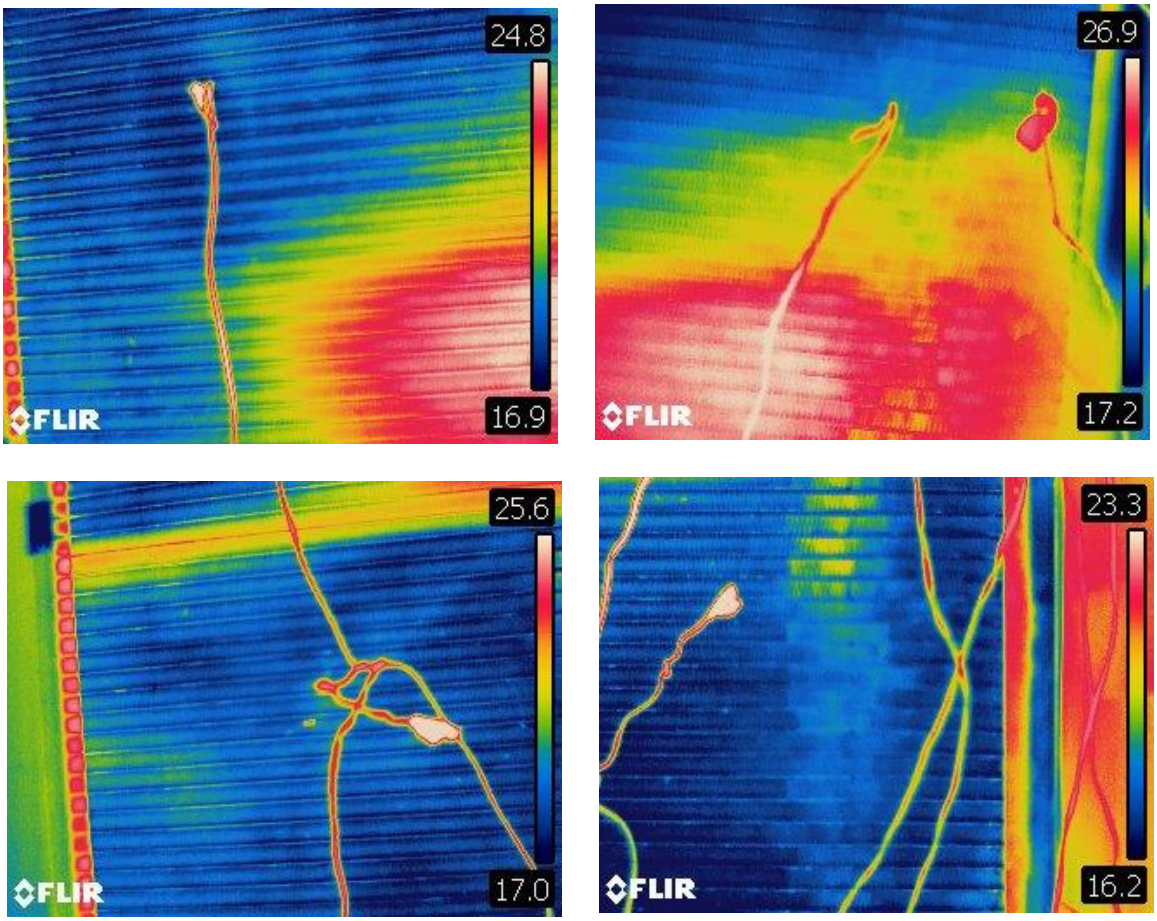

Figure 96. Refrigerant distribution in evaporator illustrated with infrared photos

The distance to the adjacent wall was very short why it was necessary to take four pictures to cover the entire surface. The pictures are overlapping at some location and there are gaps at others. This is not accurately measured but confirms the expected problems with even distribution. The lower half of the upper, outlet section is poorly fed with refrigerant. It seems reasonable to assume that inertia makes it hard for liquid droplets at high velocity to enter the first tubes in the second, upper section. In the lower, first section the distribution seems good enough to keep all tubes wetted.

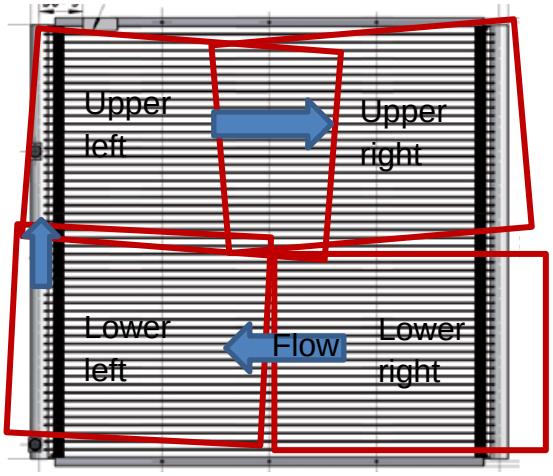

Figure 97. Evaporator sections in Figure 96

6.5.2 SD12 evaporator

The refrigerant distribution in the rebuilt SD12 evaporator was evaluated with infrared camera. The images are taken from the air outlet side and the surface of the evaporator is sprayed with black matt color. There were two distributers evaluated, A and B. The infrared camera used was a Flir One Pro, which is a unit that is attached to a smartphone. The accuracy is probably not the best so one should not pay too much attention to the absolute values but rather the distribution.

In Figure 98 the temperature distribution is illustrated at two different superheat values for distributor A. The inlet is at the top. The distribution is quite uneven where the yellow areas represent sections poorly fed, whereas the section that is blue down to the bottom outlet probably is over fed. The Max-Min temperature difference is somewhat smaller for lower superheat and the evaporating temperature is higher. This indicates better distribution and utilization of the evaporator.

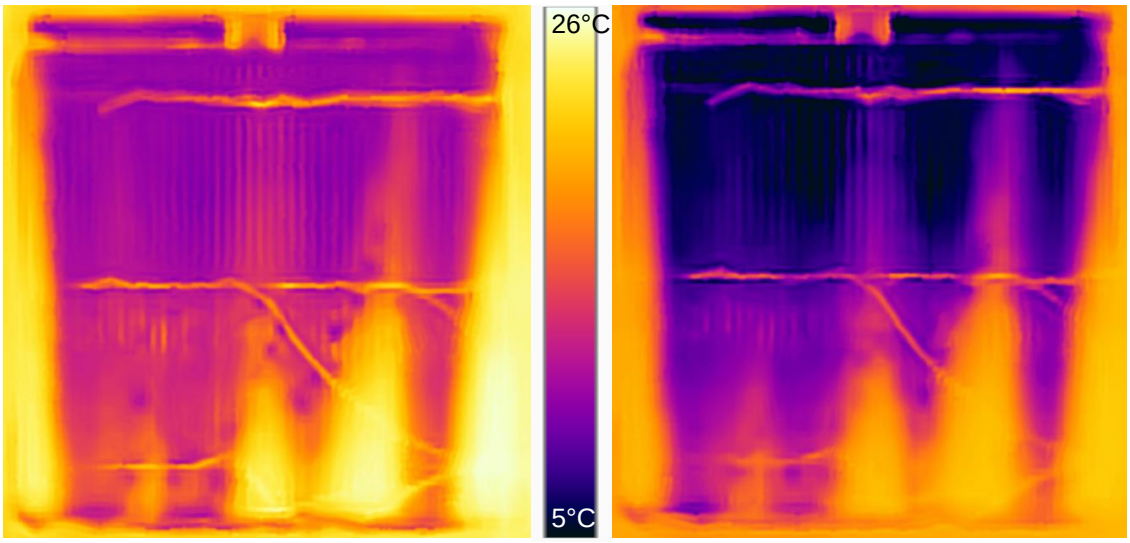

Sup.=1°C, Tair,in=26°C, T2sat=8.6°C
Max=25.5°C Min=9.1°C, Comp. 2000 rpm

Sup.=11°C, Tair,in=26°C, T2sat=6.8°C
Max=22.0°C Min=3.0°C, Comp. 2000 rpm

Figure 98. Refrigerant distribution in rebuilt SD12 evaporator at different superheat values – distributor A

Figure 99 shows the SD12 evaporator with distributor B. The distribution generally looks more even than for distributor A. The right side seems to be starved. It is hard to see any difference between 1.9 and 4.3°C superheat. A slightly worse distribution can be seen for 12.6°C superheat. If any difference, the distribution is a little more even for the higher flow rate, at 2500 rpm compressor speed, than for 2000 rpm.

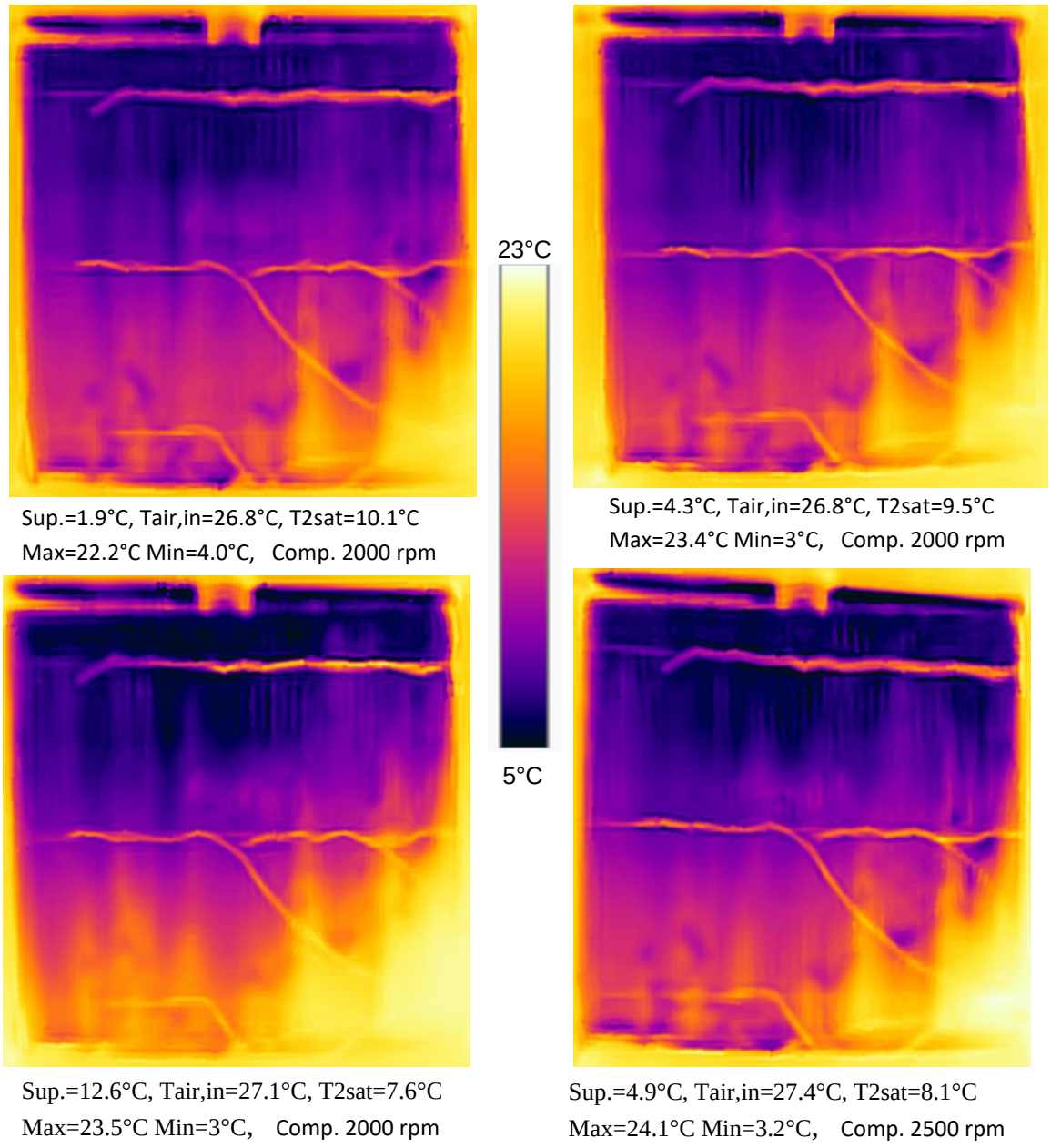

Figure 99. Refrigerant distribution in rebuilt SD12 evaporator – distributor B

Figure 100 shows the UA_2 values variation with the superheat (related to the inlet air temperature difference) for SD12 with distributor A and B respectively. The data is for similar conditions. Figure 101 and Figure 102 show the corresponding cooling capacity and COP_2. These tests are performed at the KAE site where the accuracy is not very good why only the relative differences should be considered, not absolute values. The differences are small (watch the scales) but the distributer B seems to be performing better than A.

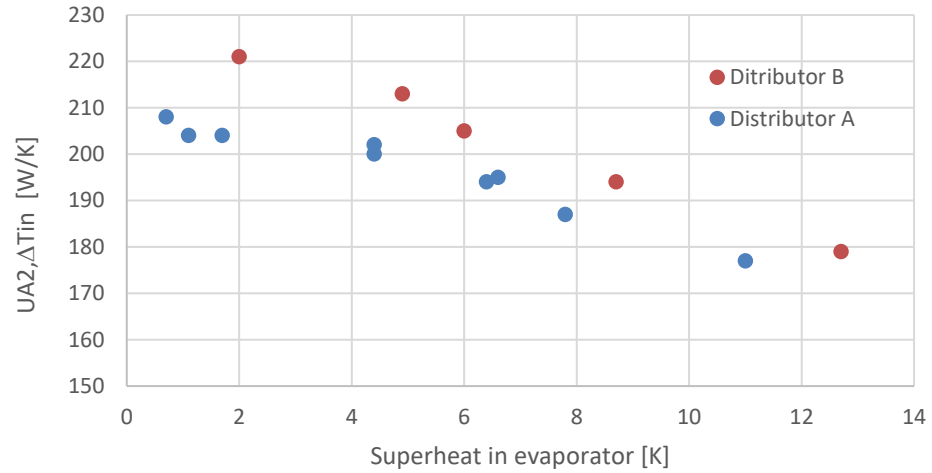

Figure 100. UA_2 values for distributor A and B at varying superheat

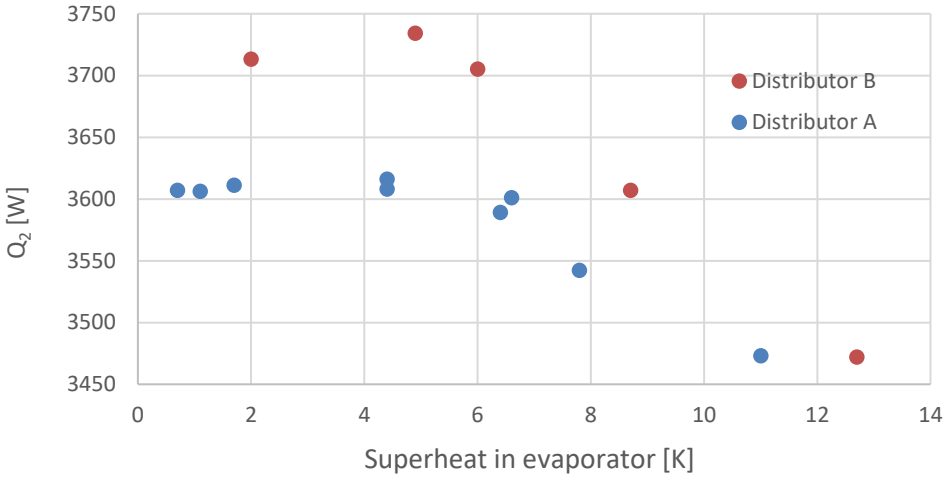

Figure 101. Capacity (Q_2) values for distributor A and B at varying superheat

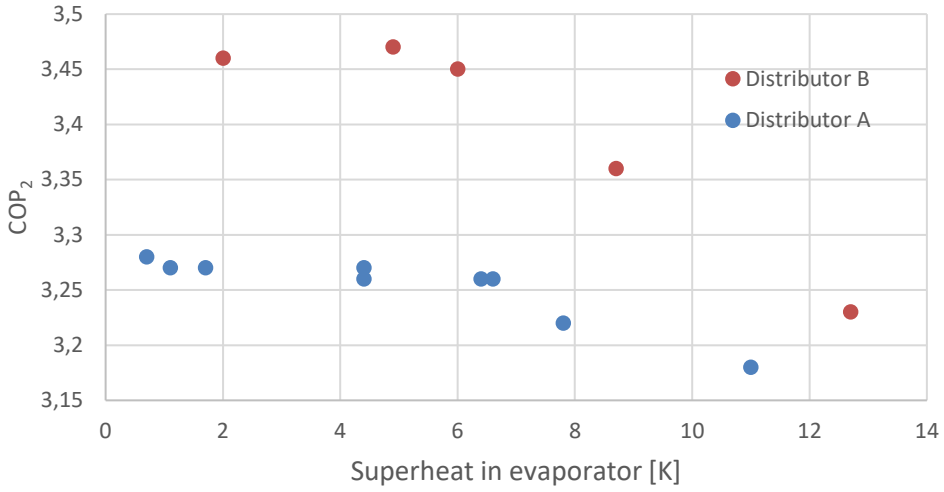

Figure 102. COP_2 values for distributor A and B at varying superheat

6.5.3 Z021 evaporator

Figure 103 illustrates the distribution from the air outlet side of the rebuilt Z021 evaporator with Sanhua distributor. The evaporator was not sprayed with color why the coefficient of emission is uncertain and consequently also the temperatures. The inlet is at the top and the distributor outlets are directed horizontally in counter direction of the air flow as illustrated in Figure 103. The distribution looks relatively even. The right side, closest to the in and outlets, seems to have lack of refrigerant.

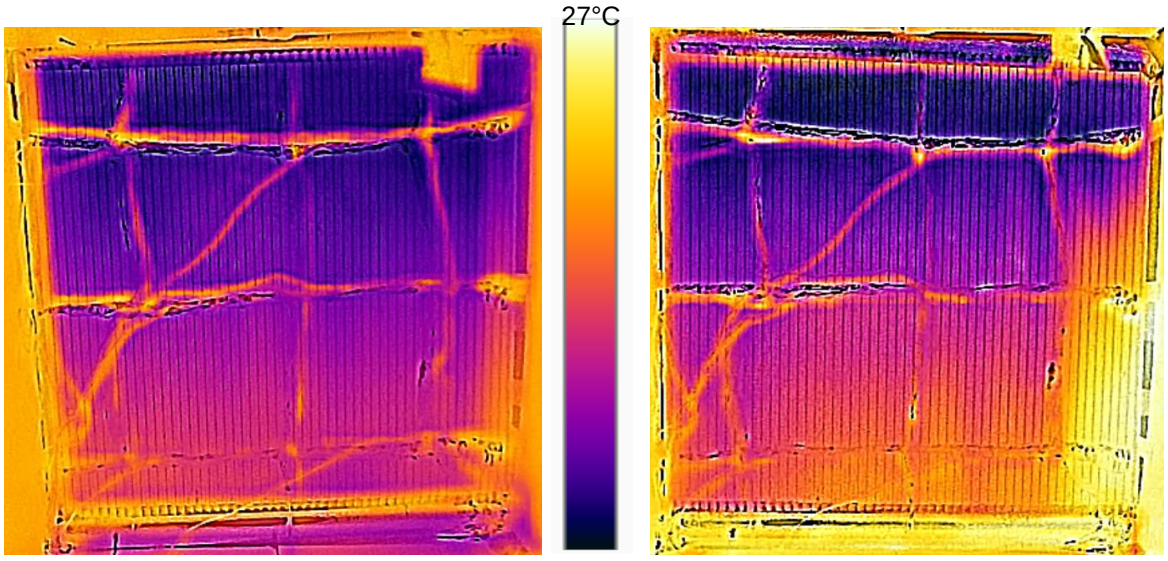

Sup.=4.6°C, Tair,in=26.1°C, T2sat=10.5°C
Max=25.1°C Min=8.6°C, Comp. 2000 rpm

Sup.=8.4°C, Tair,in=25.7°C, T2sat=8.2°C
Max=27.7°C Min=7.9°C, Comp. 2000 rpm

Figure 103. Refrigerant distribution in rebuilt Z021 evaporator at different superheat – Sanhua distributor

The outlet, bottom header for 4.6°C superheat seems quite cool, indicating liquid overflow. One hypothesis is that more refrigerant enters the channels on distributor outlet side and at the bottom, where a liquid pool might accumulate. Less is entering the opposite side of the distributor outlet, see Figure 104. This was the original arrangement of the distributer, made for tubes sticking in and injection from the bottom. For that case a bottom liquid pool might make the refrigerant enter more equally into the channels.

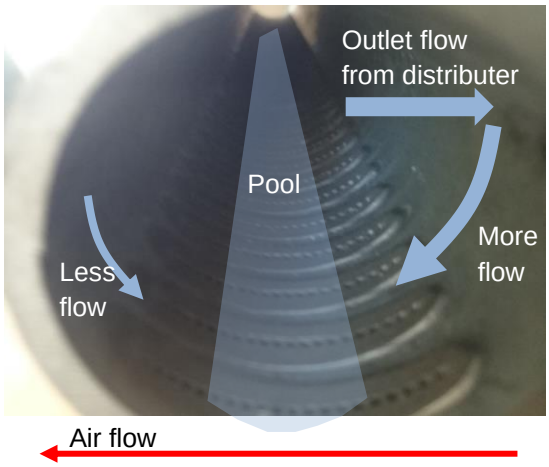

Figure 104. Illustration of hypothesis for maldistribution in Z021 due to direction of outlet flow from distributor

So even though it looks good on the infrared image, there might be overflow of liquid in channels further inwards. In the Z021 there are 20 channels in each tube.

6.6 System control

It was most of the time possible to get stable operation with very low superheat. At some situations though, oscillations of the superheat, and corresponding sub cooling was experienced. It was not systematically investigated, but it might be related to conditions with remaining liquid at the inlet to the internal heat exchanger vapor side. A hypothesis is that evaporation in the internal heat exchanger vapor side amplifies the reconnection to the liquid side by additional subcooling, reducing the restriction over the expansion valve. If so, even distribution in the evaporator, so that low superheat can be combined with high vapor fraction at the evaporator outlet, becomes extra important.

At normal situations, with no or very small oscillations, changes in the system (compressor speed, fan speed or expansion valve setting) could be made after which a new stable operation point was established more or less instantly. The high refrigerant mass flow rate, about 12-13 g/s, in relation to the total charge causes maldistribution of the refrigerant in the system to develop in seconds. This puts heavy demands on the control system. It is important to avoid that gas bubbles follow the liquid at the condenser outlet which potentialy introduce a risk of short-circuiting heat transfer between condenser and evaporator side. Despite the potential short circuiting over the internal heat exchanger, it provides extra control margin against harmful liquid entering the compressor.

The risk for short circuiting by non-condensed vapor bubbles exiting the condenser (and thus entering the internal heat exchanger) is minimized if enough subcooling is ensured in the condenser in all operation points. The system refrigerant charge has a strong influence on the condenser subcooling. Therefore a correct refrigerant charge and appropriate control of the system is important.

6.7 Tests of original evaporator Z021 in Propac #1

Earlier in the project, the Z021 evaporator in its original version was tested with the outdoor unit used in Propac #1, including the 3 m fastpipe hoses. The result from these, earlier tests are given in this chapter.

Figure 105 shows the Z021 mounted in the Propac #1 evaporator arrangement, with the radial fan and conical ducting. The refrigerant inlet is at the bottom. The evaporator is in its initial version with the tubes sticking in inside the headers as illustrated in the small photo, inserted in the upper left corner, in Figure 105. The orignal Z021 evaporator mounted in the Propac #1 indoor unit.

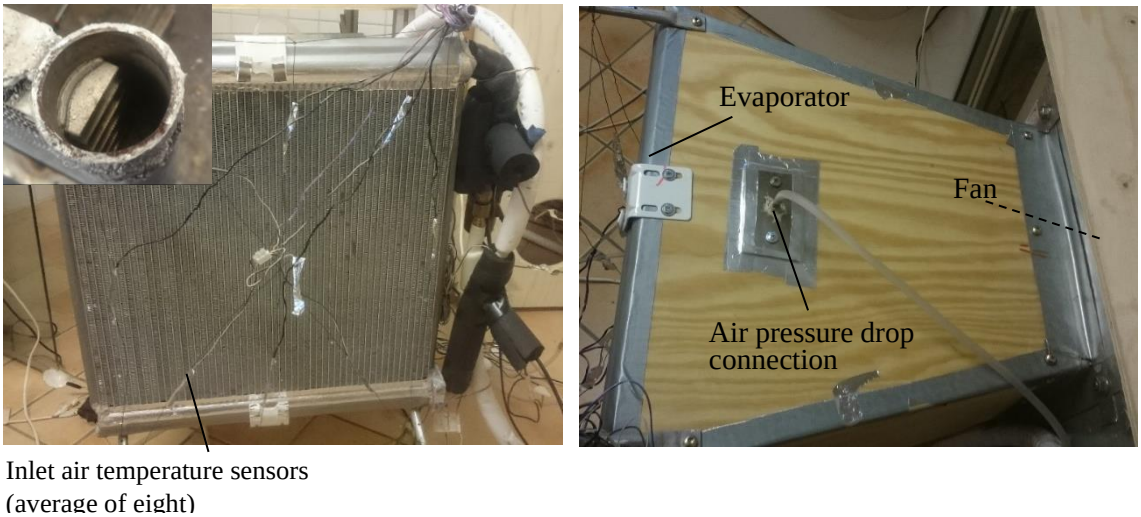

Figure 105. The orignal Z021 evaporator mounted in the Propac #1 indoor unit

The test was set up to be a direct comparison with SD13, all other part of the system unchanged. The total system refrigerant charge with the SD13 evaporator was 150 g. At that charge there were no subcooling after the condenser for the Z021 while the superheat after the evaporator was very large (>20 K). This indicates lack of refrigerant in the system. The charge was thereafter increased in steps to achieve some subcooling after the condenser in combination with a few degrees superheat after the evaporator. It ended up with 180 g. This filling sequence is illustrated in Figure 106. The compressor speed was 2000 rpm and the evaporator airflow was 12 m^3/min. At 180 g the compressor speed was increased. The subcooling was then increased and a reasonable combination of the combination of subcooling and superheat was possible to achieve. There are two possible explanations to this 1) As the compressor speed increases the evaporating temperature is decreased. The corresponding lower charge (lower density and higher vapor fraction) on the suction side increases the amount of liquid in the condenser. 2) Higher flow rates change the flow patterns in the evaporator

headers. Less separation of liquid and lower levels of liquid pools make more refrigerant available.

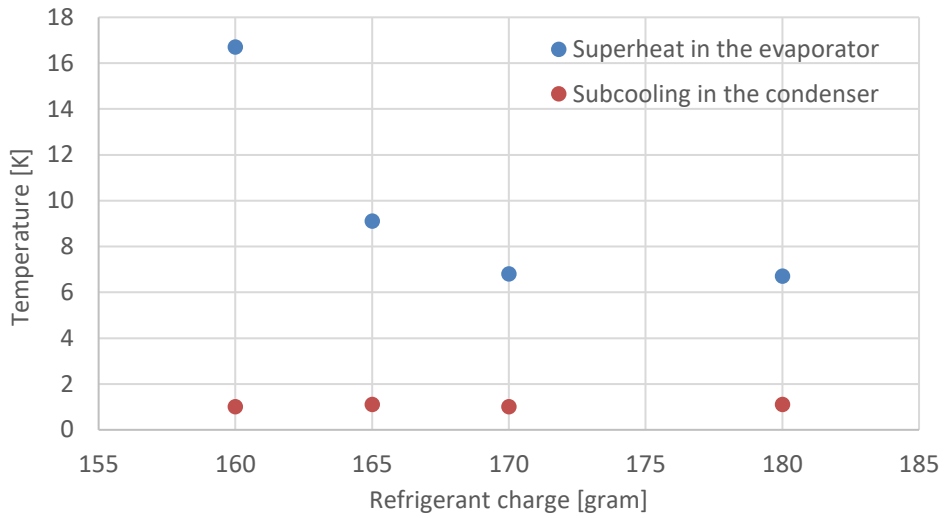

Figure 106. Superheat and subcoling in the Z021 evaporator as charge is increased.

To evaluate these explanations, a test series was performed where the compressor speed was varied with 160 g of charge. This is illustrated by the screenshot of the EasyView plot in Figure 107. The compressor speed is varied between 2000 and 3000 rpm. At 2000 rpm there is a shortage of refrigerant, which is evident from the combination of high superheat and low subcooling. At 3000 rpm, the difference between the superheat and subcooling is much smaller. The corresponding variation in evaporating temperature is relatively small. This indicates that explanation 2) is dominant.

The conclusion from this test was that the evaporator in its original version required too much charge to meet the project target. Its performance was therefore not further evaluated. Instead, it was decided to remove the part of the tubes that protrude into the headers.

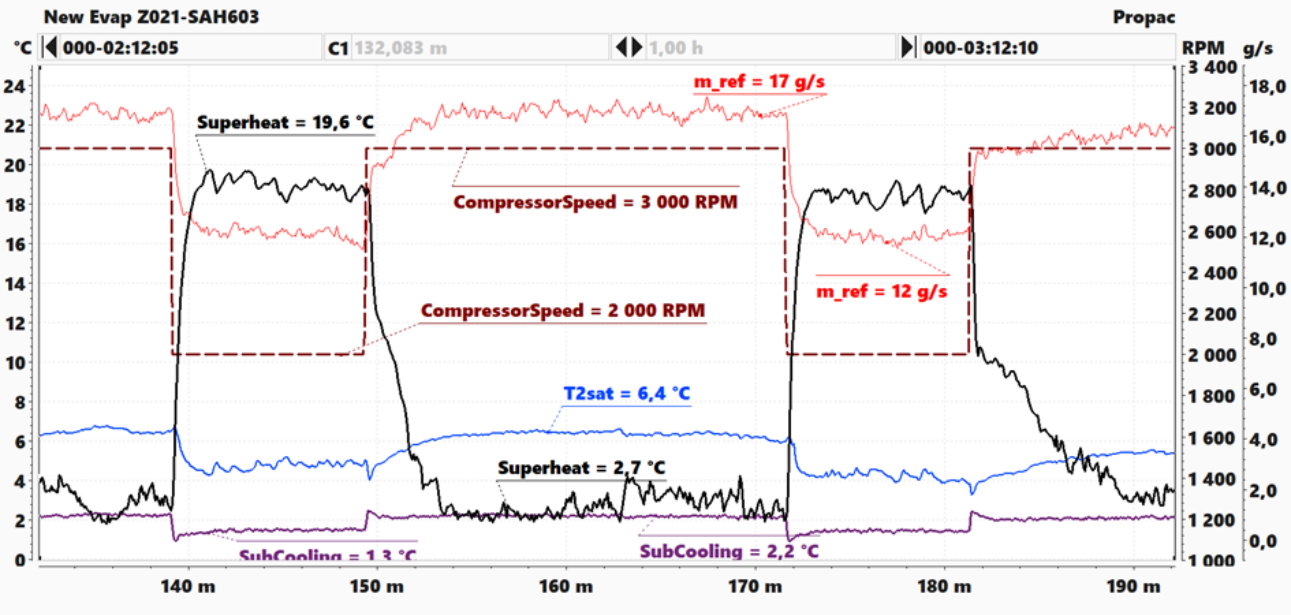

Figure 107. Superheat and subcoling in the Z021 evaporator as compressor speed is varied with 160 g of charge.

6.8 Propac #3

Propac #3 was built at the very end of the project. There was too little time to complete all details in a good manner. It was therefore only possible to perform some initial tests from which the results are doubtful. It mainly reveals some errors that need to be corrected.

- The pressure drop over the suction line was very high indicating some blockage.
- There seem to be a large overflow of liquid, not only through the evaporator, but also through the internal heat exchanger, resulting in liquid at the inlet to the compressor. That captures a lot of extra charge.
- At low superheat, the overflow of liquid in the evaporator drained the condenser so that remaining vapor condensates in the internal heat exchanger liquid side. This is a thermal short-circuiting of the system, reducing its performance.

The question was if the result from Propac #3 should be included at all. For the purpose to at least learn from these trials and errors, some results are given in the following together with some discussion on possible explanations to the phenomena experienced.

Propac #3 is a total rebuilt of Propac #2. The evaporator used was the rebuilt Sanhua Z021 with the axial fan and corresponding assembly unit from ebmpast. The outdoor unit was totally rebuilt to fit in to the standard architecture of an outdoor unit. The SD13 condenser was mounted with the axial fan in the assembly unit provided by ebmpast. The filter dryer was removed. The same 6 m connection hoses were used as in Propac #2.

The refrigerant charge was 155 gram for all tests in this chapter.

6.8.1 Compressor speed variation

In this test series both the speed of the compressor and the fans were varied. The superheat was approximately 6 K. Figure 108 shows the combination of compressor

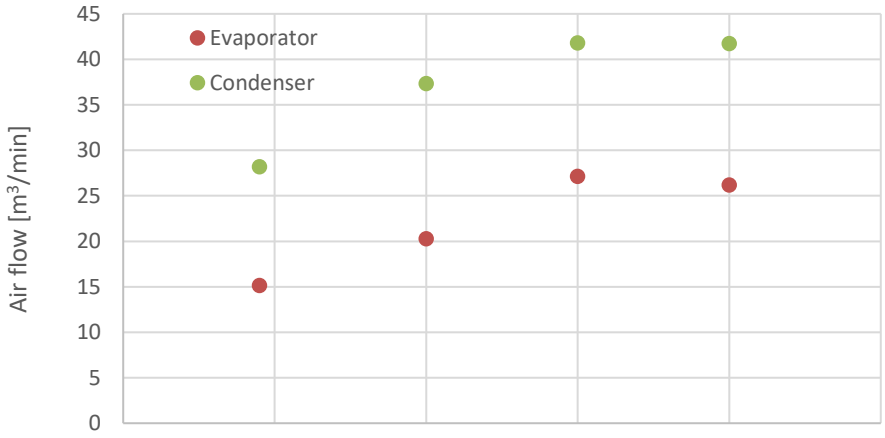

Figure 108. Combination of compressor speed and fan air flows for the Z021 test series in this chapter

speed and fan air flows. At the compressor speed 4000 and 5000 rpm, both fans were operating at their maximum setting. As a consequence of lower evaporating temperature at 5000 rpm, more water condensates on the evaporator, restricting the flow.

Figure 109 shows the cooling capacity and COP_2 for these combinations of compressor speed and air flows.

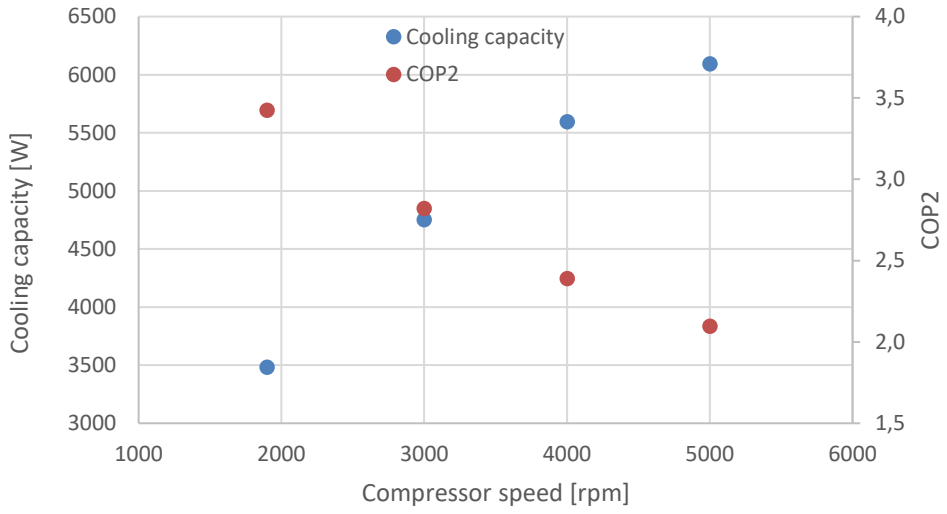

Figure 109. Cooling capacity and COP_2 for the combination of compressor speed and air flows.

Figure 110 shows the heat transfer performance for the evaporator at the combinations of cooling capacity and air flows given in the earlier figures.

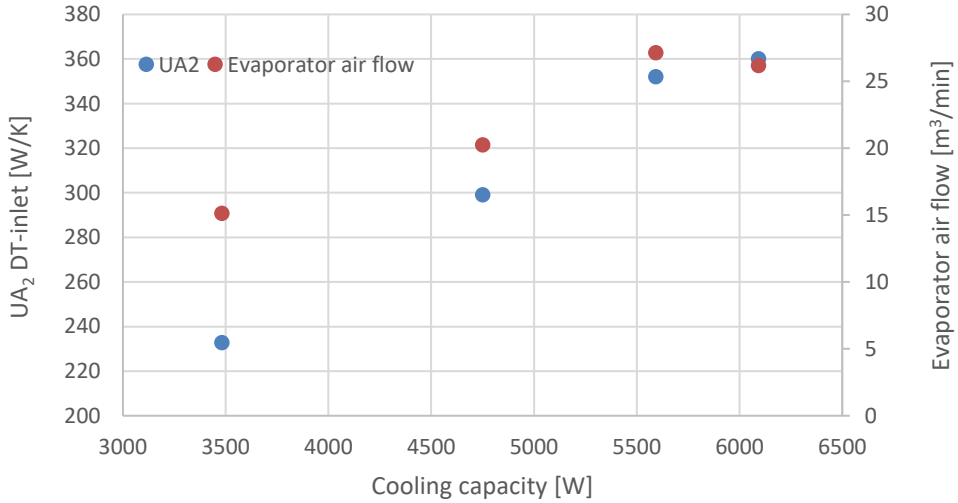

Figure 110. UA_2 for the combination of compressor speed and air flows.

Figure 111 shows the refrigerant side pressure drop over the evaporator. It is much higher than for the SD12. It could be that the connection of the differential pressure meter into the inlet header is hit by refrigerant at high velocity resulting in extra dynamic pressure. During real time measurement, large fluctuations in the pressure can be seen, indicating high degree of turbulence.

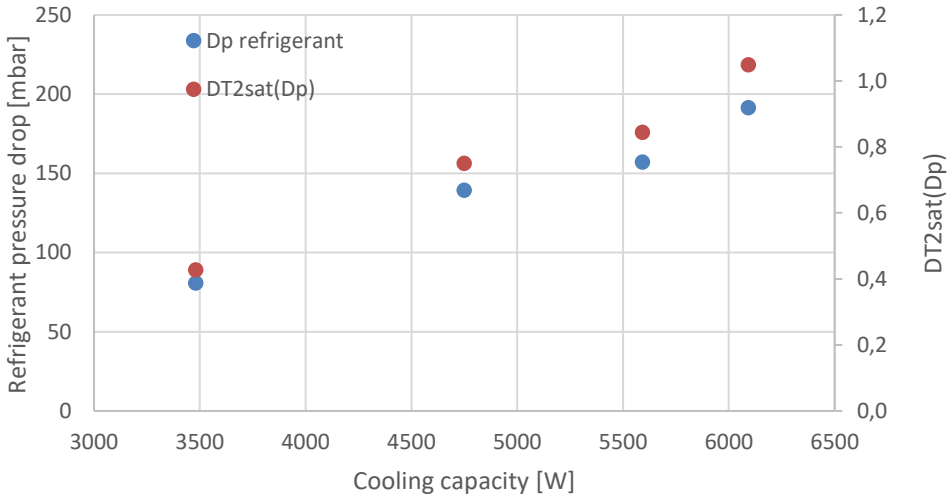

Figure 111. Pressure drop over the refrigerant side of the Z021 evaporator .

Unfortunately, the pressure drop in the suction line, from the evaporator outlet to inlet of the internal heat exchanger, had a very high pressure drop as shown in Figure 112. There is no reasonable explanation for this. It is much higher than the expected flow friction pressure drop. It might be some blockage. It could be a copper washer, used in the connections, that is misplaced. This pressure drop is devastating for the system performance. The capacity and COP_2 are typically reduced with 2-3% per degree reduced evaporating temperature.

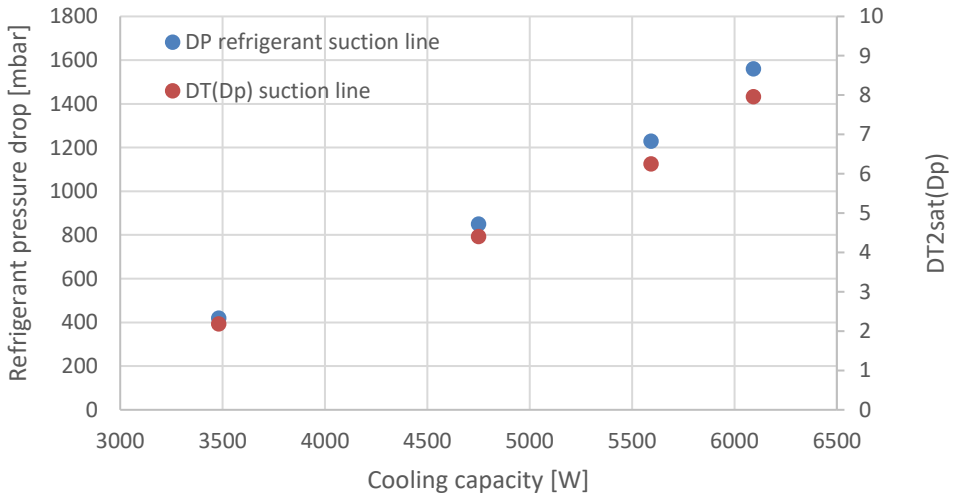

Figure 112. Pressure drop over the suction line. Evaporator to internal heat exchanger

6.8.2 Air flow variation

Only the evaporator air flow was varied since the condenser is the same as in previous tests. The condenser air flow is 28 m^3/min, the compressor speed is 1900 rpm and the superheat in the evaporator is 6 K for results given in this chapter.

Figure 113 shows the air side pressure drop over the Z021 evaporator as function of the air flow. The blue curve is for a test series at wet, standard conditions and the red curve is at dry conditions, where the evaporator temperature is above the dew point at all times. The pressure drop for the wet case has a discontinuous jump at 20 m^3/min. This corresponds to when the evaporator surface temperature passes the dew point (15.5°C). After that the evaporator surfaces dries and the dry and wet values become equal.

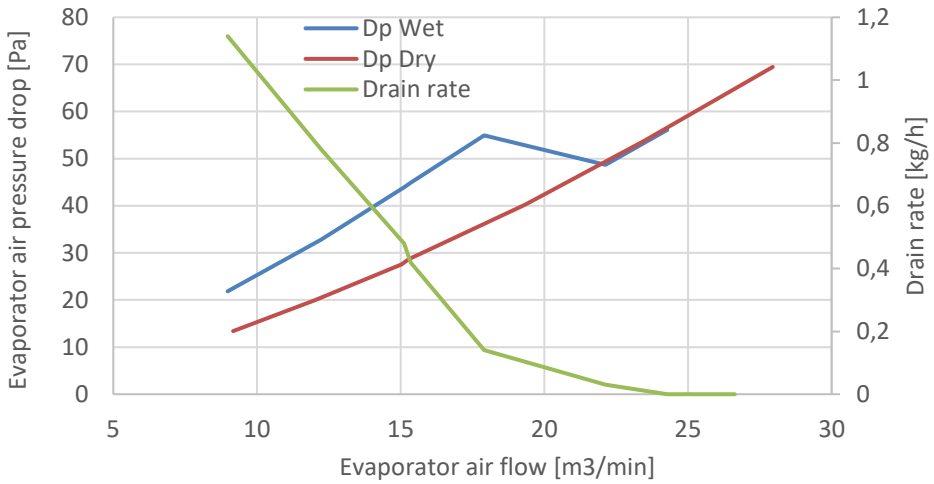

Figure 113. Air pressure drop over Z021 at wet and dry condtions with air flow variation. The green curve is the drain rate of water for the wet case.

Figure 114 shows the evaporator UA-value for the wet and dry conditions. The differences are small. For the dry case there is no water layer, reducing heat transfer from the air to the fin surface. For the wet case, latent heat transfer is added and liquid blockage increases the air velocity for given air flows, increasing the heat transfer coefficient. It seems that these phenomena compensate each other. Though it might be a weak tendency to the benefit for the wet case at the lowest air flows.

The small difference at higher air flows might be explained by the fact that there is still some water left on the fins that have not yet dried, coming from lower air flows with condensation. A lesson learned is to perform the test series coming downwards from the higher airflows. The reasons the UA-value may be affected by remaining water but not the pressure drop is probably that the remaining water mainly is located to the small gaps in-between the fin louvers. This gives a negligible blockage of the air flow but reduces heat transfer somewhat. It could be tempting not to report these results, which seems to be a mistake in the experimental routines. But perhaps this lesson learned

could be made use of in a real application as described in the following. The UA-values for the Z021 evaporator are quite similar to those for the SD12.

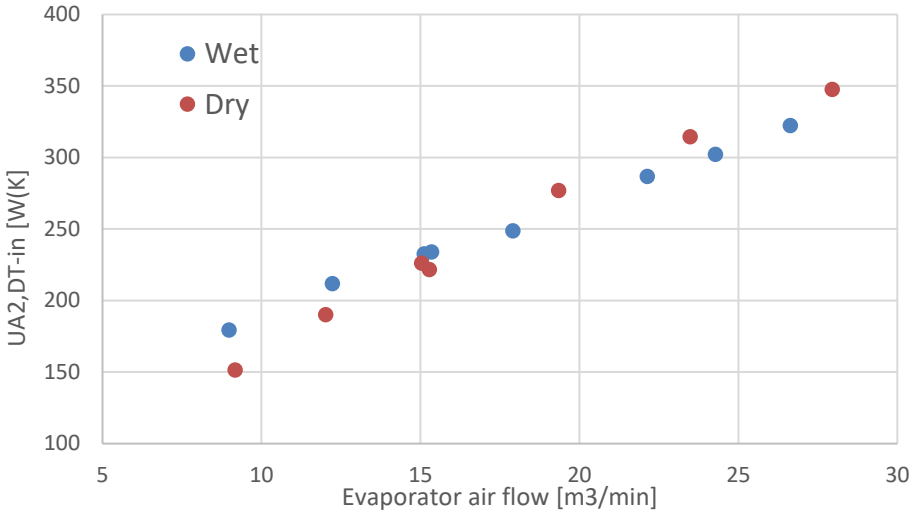

Figure 114. Heat transfer peformance for Z021 at wet and dry condtions for variation in air flow

Figure 115 and Figure 116 show the corresponding cooling capacity and COP_2 variation for wet and dry conditions respectively. The performance could be expected to be equal above 20 m^3/h, where there is no water condensation also for the wet case (drain rate zero in Figure 113). But they are not. If the explanation is remaining water, a short sequence with low compressor speed and high evaporator air flow would push up the evaporator temperature and make the fins dry more quickly. Thereafter the system can operate more efficient with dry fins.
The target performance, 3.5 kW cooling capacity and COP_2 3.5 at 15 m^3/min air flow are just reached. For dry conditions, a maximum of the COP_2 is reach at about 20 m^3/min. The cooling capacity seems to have its maximum above 30 m^3/h.

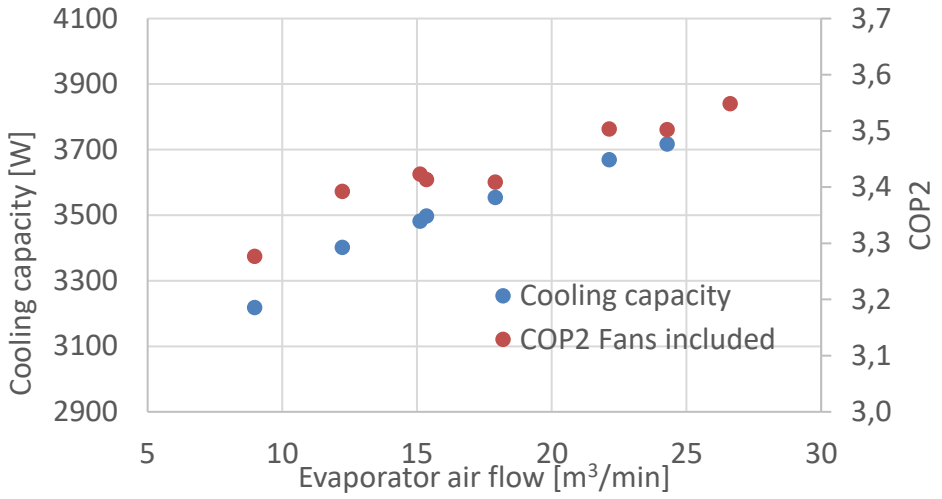

Figure 115. Cooling capacity and COP_2 at wet conditions for variation in air flow

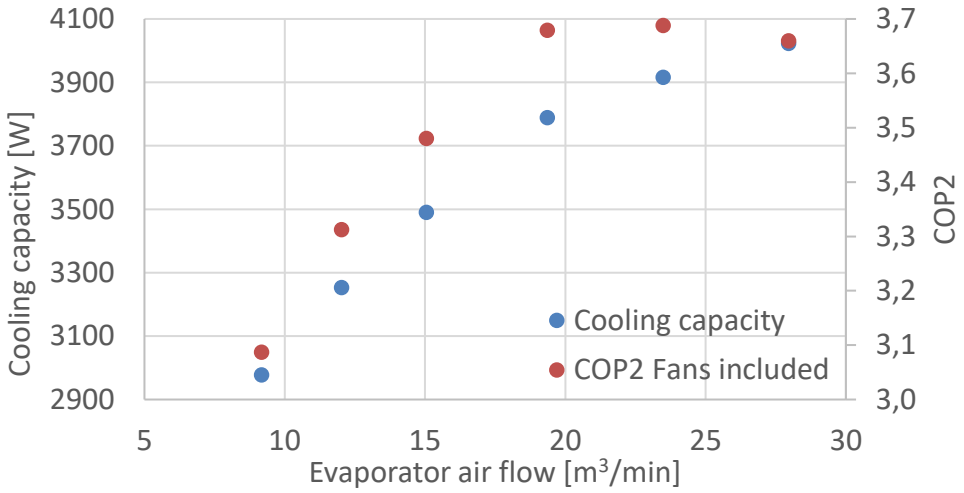

Figure 116. Cooling capacity and COP_2 at dry condtions for variation in air flow

Considering the large pressure drop in the suction line, the system is actually quite efficient.

6.8.3 Superheat variation

The tests in this chapter are performed with the compressor speed 1900 rpm, evaporator air flow 15 m^3/min and condenser air flow 28 m^3/min.

Figure 117 shows the cooling capacity and COP_2 as a function of the superheat in the evaporator at wet, standard conditions. The dependence is very small except for the lowest superheat that stands out. The reason for this is most likely remaining vapor at the outlet of the condenser that condensates at the liquid side of the internal heat exchanger, short circuiting the system. This is further discussed and explained in the "Heat balance considerations" chapter. This point is to be neglected.

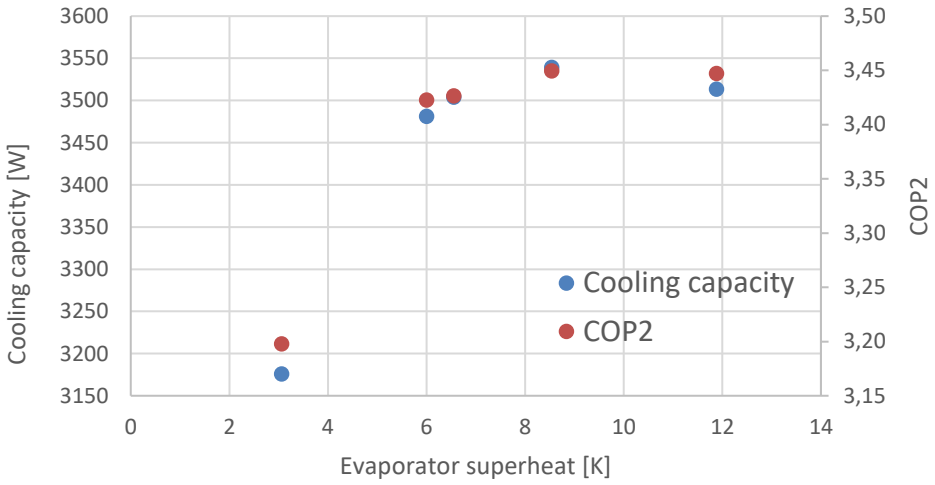

Figure 117. Cooling capacity and COP_2 variation with superheat for Z021 at wet conditions

6.8.4 Heat balance considerations

In order to validate the measurements and performance the refrigerant mass flow rate was calculated based on 1) the cooling capacity (Q_2), 2) condenser capacity (Q_1) and 3) compressor electric input power, assuming a fraction x of the power to be transferred to the refrigerant (Ec·x). From earlier measurements this fraction is estimated to be 0.87. Q_2 and Q_1 are based on the air flow and enthalpy change of the air over the respective heat exchangers.

Figure 118 shows the refrigerant mass flows calculated in these three ways for a test series when the superheat was varied. The mass flow based on the compressor capacity deviates from the two others significantly.

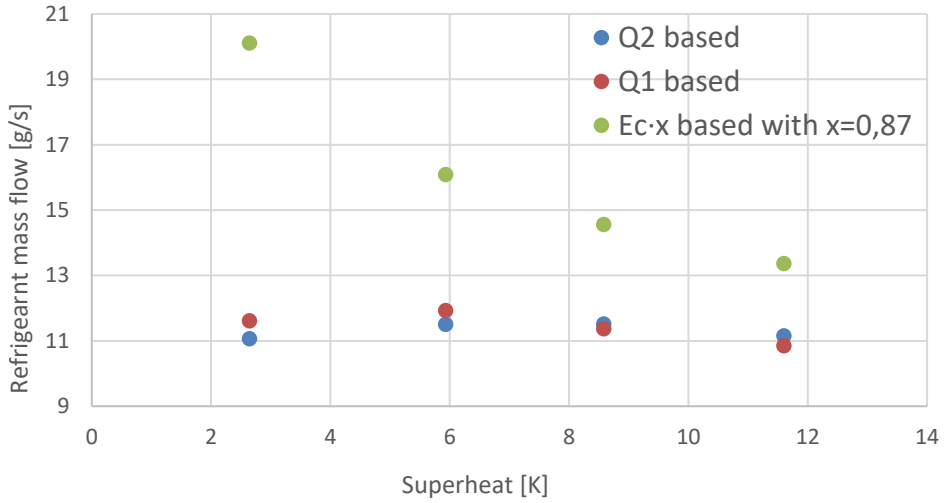

Figure 118. Refrigerant mass flow calculated in different ways assuming dry vapor at compressor inlet

Table 22.

Quality at compressor inlet	0.917	0.950	0.963	0.970
Quality at condenser outlet	0.035	0.000	0.000	0.000
Quality at evaporator outlet	0.896	0.930	0.950	0.961

The hypothesis explaining this is that there is remaining liquid droplets at the compressor inlet. The lower superheat, the more liquid overflow in the evaporator and also over the internal heat exchanger gas side.

In the same test series, it was experienced that at the lowest superheat, the subcooling and superheat were not further reduced when the expansion valve was opened more. This indicates that vapor enters the internal heat exchanger liquid side where condensation takes place. These assumptions come with unknown vapor fraction at the evaporator outlet, compressor inlet and at the internal heat exchanger liquid inlet (condenser outlet). The hypothesis is tested by introducing assumed values of these vapor fractions according to Table 22. These values make the compressor power based mass flow (the method "Ec·x" in Figure 118) come close to the mass flow from Q_2 and fulfill the heat balance $Q_{liquid,side}=Q_{vapor,side}$ for the internal heat exchanger. It also might

give an explanation to the sharp drop of Q_2 and COP_2 at low superheat as shown in Figure 117. Uncondensed vapor in the liquid exiting the condenser (estimated to 3.5%) causes a shortcut in capacity.

The corresponding comparison between the refrigerant mass flow rates then become as illustrated in Figure 119.
The possibility to get the heat balances to fit for the assumed qualities makes the hypothesis about remaining droplets at the compressor inlet likely. The relatively low vapor qualities at the evaporator outlet, despite the measured superheat, indicate that there is maldistribution of the refrigerant in the evaporator. The corresponding qualities at the compressor inlet indicate similar maldistribution problems and/or poor heat transfer performance for the internal heat exchanger that were not experience with earlier prototypes. One difference from earlier prototypes is that the inlet and outlet connections are horizontally oriented in Propac #3 while they were vertical in the earlier. Furthermore, the large liquid content at the evaporator outlet could contribute to reveal weaknesses in the internal heat exchanger performance for this situation that were not seen before.

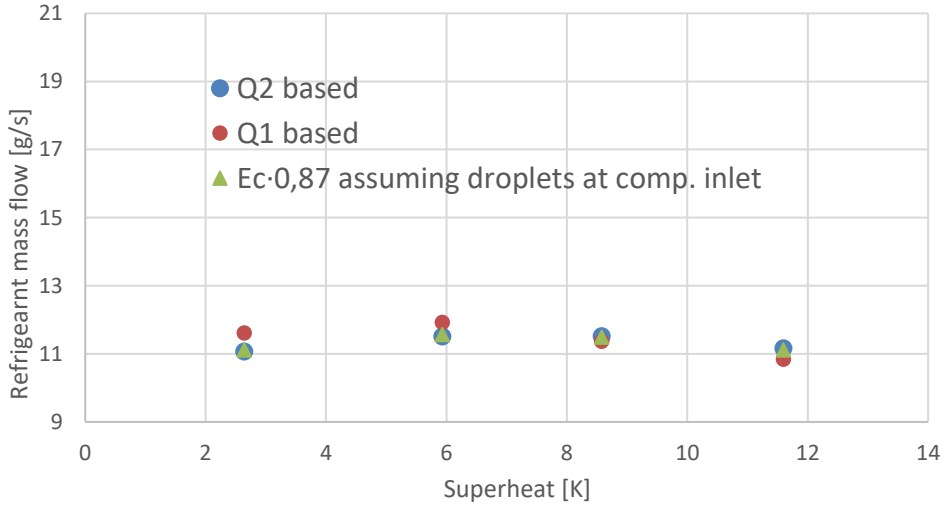

Figure 119 Refrigerant mass flow calculated in different ways assuming liquid droplets at the compressor inlet and vapor at condenser outlet for the lowest superheat as given in Table 22.

6.8.5 Summary of Propac #3 measurements

The Propac #3 prototype did not come out as well as expected. The heat transfer performance of the Z021 evaporator was expected to be higher. The great numbers of imperfections though make any conclusion regarding the potential of Z021 hard to draw. Especially the distribution needs to be further evaluated. Still, without the high pressure drop over the suction line the system performance would have come out slightly better than Propac #2.

7 Conclusions and Discussion

The Propac project has demonstrated that a split air conditioner can be built with a refrigerant charge of 143 gram propane, providing a cooling capacity of 3.5 kW at an efficiency (COP_2) of 3.5. The evaporator air flow was 13 m^3/h, which is considered to be acceptable from a noise perspective. The condenser air flow was 30 m^3/min.

The main considerations for low charge for a Propac type of system are

1. The evaporator inlet headers should be at the top with insertion of the tubes into the header kept to a minimum. This prevents separated liquid to accumulate at the bottom of the header. Consequently, the outlet header is at the bottom.
2. It is important that the refrigerant distribution in-between the many parallel evaporator channels is even.
3. Avoid liquid to enter the voluminous suction line, adding extra charge.

The system performance can be further improved if the Z021 is fully utilized. In a next step the Sanhua Z021 evaporator could be tested with a different arrangement of the distributor.

It has been demonstrated that a wide range of capacity can be provided and that the drain rate (capacity to dry humid air), an important property at many markets, is in level with products on the market. The drainage of water from the evaporator surfaces is an important property for the performance that needs to be further studied.

The minimum charge required for the system is defined at the lowest capacity. At higer capacities the optimal charge is even smaller.

The compact vehicle DC compressor and the microchannel type of heat exchangers are key technologies for minimum charge. The refrigerant distribution in the evaporator and the geometry of its headers are major areas for further reduction of the charge and improvement of the performance. Injection at the top of the evaporator reduces charge considerably.

It is recommended to use an internal heat exchanger in the type of system presented in this paper. It increases control margins, allows low superheat in the evaporator and provides a small but positive improvement of the cooling capacity and efficiency.

The control of this type of system requires new control strategies.

7.1 Discussion - Refrigerant comparison

The target cooling capacity, 3.5 kW, was achieved at a compressor speed of 1900 rpm, the maximum speed being 8500 rpm. This means that the compressor is oversized in terms of capacity which is a disadvantage for the seasonal COP_2.

Table 23. Refrigerant comparison

Given operation conditions			
$T_{1,sat}$ [°C]		50	
$T_{2,sat}$ [°C]		10	
Subcooling in condenser [K]		4	
Superheat in evaporator [K]		4	
Compressor isentropic efficiency		0.65	
Internal hex effectiveness		0.4	
Resulting states			
Refrigerant	Propane	Isobutane	R32
$p_{1,sat}$ [bar]	17.1	6.8	31.4
$p_{2,sat}$ [bar]	6.4	2.2	11.1
$\rho_{1,vapor}$ [kg/m^3]	39	18	99
$\rho_{2,vapor}$ [kg/m^3]	14	6	30
$\rho_{1,liquid}$ [kg/m^3]	449	517	839
$\rho_{2,liquid}$ [kg/m^3]	515	569	1020
T-discharge [°C]	81	73	117
T-suction gas [°C]	27	27	27
Refrigerant performance for basic, ideal cycle (Granryd)			
Volumetric cooling effect [kJ/m^3]	3414	1439	6626
COP_2 for ideal cycle and no internal hex	5.39	5.70	5.30
% Increase of Q_2 per K internal hex superheat	0.187	0.238	-0.137
% Increase of COP_2 per K internal hex superheat	0.132	0.171	-0.162

In another research project, Ecopac, at the Royal Institute of Technology the Sanden SHS33 compressor is used with isobutane (R600a) in a high temperature heat pump application. It has there been proven to work very well with isobutane. Using isobutane in the Propac system with SHS33 would lower the capacity with approximately 58%. The target capacity, 3.5 kW, would then be reached at about 4800 rpm. That would increase the seasonal COP_2 since the lowest capacity required according to the related test standard is too high with propane at the lowest speed, 800 rpm. See the “Competitor comparison” chapter for details.

The positive effect from using an internal heat exchanger is larger for R600a than for R290. Moreover, the discharge temperature is very low with R600a. This makes it possible to use an even more effective internal heat exchanger and still have reasonable discharge temperatures. At very hot conditions, Propac with isobutane would be an interesting option.

For R600a, the density of liquid is about 10% higher and for vapor about half of that for R290. The total charge for the system would not differ very much between the refrigerants. The low volumetric cooling capacity and the related low vapor density give higher refrigerant volume flow rates which require wider tubes to avoid large pressure drops. The pressures with R600a would be about 40% lower than for R290. This gives a potential for cost saving by using less material to manage required burst pressure, normally 3 times the maximum operation pressure. The efficiency for an ideal cycle is superior for R600a and the difference becomes even larger with an internal heat

exchanger since the system performance increases more with internal superheat than for propane. An interesting next step would be to test the Propac system with R600a. Some comparison data is given in Table 23, were also R32 is included.

7.2 Future work

The design of the inlet header and the distributor is a key area of further improvements for both reducing charge and improve the evaporator performance.

Strategy for control of a system of this type, in which the refrigerant flow rate is large in relation to the total charge, is an important field for further studies. Especially when an internal heat exchanger is used, that reconnects the states over the respective side. The control issue also includes charge optimization for a given application range.

It would be very interesting to test this system with isobutane (R600a) to evaluate the potential for high seasonal performance.

The new internal heat exchanger developed in the project is a starting point for further studies of an industrially and commercially feasible technique.

An interesting topic is to study techniques to introduce a reversing valve for combined refrigeration and heat pump application. Still with less than 150 gram of natural, flammable refrigerant. The big challenge is to make the heat exchangers to operate effectively both as evaporator and condenser using microchannel technique. The evaporator distribution would be a challenge.

Nomenclature

T	Temperature	$\eta_{int,hex}$	Temperature effectiveness of internal heat exchanger $\Delta T_{vapor}/\Delta T_{max}$
p	Pressure	*sat*	Saturated conditions
Nominal conditions	Q_2=3.5kW, T_1=43°C, T_2=10°C, Subcooling=4 K, Superheat=4 K, $\eta_{int,hex}$=0.4	ρ	Density
1	State at condenser inlet	*2*	State at evaporator outlet
UA_i	$Q_i/(T_i-T_{air,inlet})$	Q	capacity
COP_2	Q_2/(Compressor + Fan powers)		

References

Andersson, K. 2018. Water to water heat pump with minimum charge of propane, 13th Gustav Lorentzen Conference on natural refrigerants. Valencia, Spain.

Fernando, W. P., Palm, B., Ameel, T., Lundqvist, P. & Granryd, E. (2008). A Minichannel Aluminium Tube Heat Exchanger - Part I-III: Evaluation of Single-Phase Heat Transfer Coefficients by the Wilson Plot Method. International journal of refrigeration, 31(4), 669-680, 681-695, 696-708.

Granryd, et. Al., 2009. Refrigerating Engineering. Textbook. The department of Energy Technology, Stockholm.

Pavel Makhnatch, Gunda Mader, 2014. Refrigerants with low GWP and cost and energy efficiency optimization of vapor compression systems, Effsys Report

Refrigerant Charge Reduction, International Institute of Refrigeration, 25th Informatory Note on Refrigeration Technology

Projects scientific publications

Conference proceedings papers sent for review:

Andersson, K., Lundahl, G. & Granryd, E. 2022. AIR-AIR SPLIT AC WITH MINIMUM CHARGE OF PROPANE, 15th IIR Gustav Lorentzen Conference on Natural Refrigerants

Projects popular science publications and presentations

Research seminar at the Royal Institute of technology Institution for Energy Technology. April 2021.

Webinar for the Swedish Heat Pump and Refrigeration Association. May 2021.

Presentation for Öko-Recherche, that prepares the coming update of the EU F-gas directive for the EU commission. April 2021.

Presentation for a number of parties that has contacted the project manager during the project.